ABSTRACT

CORNEJO, LUKE R. Multilevel Methods with Multiple Grids in Energy For Multigroup Eigenvalue Transport Problems. (Under the direction of Dmitriy Y. Anistratov).

In this work we present new nonlinear multilevel methods with multiple grids in energy for solving the multigroup k-eigenvalue problems. We develop multigrid-in-energy algorithms based on a nonlinear projection operator and several advanced prolongation operators. The evaluation of the eigenvalue is performed in the space with smallest dimensionality by solving the effective one-group problem. This methodology is based on the Nonlinear Diffusion Acceleration (NDA) and Quasidiffusion (QD) methods. The multilevel method can also be used to solve diffusion problems. The homogenization in energy is based on a spatially consistent discretization of the group diffusion equations on coarse grids in energy. Prolongation is done using constant in energy or linear in energy correction factors. Various multigrid algorithms are used to iterate through the energy levels. We present numerical results of model reactor-physics problems with a very large number of groups. The results demonstrate that the multilevel method is effective for solving eigenvalue problems. Multiple energy grids are shown to be effective in reducing the total work needed to solve the problem.

Multilevel Methods with Multiple Grids in Energy For Multigroup Eigenvalue Transport Problems

by
Luke R. Cornejo

A dissertation submitted to the Graduate Faculty of
North Carolina State University
in partial fulfillment of the
requirements for the Degree of
Doctor of Philosophy

Nuclear Engineering

Raleigh, North Carolina

2019

APPROVED BY:

Yousry Y. Azmy	Robin P. Gardner
Carl T. Kelley	Dmitriy Y. Anistratov Chair of Advisory Committee

DEDICATION

I would like to dedicate this to my family and friends who supported me through this endeavor.

BIOGRAPHY

I, Luke Robert Cornejo, was born in 1992 to Roger and Jeanne Cornejo in Durham, NC. I grew up in North Carolina with four siblings and was home-schooled until I began college at North Carolina State University in 2009. I graduate from North Carolina State University with a B.S. in nuclear engineering in 2013.

ACKNOWLEDGEMENTS

I want to thank my advisor, Dr. Dmitriy Y. Anistratov, for his years of teaching and guidance in my academic and professional careers. I would also like to thank the faculty of the nuclear engineering department at North Carolina State University who instructed me in both my undergraduate and graduate education. I would especially like to thank Yousry Y. Azmy, Robin P. Gardner, and Carl T. Kelley for being part of my committee and helping direct me in my research.

I extend thanks to Bradley Rearden who provided me with my first national lab experience at Oak Ridge National Laboratory and Jae Chang for my experience at Los Alamos National Laboratory.

A special thanks to my family for encouraging me to pursue my interests in learning and supporting me throughout the process.

TABLE OF CONTENTS

LIST OF TABLES

LIST OF FIGURES

Chapter 1

Introduction

Particles transport processes play important role in various physical phenomena. For a wide class of problems, the basis for mathematical modeling of particle interactions with matter in a physical system is the linear Boltzmann equation [76]. Its solution is the particle distribution function in the phase space and time which enables to determine various characteristics of particle population and predict behavior of the physical system. The physics of nuclear reactors is dominated by the neutron transport and neutron-nuclide interactions. To design and analyze a nuclear reactor it is necessary to model dynamics of neutron population. A particular question about performance of the nuclear system is to determine physical conditions under which there is balance between neutron production and loss. These conditions can be found by solving a certain type of eigenvalue problem for the steady-state Boltzmann equation.

1.1 Transport Problems

To perform nuclear reactor design calculations the multigroup eigenvalue neutron transport problem must be solved. Solving this problem is important for finding the distribution of neutrons in the reactor and the critical parameter of the system. Current nuclear engineering calculations require the solution of these problems on fine grids in space, angle, and energy. Design processes, like coupled multi-physics problems, require the transport problem to be solved many times so it is important to be able to solve these problems quickly.

In order to solve the transport equations they are discretized in to a large system of linear equations. Let us consider the energy grid Λ_E with G intervals

$$E_{min} = E_G < \ldots < E_{g+1} < E_g < E_{g-1} < \ldots < E_0 = E_{max}\,. \tag{1.1}$$

Here E_{min} and E_{max} are some minimum and maximum energies. The energy group g is defined

by the interval of energy $[E_g, E_{g-1}]$. The transport equations with isotropic scattering are

$$\mathbf{\Omega}\cdot\boldsymbol{\nabla}\psi_g(\mathbf{r},\mathbf{\Omega})+\Sigma_{t,g}(\mathbf{r})\psi_g(\mathbf{r},\mathbf{\Omega})=\frac{1}{4\pi}\sum_{g'=1}^{G}\Sigma_{s,g'\to g}(\mathbf{r})\int_{4\pi}\psi_{g'}(\mathbf{r},\mathbf{\Omega})d\Omega + \frac{\chi_g(\mathbf{r})}{4\pi k}\sum_{g'=1}^{G}\nu_{f,g'}(\mathbf{r})\Sigma_{f,g'}(\mathbf{r})\int_{4\pi}\psi_{g'}(\mathbf{r},\mathbf{\Omega})d\Omega\,,\mathbf{r}\in G\,, \quad (1.2a)$$

$$\psi_g(\mathbf{r},\mathbf{\Omega})|_{\mathbf{r}\in\partial D_{vac}}=0 \ \text{ and}$$

$$\psi_g(\mathbf{r},\mathbf{\Omega})|_{\mathbf{r}\in\partial D_{ref}}=\psi_g(\mathbf{r},\mathbf{\Omega}^*)|_{\mathbf{r}\in\partial D_{ref}} \ \text{ for } \ \mathbf{n}\cdot\mathbf{\Omega}<0\,, \quad (1.2b)$$

$$\mathbf{\Omega}^*\cdot\mathbf{n}=-\mathbf{\Omega}\cdot\mathbf{n}, \ \ \mathbf{n}\cdot\mathbf{\Omega}\times\mathbf{\Omega}^*=0\,, \quad (1.2c)$$

$$g=1,\dots,G\,,$$

Here

$$\psi_g(\mathbf{r},\mathbf{\Omega})=\int_{E_g}^{E_{g-1}}\psi(\mathbf{r},\mathbf{\Omega},E)dE \quad (1.3)$$

is the group angular flux; $\psi(\mathbf{r},\mathbf{\Omega},E)$ is the neutron angular flux; k is the multiplication factor; $\Sigma_{t,g}$ is the group total cross section; $\Sigma_{f,g}$ is the group fission cross section; $\nu_{f,g}$ is the number of neutrons per fission in the group g; $\chi_{f,g}$ is the fission spectrum; $\Sigma_{s,g'\to g}$ is the scattering cross section from the group g' to the group g; $\mathbf{\Omega}$ is the unit vector in the direction of neutron flight; $\mathbf{n}$ is the outward normal at the boundary ∂D, ∂D_{ref} is the reflective part of the domain boundary; ∂D_{vac} is the vacuum boundary; ψ_g is the group angular flux.

Because of the integro-differential nature of the transport problem it must be solved iteratively. A classical method of power iterations [52] can converge very slowly for problems with upscattering. This is not suitable for most modern large-scale problems so faster converging methods are needed. There exist several approaches for solving the multigroup transport equation with rapidly converging iterations. One family of methods is based on the synthetic acceleration approach [52]. An example of such a method is the two-grid acceleration scheme developed to speed up iterations in fixed-source transport problems with upscattering [7]. This method uses a one-group diffusion problem for the iterative error. The one-group diffusion coefficient and cross sections are defined by means of a special spectral shape function that approximates the Fourier harmonic of the solution converging at the slowest rate. Another way to solve the k-eigenvalue transport problem is to treat it as a generalized eigenvalue problem and apply Nonlinear Krylov acceleration and Jacobian-Free Newton-Krylov methods [9, 26, 53, 31]. The iterative methods developed on such basis demonstrated efficiency of this approach. Multigrid in energy have also been used as a preconditioner for Krylov solvers [58].

A different group of iterative schemes applies the nonlinear-projective iterative (NPI) method-

ology and effectively reduces the dimensionality of the transport problem [52, 15]. These methods solve a system of equations that consist of the transport equation and a set of lower dimension equations. The low-order equations reduce the dimensionality of the problem and can form rapidly converging iterative methods. The set of equations is closed by defining linear-fractional factors. These factors are weakly dependent on the high-order which results in accelerated convergence. Over the years the NPI methods have seen wide spread used to solve multigroup neutron transport problems.

The detailed formulation of real neutron transport problems involves a very large number of energy groups. For example, the reactor-physics software SCALE for lattice physics calculations uses the 44-group and 238-group ENDF/B-V neutron cross section libraries [66]. The lattice-physics code CASMO-5 for modeling light-water reactors has the 586-group neutron library based on ENDF/B-VII nuclear data [41]. This motivates the development of iteration methods with multiple grids in energy to achieve even better efficiency for full-scale reactor-physics problems.

1.1.1 QD Method

An early NPI method is the Quasidiffusion (QD) method [52, 69, 18, 19]. The set of equations for the QD method consists of the high-order transport equations

$$\begin{aligned}\boldsymbol{\Omega}\cdot\boldsymbol{\nabla}\psi_g(\mathbf{r},\boldsymbol{\Omega})+\Sigma_{t,g}(\mathbf{r})\psi_g(\mathbf{r},\boldsymbol{\Omega}) = \frac{1}{4\pi}\sum_{g'=1}^{G}\Sigma_{s,g'\to g}(\mathbf{r})\phi_{g'}(\mathbf{r}) \\ + \frac{\chi_g(\mathbf{r})}{4\pi k}\sum_{g'=1}^{G}\nu_{f,g'}(\mathbf{r})\Sigma_{f,g'}(\mathbf{r})\phi_{g'}(\mathbf{r})\,,\mathbf{r}\in G\,, \quad (1.4)\end{aligned}$$

and the low-order QD (LOQD) equations [69, 70, 18]. The low-order QD (LOQD) equations for this method are the zeroth and first moments of the transport equation. The set of equations are closed by a set of functionals that are calculated from the high-order solution. If the functionals are exact the LOQD equations can generate the transport solution exactly. The multigroup LOQD equations in continuous form [69, 18, 19] are

$$\boldsymbol{\nabla}\cdot\boldsymbol{J}_g+\Sigma_{t,g}\phi_g=\sum_{g'=1}^{G}\Sigma_{s,g'\to g}\phi_{g'}+\frac{\chi_g}{k}\sum_{g'=1}^{G}\nu_{f,g'}\Sigma_{f,g'}\phi_{g'}\,, \quad (1.5a)$$

$$\boldsymbol{\nabla}\cdot\Big(\mathbb{E}_g\phi_g\Big)+\Sigma_{t,g}\mathbf{J}_g=0\,, \quad (1.5b)$$

where

$$E_{\alpha\beta,g} = \frac{\int_{4\pi} \Omega_\alpha \Omega_\beta \psi_g d\mathbf{\Omega}}{\int_{4\pi} \psi_g d\mathbf{\Omega}}, \quad \alpha, \beta = x, y \tag{1.6}$$

are the components of the QD (aka Eddington) tensor $\mathbb{E}_g$ that is defined to close the system of high-order transport (1.4) and LOQD equations (1.5). The boundary conditions for the LOQD equations are the following:

$$\mathbf{n} \cdot \mathbf{J}_g|_{\mathbf{r} \in \partial G_{ref}} = 0, \qquad \mathbf{n} \cdot \mathbf{J}_g|_{\mathbf{r} \in \partial G_{vac}} = C_{n,g} \phi_g|_{\mathbf{r} \in \partial G_{vac}}, \tag{1.7}$$

where the boundary factor is defined as

$$C_{n,g} = \frac{\int_{\mathbf{\Omega} \cdot \mathbf{n} \geq 0} \mathbf{n} \cdot \mathbf{\Omega} \psi_g d\mathbf{\Omega}}{\int_{\mathbf{\Omega} \cdot \mathbf{n} \geq 0} \psi_g d\mathbf{\Omega}}\Big|_{\mathbf{r} \in \partial G_{vac}}. \tag{1.8}$$

Reducing the dimensionality of the low-order problem can also be done by using coarser energy grids [69]. Methods with two energy grids, namely involving one-group (grey) low-order problems, were developed based on the Quasi-diffusion method [18, 19, 70, 71, 20, 72, 13, 24]. In the multilevel iteration scheme, the eigenvalue is determined as the solution of the problem with the smallest dimensionality, namely, of the effective one-group low-order equations. This multilevel method can be interpreted as a nonlinear multigrid method and described in terms of projection and prolongation operators. These methods demonstrated that the one-group low-order equation could accelerate the solution of the multigroup low-order equation reducing the total amount of work done in the low-order problem.

1.1.2 NDA Method

The Nonlinear Diffusion Acceleration (NDA) method is a very popular NPI method [38]. The low-order equations consist of the zeroth moment of the transport equation and the first moment in the form of a modified Fick's law equation. The NDA method is similar to the Coarse Mesh Finite Difference (CMFD) [36]. The low-order NDA equations are discretized on the same spatial mesh as the transport equations [36]. The NDA method was originally derived in descrete form [38], but the can also be written continuously [17]. The system of low-order NDA (LONDA) equations in continuous form for the multigroup transport problem (1.2) consists of the neutron balance equation

$$\boldsymbol{\nabla} \cdot \mathbf{J}_g + \Sigma_{t,g} \phi_g = \sum_{g'=1}^{G} \Sigma_{s,g' \to g} \phi_{g'} + \frac{\chi_g}{k} \sum_{g'=1}^{G} \nu_{f,g'} \Sigma_{f,g'} \phi_{g'} \tag{1.9a}$$

and the first-moment equation in the form of the generalized Fick's law

$$\mathbf{J}_g = -D_g \boldsymbol{\nabla}\phi_g + \tilde{\mathbf{D}}_g \phi_g \,, \tag{1.9b}$$

where

$$D_g = \frac{1}{3\Sigma_{t,g}} \,, \tag{1.9c}$$

$$\mathbf{J}_g = \int_{4\pi} \boldsymbol{\Omega}\psi_g d\boldsymbol{\Omega}, \tag{1.9d}$$

is the neutron current and factor $\tilde{\mathbf{D}}_g$ is defined to yield exact closure and given by

$$\tilde{\mathbf{D}}_{\alpha,g} = \frac{\int_{4\pi} \mathbf{e}_\alpha \cdot \boldsymbol{\Omega}\psi_g d\boldsymbol{\Omega} + D_g \mathbf{e}_\alpha \cdot \boldsymbol{\nabla} \int_{4\pi} \psi_g d\boldsymbol{\Omega}}{\int_{4\pi} \psi_g d\boldsymbol{\Omega}} \,, \quad \alpha = x, y \,. \tag{1.9e}$$

The boundary conditions for the low-order equations are

$$\mathbf{n}\cdot\mathbf{J}_g|_{\mathbf{r}\in\partial G_{vac}} = F_{n,g}\phi_g|_{\mathbf{r}\in\partial G_{vac}} \,, \quad F_n = \left. \frac{\int\limits_{\boldsymbol{\Omega}\cdot\mathbf{n}\geq 0} \mathbf{n}\cdot\boldsymbol{\Omega}\psi_g d\boldsymbol{\Omega}}{\int\limits_{\boldsymbol{\Omega}\cdot\mathbf{n}\geq 0} \psi_g d\boldsymbol{\Omega}} \right|_{\mathbf{r}\in\partial G_{vac}} , \tag{1.10a}$$

$$\mathbf{n}\cdot\mathbf{J}_g|_{\mathbf{r}\in\partial G_{ref}} = 0 \,. \tag{1.10b}$$

This methodology has been used to accelerate transport methods like the method of characteristics (MOC) [73] and finite element methods [63, 62] and recent work has been done to apply these methods to more types of problems like hexagonal geometries [57].

Reducing the dimensionality of the low-order problem was also done using NDA type equations. Methods were developed that reduced the dimensionality in energy and angle, using a collapsed one-group diffusion equation to calculate a spatial correction term [7, 1]. A different version of this method was developed that used a one-group transport equation instead of a diffusion equation [68]. A multilevel NDA method for multigroup eigenvalue problems have been developed and applied to 1D problems [17]. Multigroup and two-group grids were used to implement a two-level CMFD method for 2D arbitrary geometry [77]. In an application of MOC a two-group CMFD formulation was used to improve the efficiency of the multi-group CMFD accelerator [33]. A multilevel solver has been used for multigroup diffusion eigenvalue problems [2] using multigrid in space and two levels in energy. The method can be described as a power iteration method with the addition of a one-group diffusion equation, space-dependent Wielandt shift and a multigrid-in-space linear solver. This method was presented for diffusion and applied for the low-order CMFD problem in Michigan Parallel Characteristics Transport (MPACT) code. A multilevel CMFD method with two and more energy grids in the low-order

equations was implemented in the MPACT code [6]. The coarsest energy grid was defined as the two-group problem and the eigen problem was solved on this grid using shifted power iterations. Both pre- and post-sweeps are performed on each multigrid cycle.

1.1.3 pCMFD Method

The classical CMFD method has a zone of instability for certain problems with optically thick meshes in the case the system of the high-order transport equation and low-order CMFD equations is solved using a fixed-point iteration method [25, 34]. A version of CMFD, known as the partial current-based CMFD (p-CMFD) method, has been developed that formulates the low-order problem to preserve the high-order partial currents [55, 35, 54, 64]. It was shown that fixed-point iteration scheme for pCMFD system of equations has better stability properties compared to classical CMFD [55, 61]. The pCMFD equations are usually derived in discrete form. In this section we present a formulation of the pCMFD equations in continuous form. The low-order system of pCMFD equations consists of the zeroth-moment equation

$$\nabla \cdot \mathbf{J}_g + \Sigma_{t,g}\phi_g = \sum_{g'=1}^{G} \Sigma_{s,g'\to g}\phi_{g'} + \frac{\chi_g}{k}\sum_{g'=1}^{G} \nu_{f,g'}\Sigma_{f,g'}\phi_{g'} \tag{1.11}$$

and first-moment equations in the form of a generalized Fick's law. To derive the pCMFD first-moment equations, we apply the P_1 approximation of the angular flux

$$\psi_g = \frac{1}{4\pi}(\phi_g - 3D_g\mathbf{\Omega}\cdot\boldsymbol{\nabla}\phi_g)\,. \tag{1.12}$$

Integrating Eq. (1.12) with the weight $\mathbf{e}_\alpha \cdot \mathbf{\Omega}$ over $2\pi^\pm$ relative to the direction of $\mathbf{e}_\alpha$ we get the P_1-approximation for the projection of the partial currents on the direction $\mathbf{e}_\alpha$

$$J_\alpha^\pm = \frac{1}{4}\phi_g \mp \frac{1}{2}D_g\mathbf{e}_\alpha\cdot\boldsymbol{\nabla}\phi_g\,. \tag{1.13}$$

We now generalize Eq. (1.13) in the following form:

$$J_\alpha^\pm = \pm\tilde{D}_{\alpha,g}^\pm\phi_g \mp \frac{1}{2}D_g\mathbf{e}_\alpha\cdot\boldsymbol{\nabla}\phi_g\,. \tag{1.14}$$

Here we introduced factors $\tilde{D}_{\alpha,g}^\pm$ that enable one to formulate the exact closure relations for the low-order pCMFD equations. $\tilde{D}_{\alpha,g}^\pm$ are defined such that

$$\int_{2\pi^\pm} \mathbf{e}_\alpha\cdot\mathbf{\Omega}\psi_g d\mathbf{\Omega} = \pm\tilde{D}_{\alpha,g}^\pm\int_{4\pi}\psi_g d\mathbf{\Omega} \mp \frac{1}{2}D_g\mathbf{e}_\alpha\cdot\boldsymbol{\nabla}\int_{4\pi}\psi_g d\mathbf{\Omega}\,. \tag{1.15}$$

This leads to the factors defined as

$$\tilde{D}^{\pm}_{\alpha,g} = \frac{\pm \int_{2\pi^{\pm}} \mathbf{e}_\alpha \cdot \mathbf{\Omega} \psi_g d\mathbf{\Omega} \mp \frac{1}{2} D_g \mathbf{e}_\alpha \cdot \boldsymbol{\nabla} \int_{4\pi} \psi_g d\mathbf{\Omega}}{\int_{4\pi} \psi_g d\mathbf{\Omega}} \,. \tag{1.16}$$

We now take into account that α-component of the current $\mathbf{e}_\alpha \cdot \mathbf{J}_g$ is given by

$$J_{\alpha,g} = J^{+}_{\alpha,g} - J^{-}_{\alpha,g} \tag{1.17}$$

to obtain the pCMFD form of the generalized Fick's law

$$J_{\alpha,g} = -D_g \mathbf{e}_\alpha \cdot \boldsymbol{\nabla} \phi_g + (\tilde{D}^{-}_g + \tilde{D}^{+}_g)\phi_g \,. \tag{1.18}$$

Thus the low-order pCMFD equations are given by Eqs. (1.11) and (1.18). The boundary conditions for the low-order equations are defined in (1.10). Fourier analysis of pCMFD method with Step Characteristics for 1-dimensional eigenvalue problems is unconditionally stable [61]. The pCMFD method has been applied to accelerate the step characteristics method in NEWT [35]. It has also be used as an accelerator in whole-core transport solutions [64, 5].

1.2 Diffusion Problems

The phase space of neutron transport problems has high dimensionality. It includes the spatial position of the particle, its energy and the direction of particle motion. In general case, it is a 6-dimensional space. To reduce the dimensionality of the problem and complexity of neutron transport simulations, various approximate methods have been developed. One group of neutron transport models is based on the P_1 equations that belong to the family of the method of spherical harmonics also know as the P_N method [16]. The P_1 equations are defined for the first two moments of the neutron angular flux and hence of the distribution function. The moment equations are closed assuming that the angular flux linearly depends on the direction of particle motion. The P_1 equations can be reduced to the neutron diffusion equation for the zeroth angular moment of the angular flux.

For problems with isotropic scattering the P_1 equations can be reduced to the diffusion equations. The k-eigenvalue problem for the multigroup diffusion equations on the given grid

Λ_E is defined by [16]

$$-\boldsymbol{\nabla}\cdot D_g(\mathbf{r})\boldsymbol{\nabla}\phi_g(\mathbf{r})+\Sigma_{t,g}(\mathbf{r})\phi_g(\mathbf{r})=\sum_{g'=1}^{G}\Sigma_{s,g'\to g,}(\mathbf{r})\phi_{g'}(\mathbf{r}) + \frac{\chi_g(\mathbf{r})}{k}\sum_{g'=1}^{G}\nu_{f,g'}(\mathbf{r})\Sigma_{f,g'}(\mathbf{r})\phi_{g'}(\mathbf{r})\,, \quad (1.19)$$

$$\mathbf{r}\in\mathcal{D}\,,\quad g=1,\ldots,G\,,$$

with the following conditions

$$\mathbf{n}(\mathbf{r}_b)\cdot\boldsymbol{\nabla}\phi_g(\mathbf{r_b})=0\,,\quad \mathbf{r}_b\in\partial\mathcal{D}_{ref} \quad (1.20)$$

at the reflective boundary and

$$\phi_g(\mathbf{r}_b)+2D_g(\mathbf{r}_b)\mathbf{n}(\mathbf{r}_b)\cdot\boldsymbol{\nabla}\phi_g(\mathbf{r}_b)=0\,,\quad \mathbf{r}_b\in\partial\mathcal{D}_{vac} \quad (1.21)$$

at the vacuum boundary. $D_g=\frac{1}{3\Sigma_{t,g}}$ is the group diffusion coefficient; $\mathbf{n}(\mathbf{r}_b)$ is the outward normal at the boundary. The P_1 equations are given by the neutron balance equation

$$\boldsymbol{\nabla}\cdot\boldsymbol{J}_g(\mathbf{r})+\Sigma_{t,g}(\mathbf{r})\phi_g(\mathbf{r})=\sum_{g'=1}^{G}\Sigma_{s,g'\to g,}(\mathbf{r})\phi_{g'}(\mathbf{r})+\frac{\chi_g(\mathbf{r})}{k}\sum_{g'=1}^{G}\nu_{f,g'}(\mathbf{r})\Sigma_{f,g'}(\mathbf{r})\phi_{g'}(\mathbf{r}) \quad (1.22)$$

and the Fick's law

$$D_g(\mathbf{r})\boldsymbol{\nabla}\phi_g(\mathbf{r})+\boldsymbol{J}_g(\mathbf{r})=0\,. \quad (1.23)$$

The solution of the P_1 equations has limited accuracy. However, it works well for neutron transport problems in which the angular flux weakly depends on angular and spatial variables. The diffusion solution is a good approximation for problems that involve spatial homogenization [47, 65]. A lot of research has been carried out to study properties and applicability of the P_1 method and diffusion approximation [46, 23, 22, 48, 28]. The P_1 method is a reliable tool for modeling and analysis of various of physical systems [37, 11].

Basic methods for solving the multigroup diffusion equations, such as, the power and Gauss-Seidel iterations are simple algorithms, but they can converge slowly in a large class of reactor-physics problems. Advanced iteration schemes for energy-dependent particle diffusion problems has been developed [29, 30, 9, 8, 3]. There exist a group of methods for solving multigroup neutron transport and radiative transfer problems that use two grids in energy [21, 7, 13, 24, 19, 17, 2]. The two-grid approach has demonstrated that it can significantly reduce the number of times the group transport equations are solved [19]. This approach has been also

applied to develop a nonlinear two-grid (NTG) method for multigroup diffusion problems [14]. The stability properties of the NTG method for k-eigenvalue multigroup diffusion problems has been studied by means of the Fourier analysis. This analysis predicted well the rates of convergence of the eigenvalue and associated eigenfunction.

1.3 Multigrid Methods

Multigrid methods were originally developed for solving boundary value problems found in may physical systems[59, 60, 75]. A linear system of equations is formed from the elliptic partial differential equations by finite element or finite difference discretization. For this type of system of equations local relaxations, such as Gauss-Seidel and Jacobi iterations, converge very fast on the high frequency part of the solution. The low frequency component of the solution can converge much slower. The convergence of the iterative method can be improved by introducing a coarser grid and projecting the error onto it. The first effect of this is to reduce the size of the problem. The second is that the slow to converge low frequency error effectively becomes a higher frequency error on the coarser grid and can be efficiently corrected by local relaxations on that grid. Repeating this recursively yields a multigrid iterative method. The set of nested coarse grids are found by successive refinement. These types of methods are known as geometric multigrid as they are dependent on a hierarchy of geometric grids.

Algebraic multigrid is a generalization of geometric multigrid [39, 32]. It was originally developed for sets of equations similar to discretized PDEs approximated on an unstructured grid. This methodology has been extended to other types of problems and general matrices.

Multigrid method can be applied to solve neutron transport problems. Spatial multigrid methods have been developed to accelerate transport problems and be well suited for parallel computation [4]. A multilevel in space and energy method for diffusion problems has been developed that uses geometric multigrid in space linear solver [2, 3]. This method also uses two levels in energy. Multigrid has also been used as a preconditioner for solving transport problems [58].

1.4 Significance and Novelty of the Main Results

New iteration methods for solving eigenvalue problems for multigroup neutron transport and diffusion equations have been developed. They are based on multigrid-in-energy approach. For eigenvalue neutron transport problems, the nonlinear projection operator is formulated by averaging the group low-order transport equations over energy on the hierarchy of energy grids. For eigenvalue neutron diffusion problems, a similar nonlinear projection operator is defined by averaging the group diffusion equations over energy grids. Several new multilevel acceleration

transport methods for reactor-physics application are proposed based on low-order equations of the QD, NDA, CMFD, and pCMFD methods.

We defined several variants of prolongation operators based on multiplication correction of the grid solutions. The prolongation operators use constant and linear interpolation in energy between neighboring grids. We apply the partial V-cycles, partial W-cycles, and hybrid cycles to move through the hierarchy of energy grids. The estimation of the eigenvalue is performed on the coarsest grid with just one energy group. Thus, the eigenvalue problem is solved in the space with the smallest dimensionality. The proposed methods with multigrid in energy are derived for the second-order finite volume spatial discretization of the low-order transport (and diffusion) equation. They can be applied to other spatial discretizations as well, for example, finite element methods. The obtained numerical results on realistic model reactor-physics problems with 44 and 258 groups demonstrated efficiency of the developed algorithms with multigrid in energy. They enable to reduce significantly total number of low-order solves as well as accelerate transport iterations. Involving additional coarse energy grids accelerate iterations and decrease computational costs.

The proposed multilevel methods enable one to solve important class reactor physics problem. They are effective in solving the large-scale transport problems and can be used, for instance, for full-core like calculations. These methods can be applied to different transport methods to improve performance of existing reactor-physics software. The proposed multilevel algorithms can be used to develop advanced iterative methods for solving large-scale multiphysics problems with very large number of groups.

This research was presented by the candidate to members of the research community at the following venues:

- Joint International Conference on Math and Computation (M&C), Supercomputers in Nuclear Applications (SNA) and the Monte Carlo (MC) Method in Nashville, TN, April 19-23, 2015
- The Physics of Reactors (PHYSOR) Conference in Sun Valley, ID, May 1-5, 2016
- Scientific Seminar to Laboratory, Reactor and Nuclear Systems Division at Oak Ridge National in Oak Ridge, TN, July 30, 2018, and
- Scientific Seminar to Radiation Transport Group at Los Alamos National Laboratory in Los Alamos, NM, August 22, 2018,

This research has been published in peer reviewed journals Nuclear Science and Engineering [44] and Progress in Nuclear Engineering [45] (invited) and in the conference proceedings of M&C 2015 [42] and PHYSOR 2016 [43]. A paper has been also submitted for publication in Nuclear Science and Engineering [40].

The remainder of this dissertation is organized as follows. In chapter 2, we present multilevel diffusion method with multiple energy grids. In chapter 3, we describe a multilevel transport method with multiple grids in energy where the low-order equations are formulated on the same spatial mesh as the hight-order problem. In chapter 4, we describe a multilevel transport method with multiple grids in space and energy where the low-order equations are on a coarser spatial mesh than the transport problem.

Chapter 2

Multilevel Diffusion Method

In this chapter we present a nonlinear method with multiple grids in energy for solving the k-eigenvalue problem for multigroup neutron diffusion equations. We develop multigrid-in-energy algorithms based on a nonlinear projection operator and several prolongation operators. The evaluation of the eigenvalue is performed in the space with smallest dimensionality by solving the effective one-group diffusion problem. The multilevel methods are formulated in discrete form for the second-order finite volume discretization of the diffusion equation. The homogenization in energy is based on a spatially consistent discretization of the group diffusion equations on coarse grids in energy. The results of this chapter has been submitted for publication [40].

In Sec. 2.1 the hierarchy of equations is defined. Sec. 2.2 describes the multigrid cycles and Sec. 2.3 defines the prolongation operators. Numerical results are presented in Sec. 2.4.

2.1 Hierarchy of Diffusion Equations

To formulate the multilevel method for solving Eq. (1.19) we define a hierarchy of grids in energy [44, 45]

$$\{\Lambda_E^\gamma, \gamma = 1, \ldots, \Gamma : \Lambda_E^\Gamma \subset \ldots \subset \Lambda_E^\gamma \subset \Lambda_E^{\gamma-1} \subset \ldots \subset \Lambda_E^1 = \Lambda_E\}\,, \tag{2.1}$$

where γ is the grid index. The grid Λ_E^γ consists of groups with energy intervals $\delta\mathcal{E}_g^\gamma = [E_g^\gamma, E_{g-1}^\gamma]$ ($g = 1, \ldots, G^\gamma$) formed by coarsening the previous grid $\Lambda_E^{\gamma-1}$. G^γ is the number of groups in the grid Λ_E^γ. Thus, the group scalar flux on the grid Λ_E^γ is given by

$$\phi_p^\gamma = \int_{\delta\mathcal{E}_g^\gamma} \phi(\mathbf{r}, E) dE = \sum_{g' \in \omega_p^\gamma} \phi_{g'}^{\gamma-1}\,, \tag{2.2}$$

where ω_p^γ is the set of group indices of the grid $\Lambda_E^{\gamma-1}$ included in the group g of the grid Λ_E^γ. The grid Λ_E^1 is the given fine energy grid. Thus $G^1 = G$ and

$$\phi_g(\mathbf{r}) \equiv \phi_g^1(\mathbf{r})\,. \tag{2.3}$$

The coarsest grid Λ_E^Γ has only one group and $G^\Gamma = 1$. The total scalar flux is given by

$$\phi(\mathbf{r}) = \int_{E_{min}}^{E_{max}} \phi(\mathbf{r}, E)dE = \phi_1^\Gamma(\mathbf{r})\,. \tag{2.4}$$

The methods with multigrid in energy are formulated by means of projection and prolongation operators. The nonlinear projection operator is defined by integration of the diffusion equations over energy groups and their homogenization with respect to energy. The homogenization procedure transfers information from a grid to a coarser one and defines a coarse-grid correction step. The hierarchy of group diffusion equations on multiple grids in energy has the following general form:

$$-\boldsymbol{\nabla}^2\Big(\bar{\mathbb{D}}_p^\gamma(\mathbf{r})\phi_p^\gamma(\mathbf{r})\Big) + \bar{\Sigma}_{t,g}^\gamma(\mathbf{r})\phi_p^\gamma(\mathbf{r}) = \sum_{g'=1}^{G^\gamma} \bar{\Sigma}_{s,g'\to g}^\gamma(\mathbf{r})\phi_{g'}^\gamma(\mathbf{r}) + \frac{\bar{\chi}_g^\gamma(\mathbf{r})}{k}\sum_{g'=1}^{G^\gamma} \overline{\nu\Sigma}_{f,g'}^\gamma(\mathbf{r})\phi_{g'}^\gamma(\mathbf{r})\,, \tag{2.5}$$

$$\mathbf{r}\in\mathcal{D}\,,\quad g = 1,\ldots,G^\gamma\,,\quad \gamma = 1,\ldots,\Gamma-1\,,$$

$$-\boldsymbol{\nabla}^2\Big(\bar{\mathbb{D}}_1^\Gamma\phi_1^\Gamma(\mathbf{r})\Big) + \bar{\Sigma}_{a,1}^\Gamma\phi_1^\Gamma(\mathbf{r}) = \frac{1}{k}\overline{\nu\Sigma}_{f,1}^\Gamma\phi_1^\Gamma\,,\quad \mathbf{r}\in\mathcal{D}\,,\quad \gamma = \Gamma\,. \tag{2.6}$$

The cross sections and diffusion tensor $\bar{\mathbb{D}}_p^\gamma$ are averaged by the solution $\phi_g^{\gamma-1}$ on the grid $\Lambda_E^{\gamma-1}$. The averaged cross sections are given by

$$\bar{\Sigma}_{t,g}^\gamma = \frac{\sum_{g'\in\omega_g^\gamma}\bar{\Sigma}_{t,g'}^{\gamma-1}\phi_{g'}^{\gamma-1}}{\sum_{g'\in\omega_g^\gamma}\phi_{g'}^{\gamma-1}}\,,\quad \bar{\Sigma}_{a,g}^\gamma = \frac{\sum_{g'\in\omega_g^\gamma}\bar{\Sigma}_{a,g'}^{\gamma-1}\phi_{g'}^{\gamma-1}}{\sum_{g'\in\omega_g^\gamma}\phi_{g'}^{\gamma-1}}\,, \tag{2.7a}$$

$$\overline{\nu\Sigma}_{f,g}^\gamma = \frac{\sum_{g'\in\omega_g^\gamma}\overline{\nu\Sigma}_{f,g'}^{\gamma-1}\phi_{g'}^{\gamma-1}}{\sum_{g'\in\omega_g^\gamma}\phi_{g'}^{\gamma-1}}\,,\quad \bar{\chi}_g^\gamma = \sum_{g'\in\omega_g^\gamma}\bar{\chi}_{g'}^{\gamma-1}\,, \tag{2.7b}$$

$$\bar{\Sigma}_{s,g'\to g}^\gamma = \frac{\sum_{g'\in\omega_{g'}^\gamma}\Big(\sum_{g\in\omega_p^\gamma}\bar{\Sigma}_{s,g'\to g}^{\gamma-1}\Big)\phi_{g'}^{\gamma-1}}{\sum_{g'\in\omega_{g'}^\gamma}\phi_{g'}^{\gamma-1}}\,, \tag{2.7c}$$

where $\bar{\Sigma}_{t,g}^1 = \Sigma_{t,g}$, $\overline{\nu\Sigma}_{f,g}^1 = \nu_{f,g}\Sigma_{f,g}$, $\bar{\Sigma}_{s,g'\to g}^1 = \Sigma_{s,g'\to g}$, $\bar{\mathbb{D}}_p^1 = diag(D_p,\ldots,D_p)$. We note that the final form of the proposed multigrid-in-energy methods is derived for the discretized

diffusion equations. The continuous equations (2.5) and (2.6) lack some essential details. The diffusion tensor $\bar{\mathbb{D}}_p^\gamma$ and the form of the discretized differential term are defined by averaging of the discrete leakage rate density (LRD) term and depend on the spatial discretization scheme. This part of the methodology is described below.

To solve the group diffusion equations (2.5) on Λ_E^γ with $\gamma < \Gamma$, we evaluate the fission and upscattering terms by means of the solution obtained on the grid $\Lambda_E^{\gamma-1}$ and use the estimation of the eigenvalue from the previous multigrid cycle. The equation (2.5) gives rise to

$$-\boldsymbol{\nabla}^2\big(\bar{\mathbb{D}}_g^\gamma\phi_g^\gamma\big) + \bar{\Sigma}_{t,g}^\gamma\phi_g^\gamma - \sum_{g'=1}^{g}\bar{\Sigma}_{s,g'\to g}^\gamma\phi_{g'}^\gamma = \sum_{g'=g+1}^{G^\gamma}\bar{\Sigma}_{s,g'\to g}^\gamma\sum_{g'\in\omega_{g'}^\gamma}\phi_{g'}^{\gamma-1} + \frac{\bar{\chi}_g^\gamma}{k}\sum_{g'=1}^{G^\gamma}\overline{\nu\Sigma}_{f,g'}^\gamma\sum_{g'\in\omega_{g'}^\gamma}\phi_{g'}^{\gamma-1}\,, \quad (2.8)$$

$$g = 1,\ldots,G^\gamma$$

for $\gamma = 1,\ldots,\Gamma-1$. Thus, the equations for $\boldsymbol{\phi}^\gamma = (\phi_1^\gamma,\ldots,\phi_G^\gamma)^T$ have the following general form:

$$\mathcal{A}_\gamma\boldsymbol{\phi}^\gamma = \mathcal{B}_\gamma\boldsymbol{\phi}^{\gamma-1} + \frac{1}{k}\mathcal{C}_\gamma\boldsymbol{\phi}^{\gamma-1}\,, \quad (2.9)$$

where $\mathcal{A}_\gamma$ is operator of the left-hand side of Eq. (2.8) given by

$$\mathcal{A}_\gamma\boldsymbol{\phi}^\gamma \equiv -\boldsymbol{\nabla}^2\big(\bar{\mathbb{D}}_g^\gamma\phi_g^\gamma\big) + \bar{\Sigma}_{t,g}^\gamma\phi_g^\gamma - \sum_{g'=1}^{g}\bar{\Sigma}_{s,g'\to g}^\gamma\phi_{g'}^\gamma\,, \quad (2.10)$$

$\mathcal{B}_\gamma$ and $\mathcal{C}_\gamma$ are the upscattering and fission production operators, respectively, defined as

$$\mathcal{B}_\gamma\boldsymbol{\phi}^{\gamma-1} \equiv \sum_{g'=g+1}^{G^\gamma}\bar{\Sigma}_{s,g'\to g}^\gamma\sum_{g'\in\omega_{g'}^\gamma}\phi_{g'}^{\gamma-1}\,, \quad \mathcal{C}_\gamma\boldsymbol{\phi}^{\gamma-1} \equiv \bar{\chi}_g^\gamma\sum_{g'=1}^{G^\gamma}\overline{\nu\Sigma}_{f,g'}^\gamma\sum_{g'\in\omega_{g'}^\gamma}\phi_{g'}^{\gamma-1}\,. \quad (2.11)$$

The matrix-operator $\mathcal{A}_\gamma$ is lower triangular. The system of group diffusion equation (2.8) on the grid Λ_E^γ can be solved by sweeping through groups. This is equivalent to performing one Gauss-Seidel iteration over energy groups on this grid.

The eigenvalue and associated one-group eigenfunction are determined by solving the effective one-group problem (2.6). The eigenvalue problem on the coarsest grid Λ_E^Γ has the following general form:

$$\mathcal{A}_\Gamma\boldsymbol{\phi}^\Gamma = \frac{1}{k}\mathcal{C}_\Gamma\boldsymbol{\phi}^\Gamma\,, \quad (2.12)$$

where

$$\mathcal{A}_\Gamma \boldsymbol{\phi}^\Gamma \equiv -\boldsymbol{\nabla}^2\Big(\bar{\mathbb{D}}_1^\Gamma \phi_1^\Gamma\Big) + \bar{\Sigma}_{a,1}^\Gamma \phi_1^\Gamma\,, \quad \mathcal{C}_\Gamma \boldsymbol{\phi}^\Gamma = \overline{\nu\Sigma}_{f,1}^\Gamma \phi_1^\Gamma\,. \tag{2.13}$$

We consider problems in 2D Cartesian geometry with the rectangular spatial domain $\mathcal{D} = \{0 \le x \le X,\ 0 \le y \le Y\}$. The spatial grids are orthogonal and defined by the cells $C_{ij} = \{x_{i-1/2} \le x \le x_{i+1/2},\ y_{j-1/2} \le y \le y_{j+1/2}\}$, where $i = 1, \ldots, N_x$, $j = 1, \ldots, N_y$. The cross sections are assumed to be piece-wise constant functions on the set of grid cells. The group diffusion equations (1.19) on Λ_E are approximated by means of a second-order finite volume (FV) method which is derived by discretizing the P_1 equations (1.22) and (1.23). We integrate the balance equation (1.22) over the cell C_{ij} to get

$$\begin{aligned}\big(J_{g,i+1/2,j} - J_{g,i-1/2,j}\big)h_j^y + \big(J_{g,i,j+1/2} - J_{g,i,j-1/2}\big)h_i^x + \Sigma_{t,g,i,j}\phi_{g,i,j}A_{i,j} = \\ A_{i,j}\sum_{g'=1}^{G}\Sigma_{s,g'\to g,i,j}\phi_{g',i,j} + \frac{1}{k}A_{i,j}\chi_{g,i,j}\sum_{g'=1}^{G}\nu_{f,g',i,j}\Sigma_{f,g',i,j}\phi_{g',i,j}\,,\end{aligned} \tag{2.14}$$

$$h_i^x = x_{i+1/2} - x_{i-1/2}\,, \quad h_j^y = y_{j+1/2} - y_{j-1/2}\,, \quad A_{i,j} = h_i^x h_j^y\,, \tag{2.15}$$

where $\phi_{g,i,j}$ is the cell-average group scalar flux, $J_{g,i+1/2,j}$ and $J_{g,i,j+1/2}$ are the face-average group currents, $\Sigma_{t,g,i,j}$, $\Sigma_{f,g,i,j}$, $\nu_{f,g,i,j}$, $\Sigma_{s,g'\to g,i,j}$, and $\chi_{g,i,j}$ are the material parameters of the cell C_{ij}. The Fick' law (1.23) is integrated over right, left, bottom, and top halves of C_{ij}. This yields

$$D_{g,i,j}\big(\phi_{g,i+1/2,j} - \phi_{g,i,j}\big) + \frac{1}{2}J_{g,i+1/2,j}h_i^x = 0\,, \tag{2.16}$$

$$D_{g,i,j}\big(\phi_{g,i,j} - \phi_{g,i-1/2,j}\big) + \frac{1}{2}J_{g,i-1/2,j}h_i^x = 0\,, \tag{2.17}$$

$$D_{g,i,j}\big(\phi_{g,i,j} - \phi_{g,i,j-1/2}\big) + \frac{1}{2}J_{g,i,j-1/2}h_j^y = 0\,, \tag{2.18}$$

$$D_{g,i,j}\big(\phi_{g,i,j+1/2} - \phi_{g,i,j}\big) + \frac{1}{2}J_{g,i,j+1/2}h_j^y = 0\,, \tag{2.19}$$

where $\phi_{g,i+1/2,j}$ and $\phi_{g,i,j+1/2}$ are the face-average group scalar fluxes, and $D_{g,i,j} = \frac{1}{3\Sigma_{t,g,i,j}}$. Eliminating the face-average scalar fluxes in Eqs. (2.16)-(2.19), we get the following relations between the face-average currents and cell-average scalar fluxes

$$J_{g,i+1/2,j} = -\frac{D_{g,i+1/2,j}}{h_{i+1/2}^x}\big(\phi_{g,i+1,j} - \phi_{g,i,j}\big)\,, \tag{2.20}$$

$$J_{g,i,j+1/2} = -\frac{D_{g,i,j+1/2}}{h_{j+1/2}^y}\big(\phi_{g,i,j+1} - \phi_{g,i,j}\big)\,, \tag{2.21}$$

$$h^x_{i+1/2} = \frac{1}{2}(h^x_i + h^x_{i+1})\,, \quad h^y_{j+1/2} = \frac{1}{2}(h^y_j + h^y_{j+1})\,, \tag{2.22}$$

where the cell-face diffusion coefficients are given by

$$D_{g,i+1/2,j} = \frac{2D_{g,i,j}D_{g,i+1,j}h^x_{i+1/2}}{D_{g,i,j}h^x_{i+1} + D_{g,i+1,j}h^x_i}\,, \quad D_{g,i,j+1/2} = \frac{2D_{g,i,j}D_{g,i,j+1}h^y_{j+1/2}}{D_{g,i,j}h^y_{j+1} + D_{g,i,j+1}h^y_j}\,. \tag{2.23}$$

Substituting Eqs. (2.20) and (2.21) into the cell-balance equation (2.14), we obtain the discretized group diffusion equations for the cell-average group scalar fluxes $\phi_{g,i,j}$ on the given fine grid Λ_E of the following form:

$$\begin{aligned}
&-\left[\frac{D_{g,i+1/2,j}}{h^x_{i+1/2}}\big(\phi_{g,i+1,j}-\phi_{g,i,j}\big) - \frac{D_{g,i-1/2,j}}{h^x_{i-1/2}}\big(\phi_{g,i,j}-\phi_{g,i-1,j}\big)\right]h^y_j \\
&\quad -\left[\frac{D_{g,i,j+1/2}}{h^y_{j+1/2}}\big(\phi_{g,i,j+1}-\phi_{g,i,j}\big) - \frac{D_{g,i,j-1/2}}{h^y_{j-1/2}}\big(\phi_{g,i,j}-\phi_{g,i,j-1}\big)\right]h^x_i + \Sigma_{t,g,i,j}\phi_{g,i,j}A_{i,j} = \\
&\qquad A_{i,j}\sum_{g'=1}^{G}\Sigma_{s,g'\to g,i,j}\phi_{g',i,j} + \frac{1}{k}A_{i,j}\chi_{g,i,j}\sum_{g'=1}^{G}\nu_{f,g',i,j}\Sigma_{f,g',i,j}\phi_{g',i,j}\,.
\end{aligned} \tag{2.24}$$

The first two terms on the left-hand side of Eq. (2.24) define the discrete LRD term of the applied FV scheme.

The discrete group diffusion equations on the grid Λ^γ_E are formulated to be algebraically consistent with the equations on the grid $\Lambda^{\gamma-1}_E$. The homogenization of the equations over energy intervals is performed without any approximation. To derive the diffusion equations on the hierarchy of grids, we start by formulating discrete equations on Λ^2_E and sum the equations (2.24) on Λ^1_E over g-th interval of the grid Λ^2_E. The LRD term in Eq. (2.24) is summed over ω^2_g and cast in terms of $\phi^2_{g,i,j}$ in the following way:

$$\begin{aligned}
&-\frac{h^y_j}{h^x_{i+1/2}}\sum_{g\in\omega^2_p}D_{g,i+1/2,j}\big(\phi_{g,i+1,j}-\phi_{g,i,j}\big) + \frac{h^y_j}{h^x_{i-1/2}}\sum_{g\in\omega^2_p}D_{g,i-1/2,j}\big(\phi_{g,i,j}-\phi_{g,i-1,j}\big) \\
&\quad -\frac{h^x_i}{h^y_{j+1/2}}\sum_{g\in\omega^2_p}D_{g,i,j+1/2}\big(\phi_{g,i,j+1}-\phi_{g,i,j}\big) + \frac{h^x_i}{h^y_{j-1/2}}\sum_{g\in\omega^2_p}D_{g,i,j-1/2}\big(\phi_{g,i,j}-\phi_{g,i,j-1}\big) = \\
&-\frac{h^y_j}{h^x_{i+1/2}}\Big(\bar{D}^{+,2}_{g,i+1/2,j}\phi^2_{g,i+1,j} - \bar{D}^{-,2}_{g,i+1/2,j}\phi^2_{g,i,j}\Big) + \frac{h^y_j}{h^x_{i-1/2}}\Big(\bar{D}^{+,2}_{g,i-1/2,j}\phi^2_{g,i,j} - \bar{D}^{-,2}_{g,i-1/2,j}\phi^2_{g,i-1,j}\Big) \\
&\qquad -\frac{h^x_i}{h^y_{j+1/2}}\Big(\bar{D}^{+,2}_{g,i,j+1/2}\phi^2_{g,i,j+1} - \bar{D}^{-,2}_{g,i,j+1/2}\phi^2_{g,i,j}\Big) \\
&\qquad\quad +\frac{h^x_i}{h^y_{j-1/2}}\Big(\bar{D}^{+,2}_{g,i,j-1/2}\phi_{g,i,j} - \bar{D}^{-,2}_{g,i,j-1/2}\phi_{g,i,j-1}\Big)
\end{aligned} \tag{2.25}$$

where we defined the cell-face diffusion coefficients on the grid Λ_E^2

$$\bar{D}^{+,2}_{g,i+1/2,j} = \frac{\sum_{g\in\omega_g^2} D_{g,i+1/2,j}\phi_{g,i+1,j}}{\sum_{g\in\omega_g^2}\phi_{g,i+1,j}}, \quad \bar{D}^{-,2}_{g,i+1/2,j} = \frac{\sum_{g\in\omega_g^2} D_{g,i+1/2,j}\phi_{g,i,j}}{\sum_{g\in\omega_g^2}\phi_{g,i,j}}, \tag{2.26}$$

$$\bar{D}^{+,2}_{g,i,j+1/2} = \frac{\sum_{g\in\omega_g^2} D_{g,i,j+1/2}\phi_{g,i,j+1}}{\sum_{g\in\omega_g^2}\phi_{g,i,j+1}}, \quad \bar{D}^{-,2}_{g,i,j+1/2} = \frac{\sum_{g\in\omega_g^2} D_{g,i,j+1/2}\phi_{g,i,j}}{\sum_{g\in\omega_g^2}\phi_{g,i,j}}. \tag{2.27}$$

It can be shown by mathematical induction that the general form of the discrete LRD term on any coarse grid Λ_E^γ ($\gamma > 1$) has the form of the discretized LRD term on Λ_E^2. It is given by

$$\begin{aligned}\mathcal{L}^\gamma_{g,i,j}\phi^\gamma_g \equiv &-\frac{h^y_j}{h^x_{i+1/2}}\big(\bar{D}^{+,\gamma}_{g,i+1/2,j}\phi^\gamma_{g,i+1,j} - \bar{D}^{-,\gamma}_{g,i+1/2,j}\phi^\gamma_{g,i,j}\big)\\ &+\frac{h^y_j}{h^x_{i-1/2}}\big(\bar{D}^{+,\gamma}_{g,i-1/2,j}\phi^\gamma_{g,i,j} - \bar{D}^{-,\gamma}_{g,i-1/2,j}\phi^\gamma_{g,i-1,j}\big) - \frac{h^x_i}{h^y_{j+1/2}}\big(\bar{D}^{+,\gamma}_{g,i,j+1/2}\phi^\gamma_{g,i,j+1} - \bar{D}^{-,\gamma}_{g,i,j+1/2}\phi^\gamma_{g,i,j}\big)\\ &+\frac{h^x_i}{h^y_{j-1/2}}\big(\bar{D}^{+,\gamma}_{g,i,j-1/2}\phi_{g,i,j} - \bar{D}^{-,\gamma}_{g,i,j-1/2}\phi_{g,i,j-1}\big),\end{aligned} \tag{2.28}$$

where cell-face diffusion coefficients on Λ_E^γ are calculated by the solution of the previous grid as follows:

$$\bar{D}^{+,\gamma}_{g,i+1/2,j} = \frac{\sum_{g'\in\omega_g^\gamma}\bar{D}^{+,\gamma-1}_{g',i+1/2,j}\phi^{\gamma-1}_{g',i+1,j}}{\sum_{g'\in\omega_g^\gamma}\phi^{\gamma-1}_{g',i+1,j}}, \ \bar{D}^{-,\gamma}_{g,i+1/2,j} = \frac{\sum_{g'\in\omega_g^\gamma}\bar{D}^{-,\gamma-1}_{g',i+1/2,j}\phi^{\gamma-1}_{g',i,j}}{\sum_{g'\in\omega_g^\gamma}\phi^{\gamma-1}_{g',i,j}}, \tag{2.29a}$$

$$\bar{D}^{+,\gamma}_{g,i,j+1/2} = \frac{\sum_{g'\in\omega_g^\gamma}\bar{D}^{+,\gamma-1}_{g',i,j+1/2}\phi^{\gamma-1}_{g',i,j+1}}{\sum_{g'\in\omega_g^\gamma}\phi^{\gamma-1}_{g',i,j+1}}, \ \bar{D}^{-,\gamma}_{g,i,j+1/2} = \frac{\sum_{g'\in\omega_g^\gamma}\bar{D}^{-,\gamma-1}_{g',i,j+1/2}\phi^{\gamma-1}_{g',i,j}}{\sum_{g'\in\omega_g^\gamma}\phi^{\gamma-1}_{g',i,j}}, \tag{2.29b}$$

where

$$\bar{D}^{+,1}_{g,i+1/2,j} = \bar{D}^{-,1}_{g,i+1/2,j} = D_{g,i+1/2,j} \quad \bar{D}^{+,1}_{g,i,j+1/2} = \bar{D}^{-,1}_{g,i,j+1/2} = D_{g,i,j+1/2}. \tag{2.29c}$$

We note that this homogenization in energy on a coarse energy grid yields two diffusion coefficients at each face.

The final discrete form of the group diffusion equations (2.5) and (2.6) on the hierarchy of grids is the following:

$$\begin{aligned}&\mathcal{L}^\gamma_{g,i,j}\phi^\gamma_g + \bar{\Sigma}^\gamma_{t,g,i,j}\phi^\gamma_{g,i,j}A_{i,j} =\\ &\qquad A_{i,j}\sum_{g'=1}^{G}\bar{\Sigma}^\gamma_{s,g'\to g,i,j}\phi^\gamma_{g',i,j} + \frac{1}{k}\bar{\chi}^\gamma_{g,i,j}A_{i,j}\sum_{g'=1}^{G}\overline{\nu\Sigma}^\gamma_{f,g',i,j}\phi^\gamma_{g',i,j},\end{aligned} \tag{2.30}$$

$$g = 1, \ldots, G^\gamma\,, \quad \gamma = 1, \ldots, \Gamma - 1\,,$$

$$\mathcal{L}^\Gamma_{1,i,j}\phi^\Gamma_1 + \bar{\Sigma}^\Gamma_{a,1,i,j}\phi^\Gamma_{1,i,j}A_{i,j} = \frac{1}{k}A_{i,j}\overline{\nu\Sigma}^\Gamma_{f,1,i,j}\phi^\Gamma_{1,i,j}\,. \tag{2.31}$$

The cross sections and other material properties are defined according to Eqs. (2.7a)-(2.7c) by their cell-average values, for example,

$$\bar{\Sigma}^\gamma_{t,g,i,j} = \frac{\sum_{g'\in\omega^\gamma_g}\bar{\Sigma}^{\gamma-1}_{t,g',i,j}\phi^{\gamma-1}_{g',i,j}}{\sum_{g'\in\omega^\gamma_g}\phi^{\gamma-1}_{g',i,j}}\,. \tag{2.32}$$

2.2 Multigrid Cycles

To solve the multilevel system of group diffusion equations (2.30) and (2.31) on the hierarchy of grids in energy, we apply multigrid algorithms with different types of cycles. We use partial V-cycles pV-Γ which are described in Algorithm 1 and shown in Figure 2.1. The pV-Γ algorithm

$\boldsymbol{\phi}^0 \equiv \boldsymbol{\phi}^1$
for $\gamma \leftarrow 1$ *to* $\Gamma - 1$ **do**
  Solve $\boldsymbol{\phi}^\gamma = \mathcal{A}^{-1}_\gamma\mathcal{B}_\gamma\boldsymbol{\phi}^{\gamma-1} + \frac{1}{k}\mathcal{A}^{-1}_\gamma\mathcal{C}_\gamma\boldsymbol{\phi}^{\gamma-1}$
  Perform homogenization in energy to form $\mathcal{A}_{\gamma+1}$, $\mathcal{B}_{\gamma+1}$, $\mathcal{C}_{\gamma+1}$
end
Solve the eigenvalue problem $\mathcal{C}^{-1}_\Gamma\mathcal{A}_\Gamma\boldsymbol{\phi}^\Gamma = k\boldsymbol{\phi}^\Gamma$ to update k and $\boldsymbol{\phi}^\Gamma$
for $\gamma \leftarrow \Gamma - 1$ *to 1* **do**
  Perform prolongation $\boldsymbol{\phi}^\gamma \leftarrow I^{\gamma\leftarrow\gamma+1}_\alpha\boldsymbol{\phi}^{\gamma+1}$
end

Algorithm 1: pV-Γ. The multigrid algorithm with the partial V-cycle.

starts from the given fine energy grid Λ^1_E and moves through the hierarchy of grids. On each grid we solve a fixed-source multigroup problem using the eigenvalue estimated by the solution on the coarsest grid Λ^Γ_E on the previous multigrid cycle. The group diffusion equations on Λ^Γ_E for $\gamma < \Gamma$ are solved by means of just one Gauss-Seidel iteration over energy groups. Thus, there is only one relaxation step in energy. To solve the diffusion equation in the spatial domain in each group we use BiCGSTAB with the LU preconditioner. The eigenvalue and associated eigenfunction are updated on the grid Λ^Γ_E. The obtained estimation of k is then used on all grids Λ^γ_E for $\gamma < \Gamma$ on the next multigrid cycle. The effective one-group eigenvalue problem on Λ^Γ_E is solved with one Newton iteration that treats it as a generalized eigenvalue problem. On the first multigrid cycle we perform two Newton iterations on Λ^Γ_E to get better estimation of the k-eigenvalue at the initial phase of iterations.

The pV-Γ algorithm moves from the coarsest grid Λ_E^Γ towards the finest grid Λ_E^1 without solving group diffusion equations on any grid. This is shown on the cycle graphs by open circles. The prolongation procedure between grids uses one of versions of the interpolation operator $I_\alpha^{\gamma\leftarrow\gamma+1}$ described in Sec. 2.3. The subscript α indicates the type of interpolation

- $\alpha = ce$: the correction factor based on constant approximation in energy,
- $\alpha = le$: the correction factor based on linear approximation in energy,
- $\alpha = lef$: the correction factor based on linear approximation in energy with factorization.

Figure 2.1 shows various multigrid cycles. The partial V-cycle can be viewed as \-cycle. Another kind of multigrid algorithm uses nested iterations involving coarse grids. It can be interpreted as a partial W-cycle. Algorithm 2 presents the pW-$\Gamma(\gamma^*,\mu)$ algorithm, where the nested multigrid cycles start from the grid $\Lambda_E^{\gamma^*}$ and are executed μ times. Figure 2.1c illustrates the pW-3(2,1)

$\boldsymbol{\phi}^0 \equiv \boldsymbol{\phi}^1$
for $\gamma \leftarrow 1$ *to* $\Gamma - 1$ **do**
  Solve $\boldsymbol{\phi}^\gamma = \mathcal{A}_\gamma^{-1}\mathcal{B}_\gamma\boldsymbol{\phi}^{\gamma-1} + \frac{1}{k}\mathcal{A}_\gamma^{-1}\mathcal{C}_\gamma\boldsymbol{\phi}^{\gamma-1}$
  Perform homogenization in energy to form $\mathcal{A}_{\gamma+1}$, $\mathcal{B}_{\gamma+1}$, $\mathcal{C}_{\gamma+1}$
end
Solve the eigenvalue problem $\mathcal{C}_\Gamma^{-1}\mathcal{A}_\Gamma\boldsymbol{\phi}^\Gamma = k\boldsymbol{\phi}^\Gamma$ to update k and $\boldsymbol{\phi}^\Gamma$
for $m \leftarrow 1$ *to* μ **do**
  for $\gamma \leftarrow \Gamma - 1$ *to* γ^* **do**
    Perform prolongation $\boldsymbol{\phi}^\gamma \leftarrow I_\alpha^{\gamma\leftarrow\gamma+1}\boldsymbol{\phi}^{\gamma+1}$
  end
  for $\gamma \leftarrow \gamma^*$ *to* $\Gamma - 1$ **do**
    Solve $\boldsymbol{\phi}^\gamma = \mathcal{A}_\gamma^{-1}\mathcal{B}_\gamma\boldsymbol{\phi}^{\gamma-1} + \frac{1}{k}\mathcal{A}_\gamma^{-1}\mathcal{C}_\gamma\boldsymbol{\phi}^{\gamma-1}$
    Perform homogenization in energy to form $\mathcal{A}_{\gamma+1}$, $\mathcal{B}_{\gamma+1}$, $\mathcal{C}_{\gamma+1}$
  end
  Solve the eigenvalue problem $\mathcal{C}_\Gamma^{-1}\mathcal{A}_\Gamma\boldsymbol{\phi}^\Gamma = k\boldsymbol{\phi}^\Gamma$ to update k and $\boldsymbol{\phi}^\Gamma$
end
for $\gamma \leftarrow \Gamma - 1$ *to 1* **do**
  Perform prolongation $\boldsymbol{\phi}^\gamma \leftarrow I_\alpha^{\gamma\leftarrow\gamma+1}\boldsymbol{\phi}^{\gamma+1}$
end

Algorithm 2: pW-$\Gamma(\gamma^*,\mu)$. The multigrid algorithm with the partial W-cycle.

algorithm.

An important characteristic of a multigrid algorithm is the number of cycles (N_c) that it needs to achieve convergence. It is related to the ability of the algorithm to reduce the error over

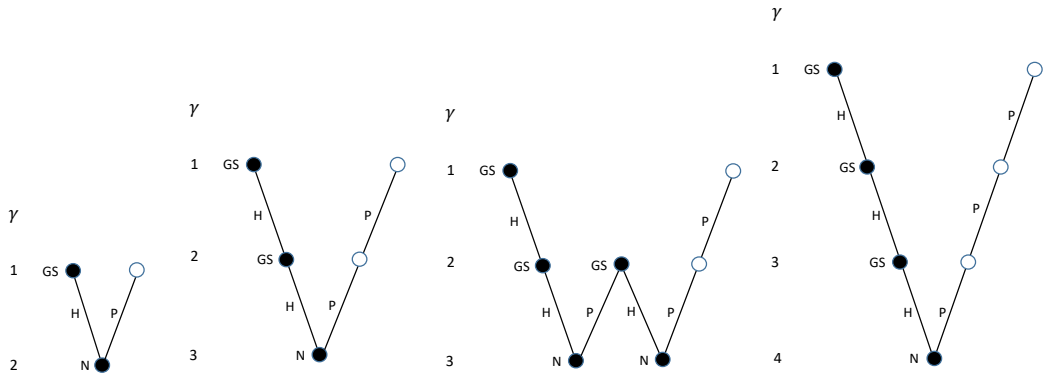

(a) pV-2 (b) pV-3 (c) pW-3(2,1) (d) pV-4

Figure 2.1: Multigrid cycles for the hierarchies of grids with Γ=2,...,4. GS - Gauss-Seidel iteration over groups on Λ_E^γ, H - homogenization over energy, N - Newton iteration, P - prolongation

a cycle. However, the cost of each cycle affects the algorithm efficiency. It varies for different algorithms. The optimum algorithm for a test is the one which requires the minimum total number of diffusion solves (N_{ds}). For the given numbers of cycles and groups in each grids, the total number of diffusion solves can be calculated as

$$N_{ds} = N_c \sum_{\gamma=1}^{\Gamma} G^\gamma + 1 \tag{2.33}$$

for the pV-Γ algorithm and

$$N_{ds} = N_c \Big(\sum_{\gamma=1}^{\Gamma} G^\gamma + \mu \sum_{\gamma=\gamma^*}^{\Gamma} G^\gamma \Big) + 1 \tag{2.34}$$

for the pW-$\Gamma(\gamma^*, \mu)$ algorithm.

2.3 Prolongation Operators

2.3.1 Prolongation with Recursive Correction

We formulate prolongation operators as an interpolation procedure based on a multiplicative correction of the solution. The corrected group scalar flux $\hat{\phi}_g^\gamma$ on the grid Λ_E^γ is defined as the product of the solution on this grid from the current multigrid iteration cycle ϕ_g^γ and the

correction factor $\mathfrak{f}_{g'}^{\gamma+1}$ computed using solutions on two neighbouring energy grids Λ_E^{γ} and $\Lambda_E^{\gamma+1}$

$$\hat{\phi}_g^{\gamma}(\vec{r}) = \phi_g^{\gamma}(\vec{r})\mathfrak{f}_{\alpha,g'}^{\gamma+1}(\vec{r})\,, \quad g \in \omega_{g'}^{\gamma+1}\,. \tag{2.35}$$

The interpolation procedure performs recursive calculation of factors and solution correction on each grid according to Algorithm 3, where $\gamma^* = 1$ for the pV-Γ cycle. In this algorithm, the correction factor generally depends on the corrected solutions on coarser grids

$$\mathfrak{f}_{\alpha,g'}^{\gamma+1} = \mathfrak{f}_{\alpha,g'}^{\gamma+1}\left[\phi^{\gamma}, \hat{\phi}^{\gamma+1}, \ldots, \hat{\phi}^{\Gamma-1}, \phi^{\Gamma}\right], \tag{2.36}$$

and hence on the corresponding factors. Hereafter we refer to this type of operator as the prolongation operator with recursive correction factors (RCF).

for $\gamma \leftarrow \Gamma - 1$ *to* γ^* **do**
  Compute correction factors $\mathfrak{f}_{\alpha,g'}^{\gamma+1}$, $g' = 1, \ldots, G^{\gamma+1}$
  Perform interpolation on the grid Λ_E^{γ} : $\hat{\phi}_g^{\gamma} = \phi_g^{\gamma}\,\mathfrak{f}_{\alpha,g'}^{\gamma+1}$, $g \in \omega_{g'}^{\gamma+1}$, $g = 1, \ldots, G^{\gamma}$
end

Algorithm 3: Prolongation operator $I_{\alpha}^{\gamma \leftarrow \gamma+1}$ with recursive correction factors

2.3.2 Prolongation Operator with Constant Approximation in Energy

The prolongation operators use different definitions of correction factors. The first variant of the prolongation operator is based on a group-local factor associated with the coarse grid $\Lambda_E^{\gamma+1}$ that involves only one energy interval on this grid. It uses constant approximation of the solution over the energy interval $\delta\mathcal{E}_g^{\gamma+1}$ and is formulated as follows:

$$\mathfrak{f}_{ce,g}^{\gamma+1}(\mathbf{r}) = \frac{\hat{\phi}_g^{\gamma+1}(\mathbf{r})}{\sum_{g' \in \omega_g^{\gamma}} \phi_{g'}^{\gamma}(\mathbf{r})}\,, \quad g = 1, \ldots, G^{\gamma+1}\,. \tag{2.37}$$

This defines the operator $I_{ce}^{\gamma \leftarrow \gamma+1}$ that is referred to as the prolongation operator with constant approximation in energy. It can be shown that application of the factor (3.28) recursively according to Algorithm 3 is equivalent to the following factorization form of the operator $I_{ce}^{\gamma \leftarrow \gamma+1}$:

$$\hat{\phi}_g^{\gamma} = \phi_g^{\gamma}\,\tilde{\mathfrak{f}}_{ce,g'}^{\gamma+1}\,\tilde{\mathfrak{f}}_{ce,g''}^{\gamma+2} \cdots \tilde{\mathfrak{f}}_{ce,1}^{\Gamma} \quad \text{for } g \in \omega_{g'}^{\gamma+1},\ g' \in \omega_{g''}^{\gamma+2} \text{ etc}\,, \tag{2.38}$$

where

$$\tilde{\mathfrak{f}}_{ce,g}^{\gamma+1}(\mathbf{r}) = \frac{\phi_g^{\gamma+1}(\mathbf{r})}{\sum_{g'\in\omega_g^\gamma}\phi_{g'}^{\gamma}(\mathbf{r})}\,, \quad g = 1,\ldots,G^{\gamma+1}\,. \tag{2.39}$$

Thus, the group scalar flux on the grid Λ_E^γ is corrected by the product of the factors (3.30) computed by the solutions on coarser grids from the current multigrid cycle.

2.3.3 Prolongation Operator with Linear Approximation in Energy

We now formulate the correction factor based on the linear approximation in energy using the solution over two energy intervals of $\Lambda_E^{\gamma+1}$. The scalar flux on the grid Λ_E^γ over intervals g and $g+1$ of the grid $\Lambda_E^{\gamma+1}$ approximated by its group-average values can be cast as follows:

$$\Phi_{g,\gamma+1}^{\gamma}(\mathbf{r},E) = \sum_{g'\in\omega_g^{\gamma+1}\cup\omega_{g+1}^{\gamma+1}} \frac{\phi_{g'}^{\gamma}(\mathbf{r})}{\Delta E_{g'}^{\gamma}}\Big(H(E-E_{g'}^{\gamma}) - H(E-E_{g'-1}^{\gamma})\Big)\,,$$

$$E\in\delta\mathcal{E}_{g+1}^{\gamma+1}\cup\delta\mathcal{E}_g^{\gamma+1}, \tag{2.40}$$

$$\Delta E_{g'}^{\gamma} = E_{g'-1}^{\gamma} - E_{g'}^{\gamma}\,, \tag{2.41}$$

where H is the Heaviside step function

$$H(x) = \begin{cases} 0 & x<0 \\ \frac{1}{2} & x=0 \\ 1 & x>0 \end{cases}\,. \tag{2.42}$$

The updated scalar flux on the grid Λ_E^γ is defined by the following interpolation function:

$$\hat{\Phi}_g^{\gamma\leftarrow\gamma+1}(\mathbf{r},E) = \Phi_{g,\gamma+1}^{\gamma}(\mathbf{r},E)F_g^{\gamma+1}(\mathbf{r},E) \quad \text{for} \quad E\in\delta\mathcal{E}_{g+1}^{\gamma+1}\cup\delta\mathcal{E}_g^{\gamma+1}\,, \tag{2.43}$$

where the factor $F_p^{\gamma+1}$ is the linear function in energy given by

$$F_g^{\gamma+1}(E) = \bar{F}_{E,g}^{\gamma+1} + \frac{2}{\Delta E_g^{\gamma+1}+\Delta E_{g+1}^{\gamma+1}}\Big(E-\bar{E}_g^{\gamma+1}\Big)\tilde{F}_{E,g}^{\gamma+1}\,, \tag{2.44}$$

$$\Delta E_g^{\gamma+1} = E_{g-1}^{\gamma+1} - E_g^{\gamma+1}\,, \quad \bar{E}_g^{\gamma+1} = \frac{1}{2}\Big(E_{g-1}^{\gamma+1}+E_{g+1}^{\gamma+1}\Big)\,. \tag{2.45}$$

The coefficients $\bar{F}_{E,g}^{\gamma+1}$ and $\tilde{F}_{E,g}^{\gamma+1}$ are determined by means of the solution on the grid $\Lambda_E^{\gamma+1}$ from the following conditions:

$$\int_{\delta\mathcal{E}_g^{\gamma+1}} \hat{\Phi}_g^{\gamma\leftarrow\gamma+1}(\mathbf{r},E)dE = \hat{\phi}_g^{\gamma+1}(\mathbf{r})\,, \tag{2.46}$$

$$\int_{\delta\mathcal{E}_{g+1}^{\gamma+1}} \hat{\Phi}_g^{\gamma\leftarrow\gamma+1}(\mathbf{r},E)dE = \hat{\phi}_{g+1}^{\gamma+1}(\mathbf{r})\,. \tag{2.47}$$

The corrected scalar flux $\hat{\Phi}_g^{\gamma\leftarrow\gamma+1}(E)$ is used to update the group scalar fluxes on the grid Λ_E^{γ} over just one interval of the grid $\Lambda_E^{\gamma+1}$. We apply it to correct the solution over the interval $\delta\mathcal{E}_{g+1}^{\gamma+1}$ as follows:

$$\hat{\phi}_{g'}^{\gamma}(\mathbf{r}) = \int_{\delta\mathcal{E}_{g'}^{\gamma}} \hat{\Phi}_g^{\gamma\leftarrow\gamma+1}(\mathbf{r},E)dE \quad \text{for} \quad g' \in \omega_{g+1}^{\gamma+1}\,. \tag{2.48}$$

This leads to the multiplicative correction of the solution on the grid Λ_E^{γ} by the solution on the coarser grid $\Lambda_E^{\gamma+1}$ given by

$$\hat{\phi}_{g'}^{\gamma}(\mathbf{r}) = \phi_{g'}^{\gamma}(\mathbf{r})\mathfrak{f}_{le,g'\leftarrow g}^{\gamma+1}(\mathbf{r})\,, \quad g' \in \omega_{g+1}^{\gamma+1}\,, \quad g' = 1,\ldots,G^{\gamma}\,, \tag{2.49}$$

where the correction factor $\mathfrak{f}_{le,g'\leftarrow g}^{\gamma+1}$ is defined as

$$\mathfrak{f}_{le,g'\leftarrow g}^{\gamma+1}(\mathbf{r}) = \frac{1}{\Delta E_{g'}^{\gamma}} \int_{\delta\mathcal{E}_{g'}^{\gamma}} F_g^{\gamma+1}(\mathbf{r},E)dE\,. \tag{2.50}$$

The interpolation procedure (2.49) is applied recursively according to Algorithm 4. This defines the prolongation operator $I_{le}^{\gamma\leftarrow\gamma+1}$. Hereafter we referred to it as the prolongation operator with linear approximation in energy.

for $\gamma \leftarrow \Gamma - 1$ *to* γ^* **do**
  Compute correction factors $\mathfrak{f}_{\alpha,g'\leftarrow g}^{\gamma+1}$, $g' = 1,\ldots,G^{\gamma}$, $g = 1,\ldots,G^{\gamma+1}$
  Perform interpolation on the grid Λ_E^{γ} : $\hat{\phi}_{g'}^{\gamma}(\mathbf{r}) = \phi_{g'}^{\gamma}(\mathbf{r})\mathfrak{f}_{\alpha,g'\leftarrow g}^{\gamma+1}(\mathbf{r})$, $g' \in \omega_{g+1}^{\gamma+1}$
end

Algorithm 4: Prolongation operator $I_{le}^{\gamma\leftarrow\gamma+1}$ with RCF.

The interpolation function (2.43) can also be applied to update group scalar fluxes on the grid Λ_E^{γ} over the interval $\delta\mathcal{E}_g^{\gamma+1}$

$$\hat{\phi}_{g'}^{\gamma}(\mathbf{r}) = \int_{\delta\mathcal{E}_{g'}^{\gamma}} \hat{\Phi}_g^{\gamma\leftarrow\gamma+1}(\mathbf{r},E)dE \quad \text{for} \quad g' \in \omega_{g}^{\gamma+1}\,. \tag{2.51}$$

This mapping is used for $g = 1$. We note that the coarsest grid Λ_E^{Γ} has only one interval. To update the solution on $\Lambda_E^{\Gamma-1}$ we use the group-local factors with constant approximation in energy and hence set

$$\mathfrak{f}_{le,g'\leftarrow g}^{\Gamma}(\mathbf{r}) = \mathfrak{f}_{ce,g}^{\Gamma}(\mathbf{r})\,, \quad g' \in \omega_g^{\Gamma}\,, \tag{2.52}$$

where $g = 1$. If the slope of the correction is large, the interpolated solution $\hat{\Phi}_g^{\gamma\leftarrow\gamma+1}(E)$ can be negative for $E \in \delta\mathcal{E}_{g+1}^{\gamma+1} \cup \delta\mathcal{E}_g^{\gamma+1}$. If this is the case, then we use the correction factor with constant approximation in energy and set

$$\mathfrak{f}_{le,g'\leftarrow g}^{\gamma+1}(\mathbf{r}) = \mathfrak{f}_{ce,g}^{\gamma+1}(\mathbf{r})\,. \tag{2.53}$$

Other slope-limiting techniques can also be applied to the interpolation factor (2.44) to adjust the slope $\tilde{F}_{E,g}^{\gamma+1}$.

2.3.4 Prolongation Operator with Linear Approximation and Factorization

To formulate prolongation operators with non-recursive factors we generalize the factorization form of the operator $I_{ce}^{\gamma\leftarrow\gamma+1}$ and define interpolation with linear approximation as a product of factors

$$\hat{\phi}_g^{\gamma} = \phi_g^{\gamma}\,\tilde{\mathfrak{f}}_{lef,g\leftarrow g'}^{\gamma+1}\,\tilde{\mathfrak{f}}_{lef,g'\leftarrow g''}^{\gamma+2}\cdots\,\tilde{\mathfrak{f}}_{ce,1}^{\Gamma} \tag{2.54}$$

where $g \in \omega_{g'+1}^{\gamma+1}$, $g' \in \omega_{g''+1}^{\gamma+2}$ etc. Here the factors $\tilde{\mathfrak{f}}_{lef,g\leftarrow g'}^{\gamma+1}$ are computed according to the methods described above in Sections 2.3.3 using the grid solutions ϕ^{γ} from the current multigrid cycle. In the case of the linear approximation in energy, the coefficients of $F_{g'}^{\gamma+1}(E)$ (Eq. (2.44)) are determined from the following conditions:

$$\int_{\delta\mathcal{E}_{g'}^{\gamma+1}} \hat{\Phi}_{g'}^{\gamma\leftarrow\gamma+1}(\mathbf{r},E)dE = \phi_{g'}^{\gamma+1}(\mathbf{r})\,, \tag{2.55}$$

$$\int_{\delta\mathcal{E}_{g'+1}^{\gamma+1}} \hat{\Phi}_{g'}^{\gamma\leftarrow\gamma+1}(\mathbf{r},E)dE = \phi_{g'+1}^{\gamma+1}(\mathbf{r})\,. \tag{2.56}$$

We refer to these operators as prolongation operators with factorization. They are described in Algorithm 5

for $\gamma \leftarrow \Gamma$ *to* $\gamma^* + 1$ **do**
  Compute correction factors $\tilde{\mathfrak{f}}_{lef,g\leftarrow g'}^{\gamma}$, $g = 1,\ldots,G^{\gamma}$, $g' = 1,\ldots,G^{\gamma+1}$
end
for $\gamma \leftarrow \Gamma - 1$ *to* γ^* **do**
  Perform interpolation on the grid Λ_E^{γ} : $\hat{\phi}_g^{\gamma} = \phi_g^{\gamma}\,\tilde{\mathfrak{f}}_{lef,g\leftarrow g'}^{\gamma+1}\,\tilde{\mathfrak{f}}_{lef,g'\leftarrow g''}^{\gamma+2}\cdots\,\tilde{\mathfrak{f}}_{ce,1}^{\Gamma}$,
  $g \in \omega_{g'+1}^{\gamma+1}$, $g' \in \omega_{g''+1}^{\gamma+2}$ ...
end

Algorithm 5: Prolongation operator $I_{lef}^{\gamma\leftarrow\gamma+1}$ with factorization.

2.4 Numerical Results

2.4.1 Definition of Tests

To demonstrate performance of the proposed methods we present results of two reactor-physics problems.

- Test A is defined by the checker-board configuration formed by quarters of fuel assemblies. It is shown in Figure 2.2. There are assemblies with two kinds of fuels: (i) UO_2 and (ii) mixed-oxide (MOX). The isotope compositions of model fuels and number densities of nuclides are presented in Tables 2.1 and 2.2. Each type of fuel pins has the same material properties. The fuel lattice pitch is 1.26 cm and the fuel pins have a radius of 1.08 cm. The space between fuel pins is filled with water. All boundaries are reflective. This problem is equivalent to the infinite spatial domain of two full assemblies next to each other.

- Test B (Figure 2.3) consists of the full-size MOX and UO_2 assemblies from Test A with large area of water that models a reflector region. The configuration of this test is shown in Figure 3.3. It is similar to C5G7 benchmark [49]. The left and bottom boundaries are reflective. The top and right boundaries are vacuum.

Both tests are defined using 44-group cross sections from SCALE 6.1 data library [66]. Figure 2.5 demonstrates $\Sigma_{t,g}$, $\nu_{f,g}\Sigma_{f,g}$, and χ_g for three different materials used in the tests. The group data values are plotted versus midpoints of group energy intervals. The scattering matrices $\Sigma_{s,g\to g'}$ are shown in Figure 2.6. The matrix elements are plotted versus the group indices.

Table 2.1: Isotope composition of UO_2 fuel and number densities [10^{24} cm^{-3}].

Nuclide	^{234}U	^{235}U	^{236}U	^{238}U	^{16}O
Density	5.93×10^{-6}	7.04×10^{-4}	3.22×10^{-6}	2.44×10^{-2}	4.62×10^{-2}

Table 2.2: Isotope composition of MOX fuel and number densities [10^{24} cm^{-3}].

Nuclide	^{234}U	^{235}U	^{238}U	^{238}Pu	^{239}Pu
Density	2.60×10^{-7}	5.43×10^{-5}	2.14×10^{-2}	4.66×10^{-5}	1.02×10^{-3}
Nuclide	^{240}Pu	^{241}Pu	^{242}Pu	^{16}O	
Density	4.83×10^{-4}	1.75×10^{-4}	1.32×10^{-4}	4.66×10^{-2}	

The spatial meshes for both problems are uniform. The cells are 0.09cm×0.09cm. The geometry and mesh of a pin cell are displayed in Figure 2.4. The convergence criteria for the

eigenvalue and associated eigenfunction on the given fine energy grid are

$$||\phi^{(s)} - \phi^{(s-1)}||_\infty \leq \varepsilon_\phi ||\phi^{(s)}||_\infty \,, \tag{2.57}$$

$$\left| k^{(s)} - k^{(s-1)} \right| \leq \varepsilon_k k^{(s)} \,, \tag{2.58}$$

where

$$||f||_\infty = \max_{i,j,g} |f_{g,i,j}| \,, \tag{2.59}$$

i and j span the spatial mesh, $g = 1, \ldots, G$, s is the index of the multigrid iteration cycle. The parameters of convergence criteria are ε_k=10^{-6} and ε_ϕ=10^{-6}. The calculated multiplication factors are (i) $k_{eff} = 1.0761$ in Test A and (ii) $k_{eff} = 1.0455$ in Test B.

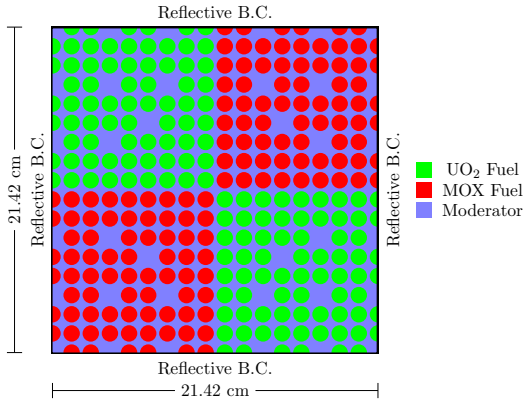

Figure 2.2: Geometry and configuration of test problem A.

Coarsening of energy grids is evaluated by the coupling of the equations between energy groups. This is done by analyzing the cross section data. There are two factors in the coupling, scattering and fission production. The group low-order equations (1.19) are coupled though the right-hand side that has the following form:

$$\mathcal{R}\boldsymbol{\phi}^1 = \mathcal{B}_1\boldsymbol{\phi}^1 + \frac{1}{k}\mathcal{C}_1\boldsymbol{\phi}^1 \,, \tag{2.60}$$

where $\mathcal{B}_1$ and $\mathcal{C}_1$ are defined by Eq. (2.11). The operator $\mathcal{R}$ accounts for scattering and fission neutron-nuclide reactions. At a spatial position, the operator $\mathcal{R}$ is defined by the matrix

$$R_{g,g'} = \Sigma_{s,g'\to g} + \frac{1}{k}\chi_g \nu_{f,g'} \Sigma_{f,g'} \,. \tag{2.61}$$

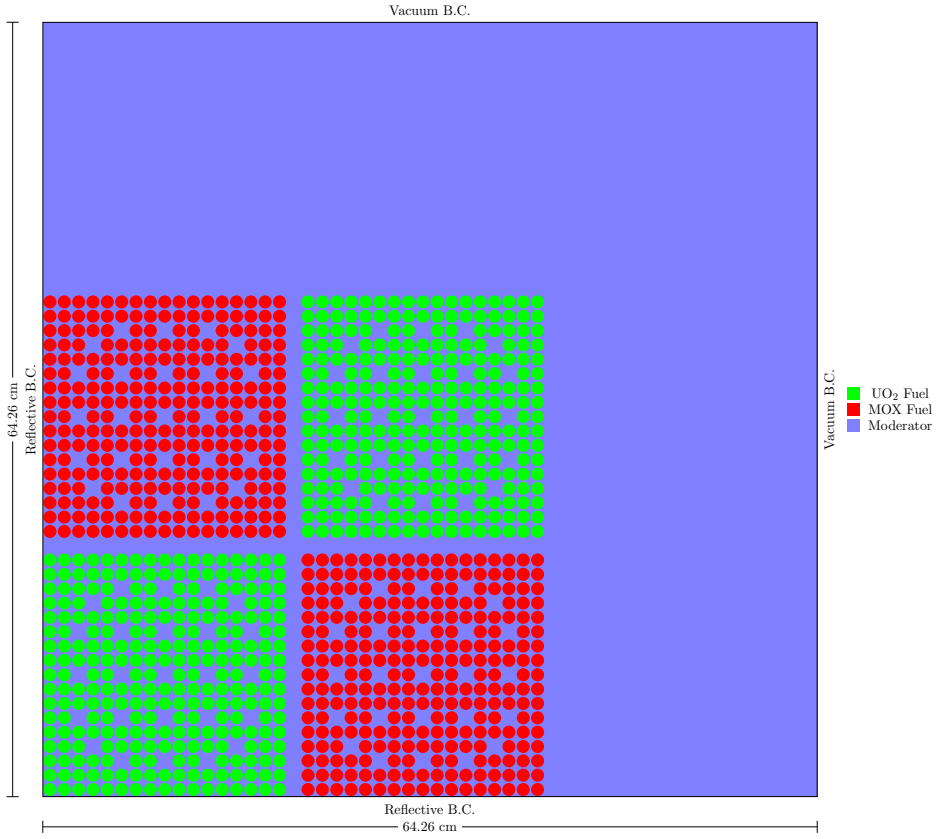

Figure 2.3: Geometry and configuration of test problem B.

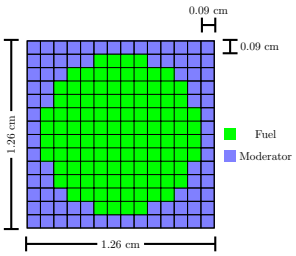

Figure 2.4: Pin-cell grid.

The strength of group connection can be measured by

$$\tilde{R}_{g,g'} = \frac{R_{g,g'}}{\max\limits_{m \neq g}\{R_{g,m}\}} \tag{2.62}$$

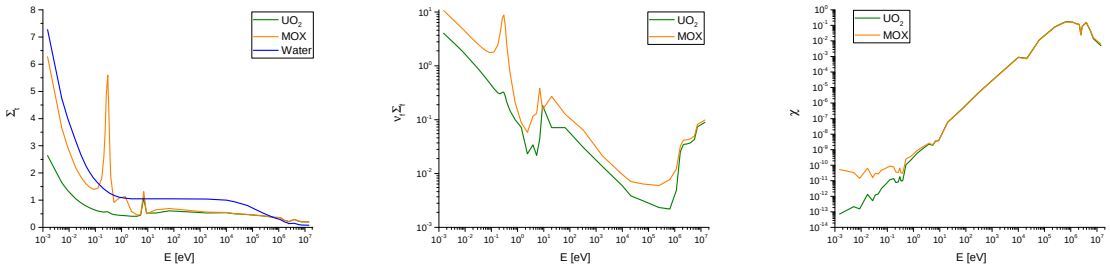

(a) $\Sigma_{t,g}$ (b) $\nu_{f,g}\Sigma_{f,g}$ (c) χ_g

Figure 2.5: The 44-group neutron cross section data generated with SCALE 6.1 data library [66].

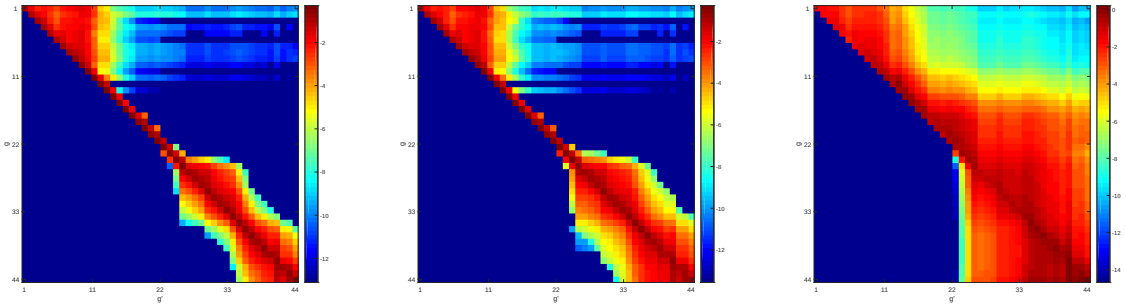

(a) UO_2 (b) MOX (c) Water

Figure 2.6: $\log(\Sigma_{s,g\to g'})$.

where $\tilde{R}_{g,g} = 0$ [67, 74]. The larger $\tilde{R}_{g,g'}$ the stronger solution in the group g is connected to the solution in the group g'. This characterizes the influence of $\phi_{g'}$ on ϕ_g. If $\tilde{R}_{g,g'}$ is small then ϕ_g is weakly coupled with $\phi_{g'}$. The measures of group connections for UO_2, MOX, and water are shown in Figure 2.7. They are calculated for $k = 1$.

2.4.2 Analysis of Results on Hierarchies of Nested Grids in Energy

Different types of hierarchies of grids in energy are applied to solve the tests. First, we use the hierarchies of nested grids which resolve both fast and thermal energies. They are formed by successive coarsening of grids and combining two or three neighboring energy intervals. These

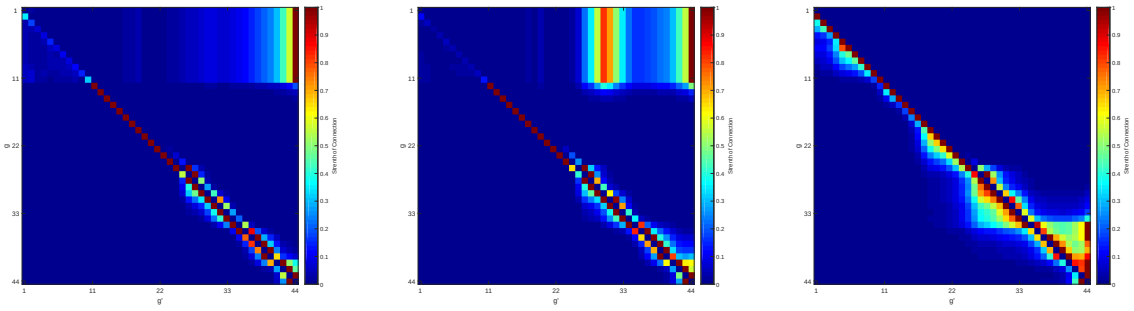

(a) UO_2 (b) MOX (c) Water

Figure 2.7: Measure of strength of group connection, $\tilde{R}_{g,g'}$.

sets of grids are built of the following nested coarse energy grids:

- $\Lambda_{E,22}$: 22 groups consisting of 11 fast and 11 thermal,
- $\Lambda_{E,8}$: 8 groups with 4 fast and 4 thermal,
- $\Lambda_{E,4}$: 4 groups with 2 fast and 2 thermal,
- $\Lambda_{E,2}$: 2 groups corresponding to fast and thermal energies.

The boundaries of energy intervals for the original 44-group data library of SCALE 6.1 and nested coarse grids are shown in Tables 2.3-2.5. Each interval of the 22-group grid $\Lambda_{E,22}$ combines two intervals of the 44-group grid. The $\Lambda_{E,8}$ grid is nested in the $\Lambda_{E,22}$ grid etc. Figure 2.8 illustrates the structure of these nested grids in energy. We use the following hierarchies of these grids: {44,2,1}, {44,4,1}, {44,8,1}, {44,22,1}, {44,8,2,1}, {44,22,4,1}, {44,8,4,2,1}, {44,22,8,2,1}, and
{44,22,8,4,2,1}.

Table 2.6 presents the results from Test A solved by means of multigrid algorithms with different prolongation operators using RCF on hierarchies of grids with $\Gamma = 3, \ldots, 6$. We also provide the data for the two-grid algorithm. This table shows the numbers of cycles N_c and diffusion solves N_{ds} (Eqs. (3.33) and (3.34)). A similar collection of results for Test B is presented in Tables 2.7.

Table 2.3: Boundaries of energy intervals E_g in eV of the 44-group data library of SCALE 6.1.

$i\backslash j^*$	0	1	2	3	4	5	6	7	8	9
0	$2.\times10^{7}$	8.1873×10^{6}	6.434×10^{6}	4.8×10^{6}	$3.\times10^{6}$	2.479×10^{6}	2.354×10^{6}	1.85×10^{6}	1.4×10^{6}	$9.\times10^{5}$
10	$4.\times10^{5}$	$1.\times10^{5}$	2.5×10^{4}	1.7×10^{4}	$3.\times10^{3}$	5.5×10^{2}	$1.\times10^{2}$	$3.\times10^{1}$	$1.\times10^{1}$	8.1
20	6.	4.75	3.	1.77	1.	6.25×10^{-1}	$4.\times10^{-1}$	3.75×10^{-1}	3.5×10^{-1}	3.25×10^{-1}
30	2.75×10^{-1}	2.5×10^{-1}	2.25×10^{-1}	$2.\times10^{-1}$	1.5×10^{-1}	$1.\times10^{-1}$	$7.\times10^{-2}$	$5.\times10^{-2}$	$4.\times10^{-2}$	$3.\times10^{-2}$
40	2.53×10^{-2}	$1.\times10^{-2}$	7.5×10^{-3}	$3.\times10^{-3}$	$1.\times10^{-5}$					

$^*g = i + j$

Table 2.4: Boundaries of energy intervals E_g in eV of the 22-group energy grid $\Lambda_{E,22}$.

$i\backslash j^*$	0	1	2	3	4	5	6	7	8	9
0	$2.\times10^{7}$	6.434×10^{6}	$3.\times10^{6}$	2.354×10^{6}	1.4×10^{6}	$4.\times10^{5}$	2.5×10^{4}	$3.\times10^{3}$	$1.\times10^{2}$	$1.\times10^{1}$
10	6.	3.	1.	$4.\times10^{-1}$	3.5×10^{-1}	2.75×10^{-1}	2.25×10^{-1}	1.5×10^{-1}	$7.\times10^{-2}$	$4.\times10^{-2}$
20	2.53×10^{-2}	7.5×10^{-3}	$1.\times10^{-5}$							

$^*g = i + j$

Table 2.5: Boundaries of energy intervals E_g in eV of the nested energy grids $\Lambda_{E,8}$, $\Lambda_{E,4}$, and $\Lambda_{E,2}$.

g	0	1	2	3	4	5	6	7	8
$\Lambda_{E,8}$	$2.\times10^{7}$	2.354×10^{6}	2.5×10^{4}	$1.\times10^{1}$	3.	$4.\times10^{-1}$	2.25×10^{-1}	$4.\times10^{-2}$	$1.\times10^{-5}$
$\Lambda_{E,4}$	$2.\times10^{7}$	2.5×10^{4}	3.	2.25×10^{-1}	$1.\times10^{-5}$				
$\Lambda_{E,2}$	$2.\times10^{7}$	3.	$1.\times10^{-5}$						

Figures 2.9-2.12 show the ∞-norm of the error of the solution $\phi_g(\mathbf{r})$ on the given 44-group grid for the pV-Γ algorithms with $I_{ce}^{\gamma\leftarrow\gamma+1}$ and RCF during iteration cycles. Each of these figures demonstrates the results for both tests. The ∞-norm of the error is plotted versus computational costs measured in numbers of diffusion solves. To compute these errors (a) the correction factors of the multigrid algorithm are calculated after obtaining the solution on each energy grid Λ_E^γ, (b) then the updated factors are applied to correct the solution on the fine grid Λ_E^1, (c) this updated solution ϕ^1 is compared in the ∞-norm with the converged numerical solution of the problem. Figure 2.9 demonstrates the effect of adding extra energy grids in case of the pV-Γ algorithms with the correction factor based on constant approximation in energy ($I_{ce}^{\gamma\leftarrow\gamma+1}$). Figure 2.10 shows performance of the pV-3 algorithm with $I_{ce}^{\gamma\leftarrow\gamma+1}$ on different sets of grids. The plots of errors of the pV-Γ algorithms with $I_{ce}^{\gamma\leftarrow\gamma+1}$ on larger number of grids ($\Gamma = 4, 5$) are presented in Figures 2.11-2.12. Figures 2.13-2.15 show comparison of convergence of the pV-Γ algorithms with different prolongation operators on the hierarchies with four, five and six grids.

Table 2.6: Test A results on nested grids.

Multigrid Algorithm	Hierarchy of Grids	Prolongation Operator								
		$I_{ce}^{\gamma\leftarrow\gamma+1}$			$I_{le}^{\gamma\leftarrow\gamma+1}$			$I_{lef}^{\gamma\leftarrow\gamma+1}$		
		N_c	N_{ds}	N_{ds}/G	N_c	N_{ds}	N_{ds}/G	N_c	N_{ds}	N_{ds}/G
pV-2	{44,1}	25	1126	25.6	N/A			N/A		
pV-3	{44,2,1}	15	706	16.0	17	800	18.2	N/A		
pV-3	{44,4,1}	11	540	12.3	11	540	12.3	N/A		
pW-3(2,1)	{44,4,1}	11	595	13.5	11	595	13.5	N/A		
pV-3	{44,8,1}	9	478	10.9	8	425	9.7	N/A		
pV-3	{44,22,1}	13	872	19.8	13	872	19.8	N/A		
pW-3(2,1)	{44,22,1}	8	721	16.4	8	721	16.4	N/A		
pW-3(2,2)	{44,22,1}	6	679	15.4	7	792	18.0	N/A		
pV-4	{44,8,2,1}	8	441	10.0	9	496	11.3	9	496	11.3
pV-4	{44,22,4,1}	5	356	8.1	7	498	11.3	7	498	11.3
pV-5	{44,8,4,2,1}	8	473	10.8	9	532	12.1	9	532	12.1
pV-5	{44,22,8,2,1}	6	463	10.5	7	540	12.3	6	463	10.5
pV-6	{44,22,8,4,2,1}	6	487	11.0	7	568	12.9	6	487	11.1

N/A - Not applicable on this grid sequence.

Table 2.7: Test B results on nested grids.

Multigrid Algorithm	Hierarchy of Grids	Prolongation Operator								
		$I_{ce}^{\gamma\leftarrow\gamma+1}$			$I_{le}^{\gamma\leftarrow\gamma+1}$			$I_{lef}^{\gamma\leftarrow\gamma+1}$		
		N_c	N_{ds}	N_{ds}/G	N_c	N_{ds}	N_{ds}/G	N_c	N_{ds}	N_{ds}/G
pV-2	{44,1}	30	1351	30.7	N/A			N/A		
pV-3	{44,2,1}	15	706	16.0	17	800	18.2	N/A		
pV-3	{44,4,1}	12	589	13.4	12	589	13.4	N/A		
pV-3	{44,8,1}	18	955	21.7	17	902	20.5	N/A		
pW-3(2,1)	{44,8,1}	10	621	14.1	10	621	14.1	N/A		
pV-3	{44,22,1}	23	1542	35.0	23	1542	35.0	N/A		
pW-3(2,1)	{44,22,1}	13	1171	26.6	13	1171	26.6	N/A		
pW-3(2,2)	{44,22,1}	10	1131	25.7	10	1131	25.7	N/A		
pV-4	{44,8,2,1}	8	441	10.0	10	551	12.5	10	551	12.5
pV-4	{44,22,4,1}	10	711	16.2	10	711	16.2	10	711	16.2
pV-5	{44,8,4,2,1}	8	473	10.8	10	591	13.4	10	591	13.4
pV-5	{44,22,8,2,1}	7	540	12.3	9	694	15.8	8	617	14.0
pV-6	{44,22,8,4,2,1}	6	487	11.0	9	730	16.6	8	649	14.8

N/A - Not applicable on this grid sequence.

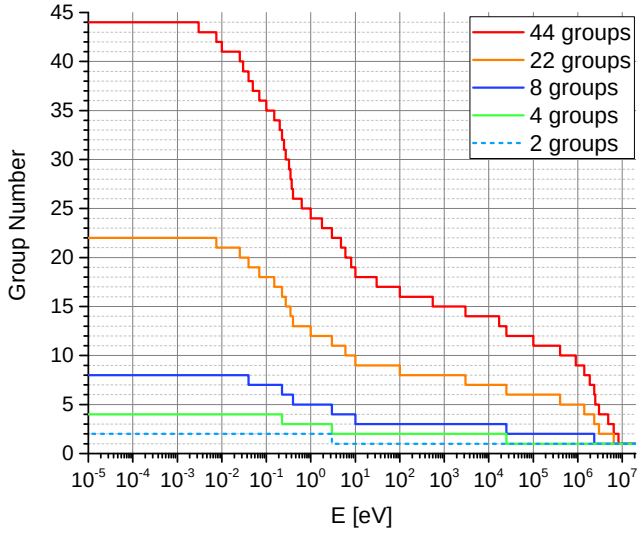

Figure 2.8: The structure of nested energy grids based on the 44-group data library.

The results indicate that involving extra energy grids can reduce both the number of cycles and the total number of diffusion solves. Going from two grids to any of the three grid sequences leads to a significant reduction in the number of diffusion solves. Of the three-grid methods for Test A the {44,8,1} hierarchy takes the least work. The pV-3 algorithm with $I_{le}^{\gamma\leftarrow\gamma+1}$ is the most efficient in this case. For Test B the pV-3 algorithms with $I_{ce}^{\gamma\leftarrow\gamma+1}$ and $I_{le}^{\gamma\leftarrow\gamma+1}$ on the {44,4,1} set have the fewest number of diffusion solves. These results on three-grid hierarchies also show that using the second grid with large number of groups doesn't lead to better efficiency. The pV-4 algorithms have even better performance than pV-3 algorithms. The pW-4 algorithms don't reduce the total number of cycles, but executing nested iterations for the four-grid sequences only increases the cost of each cycle. In Test A the pV-4 algorithm with $I_{ce}^{\gamma\leftarrow\gamma+1}$ on the hierarchy {44,22,4,1} shows the best performance with $N_{ds} = 356$. In Test B this method also is the most efficient with $N_{ds} = 441$. It works better on the hierarchy {44,8,2,1}.

In both tests, the pV-4 algorithm with $I_{ce}^{\gamma\leftarrow\gamma+1}$ is the most efficient. Some algorithms with five and six grids require small number of cycles, but relatively higher cost of each cycle makes them less efficient than the four-grid algorithms. On most grids the pV-Γ algorithms with $I_{ce}^{\gamma\leftarrow\gamma+1}$ have the best performance. The algorithms with $I_{le}^{\gamma\leftarrow\gamma+1}$ work rather similarly and require the numbers of cycles that are close to the numbers of the method with $I_{ce}^{\gamma\leftarrow\gamma+1}$. We notice that the pV-Γ algorithm with $I_{le}^{\gamma\leftarrow\gamma+1}$ and factorization converges more rapidly for $\Gamma = 6$ compared to this algorithm with RCF. These results are indicative of certain advantage of

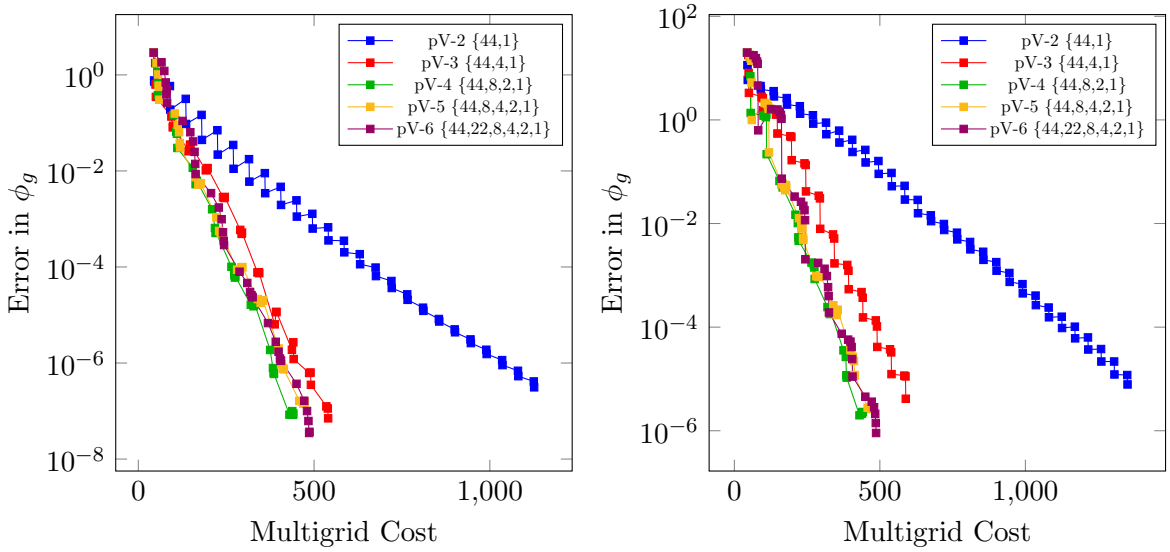

(a) Test A (b) Test B

Figure 2.9: Evolution of the ∞-norm of the error for pV-Γ with $I_{ce}^{\gamma\leftarrow\gamma+1}$ on hierarchies of grids with different number of levels.

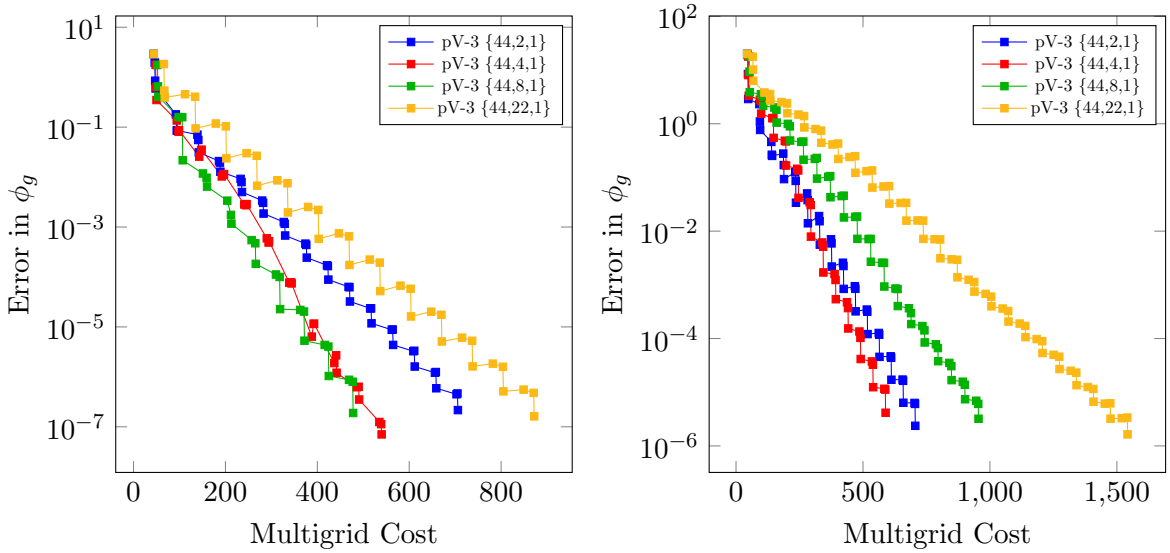

(a) Test A (b) Test B

Figure 2.10: Evolution of the ∞-norm of the error for pV-3 with $I_{ce}^{\gamma\leftarrow\gamma+1}$ on different hierarchies of grids.

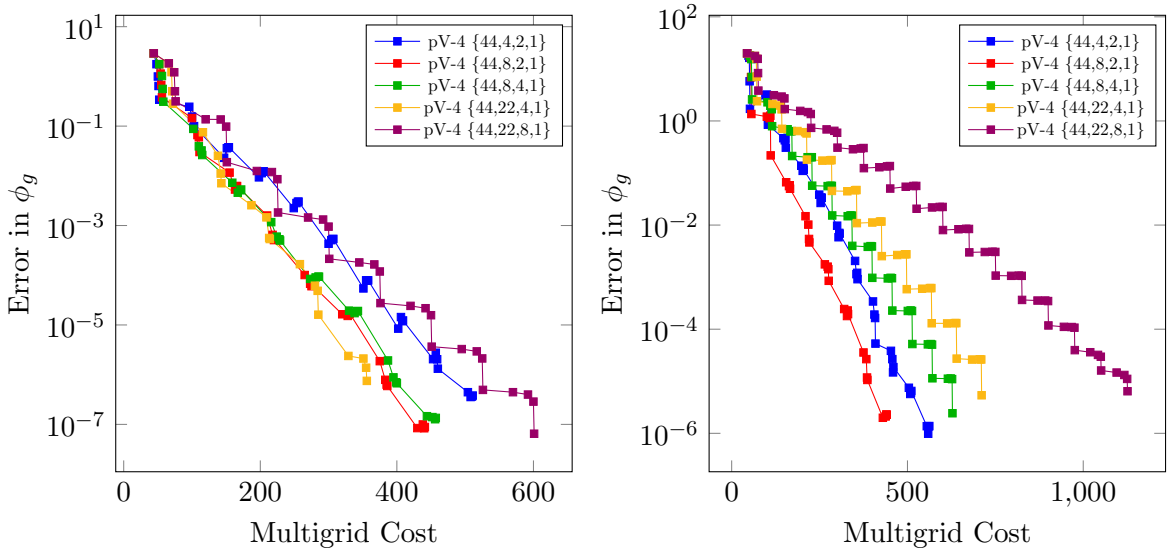

(a) Test A (b) Test B

Figure 2.11: Evolution of the ∞-norm of the error for pV-4 with $I_{ce}^{\gamma \leftarrow \gamma+1}$ on different hierarchies of grids.

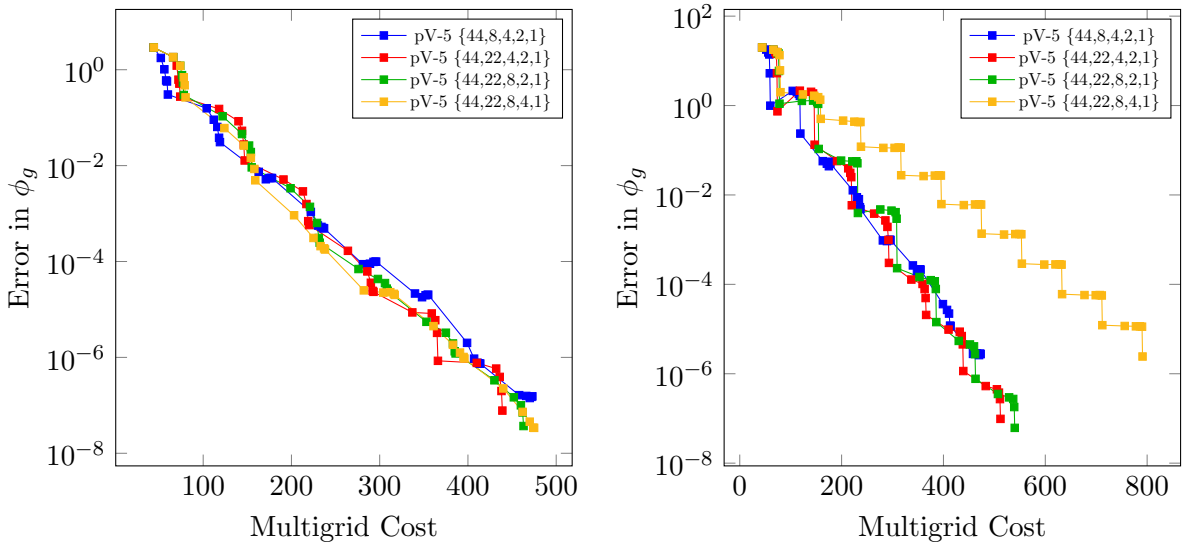

(a) Test A (b) Test B

Figure 2.12: Evolution of the ∞-norm of the error for pV-5 with $I_{ce}^{\gamma \leftarrow \gamma+1}$ on different hierarchies of grids.

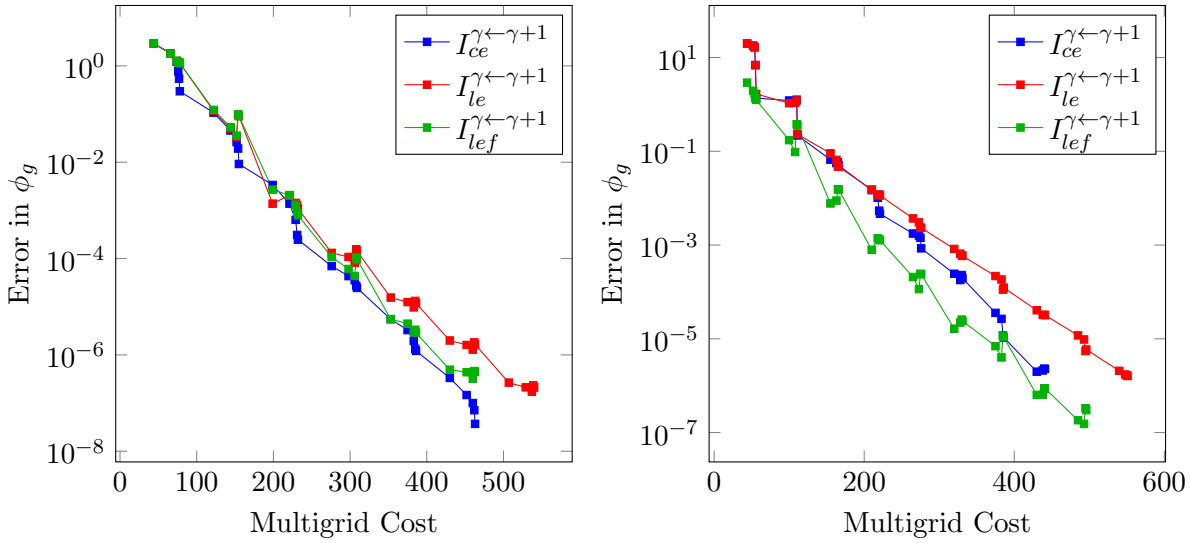

(a) Test A (b) Test B

Figure 2.13: Evolution of the ∞-norm of the error for pV-4 with $I_{ce}^{\gamma\leftarrow\gamma+1}$ and $I_{le}^{\gamma\leftarrow\gamma+1}$ on the hierarchy of grids {44,8,2,1}.

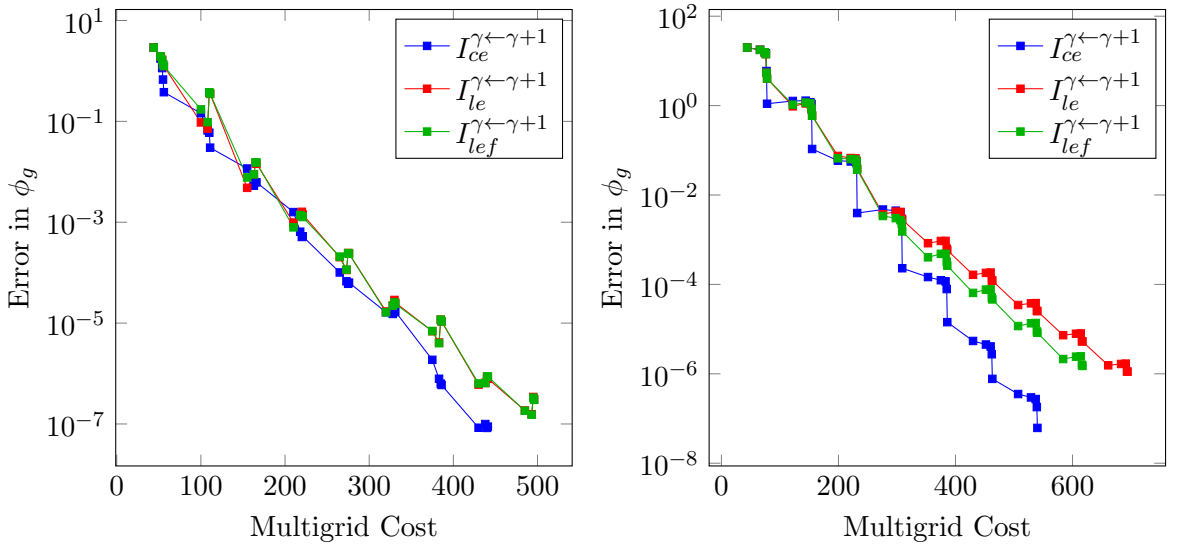

(a) Test A (b) Test B

Figure 2.14: Evolution of the ∞-norm of the error for pV-5 with $I_{ce}^{\gamma\leftarrow\gamma+1}$ and $I_{le}^{\gamma\leftarrow\gamma+1}$ on the hierarchy of grids {44,8,4,2,1}.

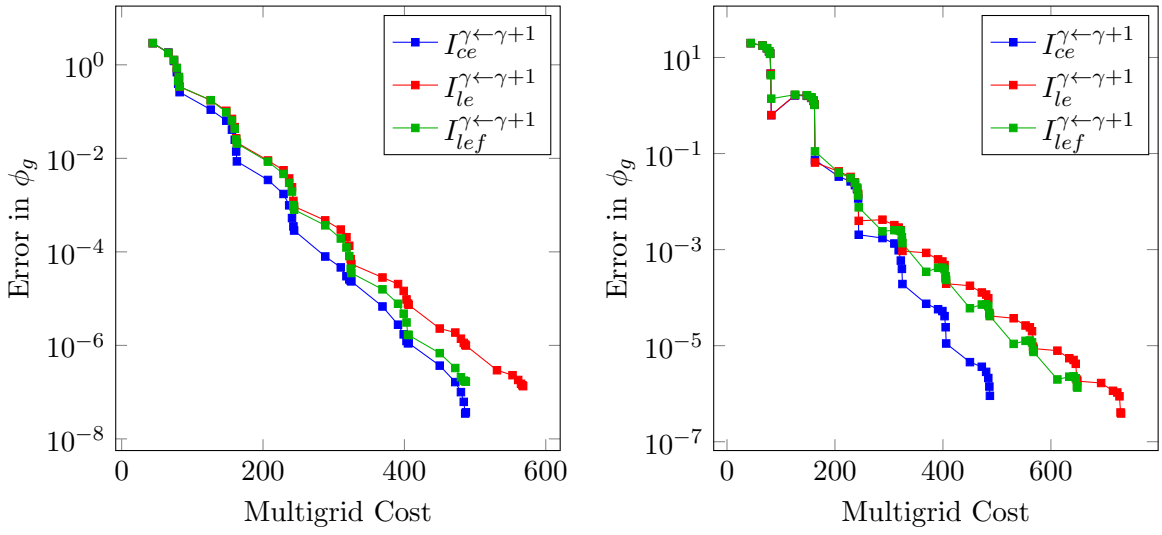

(a) Test A

(b) Test B

Figure 2.15: Evolution of the ∞-norm of the error for pV-6 with $I_{ce}^{\gamma\leftarrow\gamma+1}$ and $I_{le}^{\gamma\leftarrow\gamma+1}$ on the hierarchy of grids {44,22,8,4,2,1}.

prolongation operators with factorization.

The multigrid algorithms have different patterns of convergence during a multigrid cycle. The methods with large number of grids exhibit rather steady convergence during cycles. An example is performance of the pV-6 algorithms with $I_{ce}^{\gamma\leftarrow\gamma+1}$ and $I_{le}^{\gamma\leftarrow\gamma+1}$ with RCF (see Fig. 2.15). The error in the solution of the pV-3 algorithms on various hierarchies of grids is reduced significantly on the coarsest grid where the effective one-group eigenvalue problem is solved (see Fig. 2.10). In fast pV-4 algorithms, the error in the solution is decreased efficiently after the solve on the fine grid Λ_E^1. The examples are the pV-4 algorithms on the {44,8,2,1} set in both tests (see Fig. 2.13). Some multigrid algorithms on a certain set of grids have increase in the error in ϕ_g on one of stages of the iteration cycle. We see this, for example, in the error histories of the pV-4 algorithms on the {44,8,2,1} set with $I_{le}^{\gamma\leftarrow\gamma+1}$ in Test A (see Fig. 2.13). In most cases, such behavior doesn't cause a problem for convergence.

2.4.3 Analysis of Results on Hierarchies of Grids with Agglomeration

The multigrid algorithms are also analyzed on grids with agglomeration in which fast groups are combined to form a macroelement in energy. As a result these grids don't resolve the fast energy range. This type of grids are defined as follows:

- $\Lambda_{E,13}$: 13 groups consisting of 2 fast and 11 thermal,

- $\Lambda_{E,12}$: 12 groups consisting of 1 fast and 11 thermal,
- $\Lambda_{E,5}$: 5 groups with 1 fast and 4 thermal,
- $\Lambda_{E,3}$: 3 groups with 1 fast and 2 thermal.

These energy grids are shown in Figure 2.16. We consider several hierarchies of such grids: {44,3,1}, {44,5,1}, {44,12,1}, {44,12,3,1}, {44,13,5,2,1}, and {44,13,5,3,2,1}. Each of these sets has a corresponding sequence of nested grids with the resolved fast range. They are presented in Table 2.8.

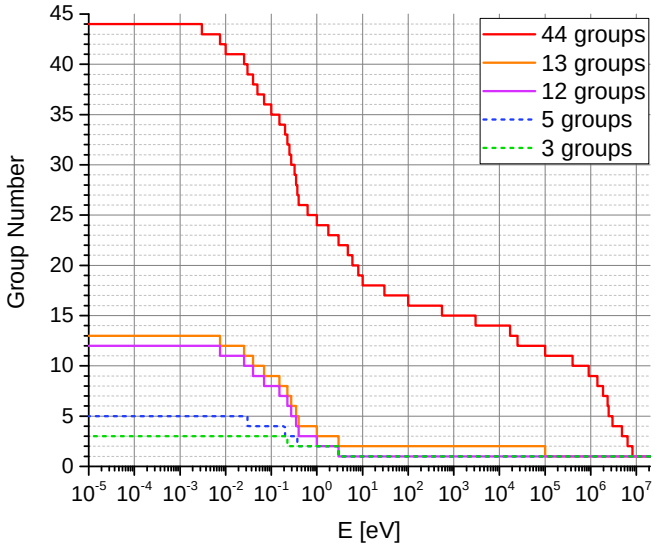

Figure 2.16: The structure of energy grids with agglomeration based on 44-group library.

Table 2.9 shows the results of Test A on hierarchies of grids with agglomeration obtained by the multigrid algorithms using prolongation operators with RCF and factorization. The results for Test B are summarized in Table 2.10. In most cases, the pV-Γ and pW-Γ algorithms on these hierarchies of grids have the same number of circles as in the case of corresponding nested grids. Some algorithms have even less cycles. Note that this is in spite of the fact that the fast range isn't resolved. All these hierarchies of grids have fewer number of groups. This leads to high efficiency of the multigrid algorithms. Such kind of grids also enable us to use advantages of five- and six-grid algorithms to achieve even better performance. The most efficient algorithm in Test B is pV-5 with $I_{ce}^{\gamma\leftarrow\gamma+1}$ and RCF on the {44,13,5,2,1} set. It requires 391 diffusion solves.

Table 2.8: Hierarchies of grids with agglomeration and corresponding sets of nested grids.

Γ	Hierarchy of Grids with Agglomeration	Hierarchy of Grids with Resolved Fast Range
3	{44,3,1}	{44,4,1}
	{44,5,1}	{44,8,1}
	{44,12,1}	{44,22,1}
4	{44,5,3,1}	{44,8,4,1}
5	{44,13,5,2,1}	{44,22,8,2,1}
6	{44,13,5,3,2,1}	{44,22,8,4,2,1}

Table 2.9: Test A results on grids with agglomeration.

Multigrid Algorithm	Hierarchy of Grids	Prolongation Operator								
		$I_{ce}^{\gamma\leftarrow\gamma+1}$			$I_{le}^{\gamma\leftarrow\gamma+1}$			$I_{lef}^{\gamma\leftarrow\gamma+1}$		
		N_c	N_{ds}	N_{ds}/G	N_c	N_{ds}	N_{ds}/G	N_c	N_{ds}	N_{ds}/G
pV-3	{44,3,1}	11	529	12.0	11	529	12.0	N/A		
pV-3	{44,5,1}	9	451	10.3	10	501	11.4	N/A		
pV-3	{44,12,1}	12	685	15.6	13	742	16.9	N/A		
pW-3(2,1)	{44,12,1}	8	561	12.8	8	561	12.8	N/A		
pW-3(2,2)	{44,12,1}	6	499	11.3	6	501	11.4	N/A		
pV-4	{44,12,3,1}	6	361	8.2	8	481	10.9	7	421	9.6
pV-5	{44,13,5,2,1}	6	391	8.9	7	456	10.4	7	456	10.4
pV-6	{44,13,5,3,2,1}	6	409	9.3	7	477	10.8	7	477	10.8

N/A - Not applicable on this grid sequence.

Table 2.10: Test B results on grids with agglomeration.

Multigrid Algorithm	Hierarchy of Grids	Prolongation Operator								
		$I_{ce}^{\gamma\leftarrow\gamma+1}$			$I_{le}^{\gamma\leftarrow\gamma+1}$			$I_{lef}^{\gamma\leftarrow\gamma+1}$		
		N_c	N_{ds}	N_{ds}/G	N_c	N_{ds}	N_{ds}/G	N_c	N_{ds}	N_{ds}/G
pV-3	{44,3,1}	12	577	13.1	14	673	15.3	N/A		
pV-3	{44,5,1}	18	901	20.5	17	851	19.3	N/A		
pV-3	{44,12,1}	22	1255	28.5	22	1255	28.5	N/A		
pW-3(2,1)	{44,12,1}	12	841	19.1	13	898	20.4	N/A		
pW-3(2,2)	{44,12,1}	9	748	17.0	9	748	17.0	N/A		
pV-4	{44,5,3,1}	8	417	9.5	10	521	11.8	10	521	11.8
pV-5	{44,13,5,2,1}	6	391	8.9	9	586	13.3	8	521	11.8
pV-6	{44,13,5,3,2,1}	6	409	9.3	10	681	15.5	8	545	12.4

N/A - Not applicable on this grid sequence.

2.5 Summary

New iteration methods for solving eigenvalue problems for multigroup diffusion equations have been developed. They are based on multigrid-in-energy approach. The nonlinear projection

operator is formulated by means of averaging the group diffusion equations over energy on the hierarchy of energy grids. We defined several variants of prolongation operators based on multiplication correction of the grid solutions. One prolongation uses correction factors with a constant approximation in energy and the other uses correction factors with linear approximation in energy. The linear in energy prolongation operators use linear interpolation in energy between neighboring grids. We apply the partial V- and W-cycles to move through the hierarchy of energy grids. The estimation of the eigenvalue is performed on the coarsest grid with just one energy group. Thus, the eigenvalue problem is solved in the space with the smallest dimensionality. The proposed methods with multigrid in energy were derived for the second-order finite volume spatial approximation of the diffusion equation. They can be applied to other spatial discretizations as well, for example, finite element methods. The obtained numerical results on realistic model reactor-physics problems with 44 groups demonstrated efficiency of the developed algorithms with multigrid in energy. They enable to reduce significantly total number of diffusion solves. Involving additional coarse energy grids can accelerate iterations and decrease computational costs. The algorithms with new prolongation operators can be applied to develop advanced iterative methods for solving the multigroup transport problems with very large number of groups and large-scale multiphysics problems. The NDA and QD methods are both discrete ordinate transport methods, but the low-order equations used to accelerate them are diffusion like. This multilevel with multigrid in energy methodology can be used to reduce the work in the work in the low-order problems of NDA and QD.

Chapter 3

Multilevel Transport Method with Multigrid in Energy

This chapter presents a transport method that solves the multigroup k-eigenvalue equations. It uses a set of low-order equations to accelerate the transport solution. We consider multigroup k-eigenvalue transport problems with isotropic scattering in 2D Cartesian geometry (1.2a). The high-order transport equations are discretized on rectangular mesh using the conservative method of short characteristics with sub-cell balance [51, 10, 56], however the methodology can be applied to other existing transport discretization schemes. The hyperbolic system of transport equations is solved as a fixed source problem by sweeping through space along each angle. The total source terms for these sweeps is calculated by means of the solution from the low-order problem. The low-order equations have been formulated using both Quasidiffusion and Nonlinear Diffusion Acceleration. The low-order problem is defined on a sequence of coarsening grids in energy. These problems on multiple energy grids are used to accelerate the solution of the transport eigenvalue problem on the original grid. On each iteration cycle, the eigenvalue is estimated from the solution of the low-order problem with the lowest dimensionality which is the one-group problem. Various multigrid algorithms are used to move through these different grids and solve the set of low-order equations. A consistent discretization of the low-order Quasidiffusion equations is derived that is based on a second-order finite volume scheme and uses special compensation (consistency) terms. Thus both of the proposed multilevel methods are pure acceleration methods. The iterative method with multigrid in energy based on the QD method can use independent discretization of high-order and low-order equations and provide certain advantages from the viewpoint of stability of iterations. The results of this chapter has been published in [42, 43, 44, 45].

The following sections describe two variants of the proposed methodology by formulating the multigroup low-order NDA and QD equations. The discretized NDA equations are presented

in Sec. 3.1 and the discretized Quasidiffusion equations are described in Sec. 3.2. A hierarchy of low-order equations is defined in 3.3 and the multigrid algorithms are described 3.4. Some results are presented in Sec. 3.5. Sec. 3.6 presents a modified grid sequence where the low-order problem is formulated on a coarser energy grid than the original transport problem.

3.1 Formulation of the Multigroup Low-Order NDA Equations

The low-order NDA equations were presented earlier in continuous form, however they were originally defined in discretized form. The idea behind formulating the LONDA equations in discrete form is to take some discretization of the P_1 equations as a basis then (i) modify it by introducing compensation terms in the discretized first-moment equations and (ii) define exact closure relations [36, 38].

Let us consider transport problems in two-dimensional Cartesian geometry for $G = \{0 \leq x \leq X, 0 \leq y \leq Y\}$ with rectangular spatial grids $\{x_{i-1/2}, i = 1, \ldots, N_x,\ y_{j-1/2}, j = 1, \ldots, N_y\}$. The high-order transport and LONDA equations are approximated on the same spatial grids. To derive the LONDA equations we apply classical formulation by means of a finite-volume scheme for the P_1 equations. For the cell (i, j) the system of LONDA equations for the multigroup transport problem (1.2) consists of the balance equation

$$(J_{x,g,i+1/2,j} - J_{x,g,i-1/2,j})\Delta y_j + (J_{y,g,i,j+1/2} - J_{y,g,i,j-1/2})\Delta x_i + \Sigma_{t,g,i,j} A_{i,j}\phi_{g,i,j} = A_{i,j}\sum_{g'=1}^{G}\Sigma_{s,g'\to g,i,j}\phi_{g',i,j} + \frac{1}{k}A_{i,j}\chi_{g,i,j}\sum_{g'=1}^{G}\nu\Sigma_{f,g',i,j}\phi_{g',i,j} \quad (3.1a)$$

and the first-moment equations of the following form:

$$J_{x,g,i+1/2,j} = -\frac{D_{g,i+1/2,j}(\phi_{g,i+1,j} - \phi_{g,i,j})}{\Delta x_{i+1/2}} + \frac{1}{2}\tilde{D}_{g,i+1/2,j}(\phi_{g,i+1,j} + \phi_{g,i,j})\,, \quad (3.1b)$$

$$J_{y,g,i,j+1/2} = -\frac{D_{g,i,j+1/2}(\phi_{g,i,j+1} - \phi_{g,i,j})}{\Delta y_{j+1/2}} + \frac{1}{2}\tilde{D}_{g,i,j+1/2}(\phi_{g,i,j+1} + \phi_{g,i,j})\,, \quad (3.1c)$$

where

$$\Delta x_i = x_{i+1/2} - x_{i-1/2}\,, \quad \Delta y_j = y_{j+1/2} - y_{j-1/2}\,, \quad A_{i,j} = \Delta x_i \Delta y_j\,, \quad (3.2)$$

$$\Delta x_{i+1/2} = \frac{1}{2}(\Delta x_{i+1} + \Delta x_i)\,, \quad \Delta y_{j+1/2} = \frac{1}{2}(\Delta y_{j+1} + \Delta y_j)\,, \quad (3.3)$$

$J_{x,g,i+1/2,j}$ and $J_{y,g,i,j+1/2}$ are cell-face group currents, $\phi_{g,i,j}$ $(i = 1, \ldots, N_x, j = 1, \ldots, N_y)$ are cell-average group scalar fluxes, $\phi_{g,i,j}$, $\phi_{g,N_x+1,j}$, $\phi_{g,i,0}$, ϕ_{g,i,N_y+1} are cell-face group scalar fluxes

in boundary spatial cells. The boundary conditions are

$$J_{x,g,1/2,j} = F^L_{x,g,j}\phi_{g,0,j}\,, \quad J_{x,g,N_x+1/2,j} = F^R_{x,g,j}\phi_{g,N_x+1,j}\,, \tag{3.4}$$

$$J_{y,g,i,1/2} = F^B_{y,g,i}\phi_{g,i,0}\,, \quad J_{y,g,i,N_y+1/2} = F^T_{y,g,i}\phi_{g,i,N_y+1}\,. \tag{3.5}$$

The cell-face diffusion coefficients are defined by means of cell-average coefficients

$$D_{g,i+1/2,j} = \frac{2D_{g,i,j}D_{g,i+1,j}\Delta x_{i+1/2}}{D_{g,i,j}\Delta x_{i+1} + D_{g,i+1,j}\Delta x_i}\,, \tag{3.6a}$$

$$D_{g,i,j+1/2} = \frac{2D_{g,i,j}D_{g,i,j+1}\Delta y_{j+1/2}}{D_{g,i,j}\Delta y_{j+1} + D_{g,i,j+1}\Delta y_j}\,. \tag{3.6b}$$

The compensation factors are formulated to make the high-order and low-order equations consistent. They are given by

$$\tilde{D}_{g,i+1/2,j} = \frac{\tilde{J}_{x,g,i+1/2,j} + \frac{1}{\Delta x_{i+1/2}}D_{g,i+1/2,j}(\tilde{\phi}_{g,i+1,j} - \tilde{\phi}_{g,i,j})}{0.5(\tilde{\phi}_{g,i+1,j} + \tilde{\phi}_{g,i,j})}\,, \tag{3.7a}$$

$$\tilde{D}_{g,i,j+1/2} = \frac{\tilde{J}_{x,g,i,j+1/2} + \frac{1}{\Delta y_{j+1/2}}D_{g,i,j+1/2}(\tilde{\phi}_{g,i,j+1} - \tilde{\phi}_{g,i,j})}{0.5(\tilde{\phi}_{g,i,j+1} + \tilde{\phi}_{g,i,j})}\,, \tag{3.7b}$$

where $\tilde{\phi}_g$ and $\tilde{J}_{\alpha,g}$ are defined by the solution of the high-order transport problem and hence

$$\tilde{\phi}_{g,i,j} = \sum_m \psi_{g,m,i,j}w_m\,, \tag{3.8a}$$

$$\tilde{J}_{x,g,i+1/2,j} = \sum_m \Omega_{x,m}\psi_{g,m,i+1/2,j}w_m\,, \tag{3.8b}$$

$$\tilde{J}_{y,g,i+1/2,j} = \sum_m \Omega_{y,m}\psi_{g,m,i+1/2,j}w_m\,. \tag{3.8c}$$

Here $\psi_{g,m}$ is the angular flux for the discrete direction $\mathbf{\Omega}_m$ and w_m is the quadrature weight.

The first-moment equations (3.1b) and (3.1b) can be cast as

$$J_{x,g,i+1/2,j} = -\frac{1}{\Delta x_{i+1/2}}\left(D^+_{g,i+1/2,j}\phi_{g,i+1,j} - D^-_{g,i+1/2,j}\phi_{g,i,j}\right), \tag{3.9a}$$

$$J_{y,g,i,j+1/2} = -\frac{1}{\Delta y_{j+1/2}}\left(D^+_{g,i,j+1/2}\phi_{g,i,j+1} - D^-_{g,i,j+1/2}\phi_{g,i,j}\right), \tag{3.9b}$$

where the factors

$$D^\pm_{g,i+1/2,j} = D_{g,i+1/2,j} \mp \frac{1}{2}\tilde{D}_{x,g,i+1/2,j}\Delta x_{i+1/2}\,, \tag{3.10a}$$

$$D^{\pm}_{g,i,j+1/2} = D_{g,i,j+1/2} \mp \frac{1}{2}\tilde{D}_{y,g,i,j+1/2}\Delta y_{j+1/2} \tag{3.10b}$$

are modified diffusion coefficients of the generalized Fick's law. Substituting equation (3.9) into the balance equation (3.1a) yields the diffusion-like equation

$$\mathbb{L}_g[D^{\pm}_g]\phi_{g,i,j} + \Sigma_{t,g,i,j}A_{i,j}\phi_{g,i,j} = A_{i,j}\sum_{g'=1}^{G}\Sigma_{s,g'\to g,i,j}\phi_{g',i,j} + \frac{1}{k}A_{i,j}\chi_{g,i,j}\sum_{g'=1}^{G}\nu\Sigma_{f,g',i,j}\phi_{g',i,j}, \tag{3.11a}$$

$$\begin{aligned}\mathbb{L}_g[D^{\pm}_g]\phi_{g,i,j} = -\Bigg[&\frac{(D^{+}_{g,i+1/2,j}\phi_{g,i+1,j} - D^{-}_{g,i+1/2,j}\phi_{g,i,j})}{\Delta x_{i+1/2}} \\ &- \frac{(D^{+}_{g,i-1/2,j}\phi_{g,i,j} - D^{-}_{g,i-1/2,j}\phi_{g,i-1,j})}{\Delta x_{i-1/2}}\Bigg]\Delta y_j - \Bigg[\frac{(D^{+}_{g,i,j+1/2}\phi_{g,i,j+1} - D^{-}_{g,i,j+1/2}\phi_{g,i,j})}{\Delta y_{j+1/2}} \\ &- \frac{(D^{+}_{g,i,j-1/2}\phi_{g,i,j} - D^{-}_{g,i,j-1/2}\phi_{g,i,j-1})}{\Delta y_{j-1/2}}\Bigg]\Delta x_i\,.\end{aligned} \tag{3.11b}$$

where the leakage operator $\mathbb{L}_g$ is defined by a five-point stencil.

3.2 Formulation of the Multigroup Low-Order Quasidiffusion Equations

The low-order QD equations (1.5a)-(1.5b) can be discretized on a rectangular spatial mesh by means of a second-order finite volume method. The balance equation (1.5a) is integrated over each cell (i, j) to obtain

$$\begin{aligned}(J_{x,g,i+1/2,j} - J_{x,g,i-1/2,j})\Delta y_j + (J_{y,g,i,j+1/2} - J_{y,g,i,j-1/2})\Delta x_i + \Sigma_{t,g,i,j}A_{i,j}\phi_{g,i,j} = \\ A_{i,j}\sum_{g'=1}^{G}\Sigma_{s,g'\to g,i,j}\phi_{g',i,j} + A_{i,j}\frac{\chi_{g,i,j}}{k}\sum_{g'=1}^{G}\nu_{f,g',i,j}\Sigma_{f,g',i,j}\phi_{g',i,j}\,.\end{aligned} \tag{3.12}$$

The x-component of the first moment equation (1.5b) is integrated over the left and right halves of the cell (i, j) and compensation terms are added to enable the solution of the low-order equations to reproduce angular moments of the discrete high-order transport solution on

any spatial grid [12]. The corresponding discretized first moment equations are given by

$$\Big(\big(E_{xx,g,i,j}+\xi^{L-}_{x,g,i,j}\big)\phi_{g,i,j}-\big(E_{xx,g,i-1/2,j}+\xi^{L+}_{x,g,i,j}\big)\phi_{g,i-1/2,j}\Big)\Delta y_j+\frac{1}{2}\Big(E_{xy,g,i,j+1/2}\phi_{g,i,j+1/2} - E_{xy,g,i,j-1/2}\phi_{g,i,j-1/2}\Big)\Delta x_i+\frac{1}{2}\Sigma_{t,g,i,j}A_{i,j}J_{x,g,i-1/2,j}=0\,, \quad (3.13a)$$

$$\Big(\big(E_{xx,g,i+1/2,j}+\xi^{R-}_{x,g,i,j}\big)\phi_{g,i+1/2,j}-\big(E_{xx,g,i,j}+\xi^{R+}_{x,g,i,j}\big)\phi_{g,i,j}\Big)\Delta y_j+\frac{1}{2}\Big(E_{xy,g,i,j+1/2}\phi_{g,i,j+1/2} - E_{xy,g,i,j-1/2}\phi_{g,i,j-1/2}\Big)\Delta x_i+\frac{1}{2}\Sigma_{t,g,i,j}A_{i,j}J_{x,g,i+1/2,j}=0\,, \quad (3.13b)$$

$$E_{\alpha\beta,g,k,l}=\frac{\sum_{m=1}^{M}\Omega_{\alpha,m}\Omega_{\beta,m}\psi_{m,g,k,l}w_m}{\sum_{m=1}^{M}\psi_{m,g,k,l}w_m}\,, \quad (3.14)$$

where $(k,l)=\{(i,j),(i+1/2,j),(i,j+1/2)\}$ are indices corresponding to cell-average or face-average grid functions, $\mathbf{\Omega}_m$ and w_m $(m=1,\ldots,M)$ are discrete directions and quadrature weights, respectively. The compensation terms are defined as follows:

$$\xi^{L-}_{x,g,i,j}=\begin{cases}-\frac{\gamma^{L}_{x,g,i,j}}{\tilde{\phi}_{g,i,j}\Delta y_j}, & \text{if } \gamma^{L}_{x,g,i,j}\le 0,\\ 0, & \text{if } \gamma^{L}_{x,g,i,j}>0,\end{cases}\quad \xi^{L+}_{x,g,i,j}=\begin{cases}0, & \text{if } \gamma^{L}_{x,g,i,j}\le 0,\\ \frac{\gamma^{L}_{x,g,i,j}}{\tilde{\phi}_{g,i-1/2,j}\Delta y_j}, & \text{if } \gamma^{L}_{x,g,i,j}>0,\end{cases} \quad (3.15a)$$

$$\xi^{R-}_{x,g,i,j}=\begin{cases}-\frac{\gamma^{R}_{x,g,i,j}}{\tilde{\phi}_{g,i+1/2,j}\Delta y_j}, & \text{if } \gamma^{R}_{x,g,i,j}\le 0,\\ 0, & \text{if } \gamma^{R}_{x,g,i,j}>0,\end{cases}\quad \xi^{R+}_{x,g,i,j}=\begin{cases}0, & \text{if } \gamma^{R}_{x,g,i,j}\le 0,\\ \frac{\gamma^{R}_{x,g,i,j}}{\tilde{\phi}_{g,i,j}\Delta y_j}, & \text{if } \gamma^{R}_{x,g,i,j}>0,\end{cases} \quad (3.15b)$$

$$\gamma^{L}_{x,g,i,j}=\Big(E_{xx,g,i,j}\tilde{\phi}_{g,i,j}-E_{xx,g,i-1/2,j}\tilde{\phi}_{g,i-1/2,j}\Big)\Delta y_j + \Big(E_{xy,g,i,j+1/2}\tilde{\phi}_{g,i,j+1/2}-E_{xy,g,i,j-1/2}\tilde{\phi}_{g,i,j-1/2}\Big)\frac{\Delta x_i}{2}+\frac{1}{2}\Sigma_{t,g,i,j}A_{i,j}\tilde{J}_{x,g,i-1/2,j}\,, \quad (3.15c)$$

$$\gamma^{R}_{x,g,i,j}=\Big(E_{xx,g,i+1/2,j}\tilde{\phi}_{g,i+1/2,j}-E_{xx,g,i,j}\tilde{\phi}_{g,i,j}\Big)\Delta y_j + \Big(E_{xy,g,i,j+1/2}\tilde{\phi}_{g,i,j+1/2}-E_{xy,g,i,j-1/2}\tilde{\phi}_{g,i,j-1/2}\Big)\frac{\Delta x_i}{2}+\frac{1}{2}\Sigma_{t,g,i,j}A_{i,j}\tilde{J}_{x,g,i-1/2,j}\,, \quad (3.15d)$$

where

$$\tilde{\phi}_{g,k,l}=\sum_m \psi_{m,g,k,l}w_m\,,\quad \tilde{J}_{\alpha,g,k,l}=\sum_m \Omega_{\alpha,m}\psi_{m,g,k,l}w_m \quad (3.16)$$

are the angular moments of the high-order transport solution. To discretize the y-component of the first moment equation (1.5b) we integrate it over the top and bottom halves of the cell

(i,j) and introduce corresponding compensation terms. This yields the following discretization of Eq. (1.5b):

$$\frac{1}{2}\Big(E_{xy,g,i+1/2,j}\phi_{g,i+1/2,j} - E_{xy,g,i-1/2,j}\phi_{g,i-1/2,j}\Big)\Delta y_j + \Big((E_{yy,g,i,j} + \xi^{B-}_{g,i,j})\phi_{g,i,j} - (E_{yy,g,i,j-1/2} + \xi^{B+}_{g,i,j})\phi_{g,i,j-1/2}\Big)\Delta x_i + \frac{1}{2}\Sigma_{t,g,i,j}J_{y,g,i,j-1/2}A_{i,j} = 0\,, \quad (3.17a)$$

$$\frac{1}{2}\Big(E_{xy,g,i+1/2,j}\phi_{g,i+1/2,j} - E_{xy,g,i-1/2,j}\phi_{g,i-1/2,j}\Big)\Delta y_j + \Big((E_{yy,g,i,j+1/2} + \xi^{T-}_{g,i,j})\phi_{g,i,j+1/2} - (E_{yy,g,i,j} + \xi^{T+}_{g,i,j})\phi_{g,i,j}\Big)\Delta x_i + \frac{1}{2}\Sigma_{t,g,i,j}J_{y,g,i,j+1/2}A_{i,j} = 0\,, \quad (3.17b)$$

where

$$\xi^{B-}_{g,i,j} = \begin{cases} -\frac{\gamma^B_{g,i,j}}{\tilde{\phi}_{g,i,j}\Delta x_i} & \text{for } \gamma^B_{g,i,j} \le 0\,, \\ 0 & \text{for } \gamma^B_{g,i,j} > 0\,, \end{cases} \quad \xi^{B+}_{g,i,j} = \begin{cases} 0 & \text{for } \gamma^B_{g,i,j} \le 0\,, \\ \frac{\gamma^B_{g,i,j}}{\tilde{\phi}_{g,i,j-1/2}\Delta x_i} & \text{for } \gamma^B_{g,i,j} > 0\,, \end{cases} \quad (3.18a)$$

$$\xi^{T-}_{g,i,j} = \begin{cases} -\frac{\gamma^T_{g,i,j}}{\tilde{\phi}_{g,i,j+1/2}\Delta x_i} & \text{for } \gamma^T_{g,i,j} \le 0\,, \\ 0 & \text{for } \gamma^T_{g,i,j} > 0\,, \end{cases} \quad \xi^{T+}_{g,i,j} = \begin{cases} 0 & \text{for } \gamma^T_{g,i,j} \le 0\,, \\ \frac{\gamma^T_{g,i,j}}{\tilde{\phi}_{g,i,j}\Delta x_i} & \text{for } \gamma^T_{g,i,j} > 0\,, \end{cases} \quad (3.18b)$$

$$\gamma^B_{g,i,j} = \frac{1}{2}\Big(E_{xy,g,i+1/2,j}\tilde{\phi}_{g,i+1/2,j} - E_{xy,g,i-1/2,j}\tilde{\phi}_{g,i-1/2,j}\Big)\Delta y_j + \Big(E_{yy,g,i,j}\tilde{\phi}_{g,i,j} - E_{yy,g,i,j-1/2}\tilde{\phi}_{g,i,j-1/2}\Big)\Delta x_i + \frac{1}{2}\Sigma_{t,g,i,j}\tilde{J}_{y,g,i,j-1/2}A_{i,j}\,, \quad (3.19a)$$

$$\gamma^T_{g,i,j} = \frac{1}{2}\Big(E_{xy,g,i+1/2,j}\tilde{\phi}_{g,i+1/2,j} - E_{xy,g,i-1/2,j}\tilde{\phi}_{g,i-1/2,j}\Big)\Delta y_j + \Big(E_{yy,g,i,j+1/2}\tilde{\phi}_{g,i,j+1/2} - E_{yy,g,i,j}\tilde{\phi}_{g,i,j}\Big)\Delta x_i + \frac{1}{2}\Sigma_{t,g,i,j}\tilde{J}_{y,g,i,j+1/2}A_{i,j}\,. \quad (3.19b)$$

The first moment equations can be substituted into the balance equation to eliminate the currents yielding the equations in the form

$$\mathbb{L}_g[G^*_g]\phi_{g,i,j} + \Sigma_{t,g,i,j}\phi_{g,i,j} = \sum_{g'=1}^{G}\Sigma_{s,g'\to g,i,j}\phi_{g',i,j} + \frac{\chi_{g,i,j}}{k}\sum_{g'=1}^{G}\nu_{f,g',i,j}\Sigma_{f,g',i,j}\phi_{g',i,j}\,, \quad (3.20a)$$

where the leakage operator is

$$\mathbb{L}_g[G^*_g]\phi_{g,i,j} = -\frac{2}{\Delta x_i^2}\Big(G^R_{xx,g,i,j}\phi_{g,i+1/2,j} - (G^{CR}_{xx,g,i,j} + G^{CL}_{xx,g,i,j})\phi_{g,i,j} + G^L_{xx,g,i,j}\phi_{g,i-1/2,j}\Big) - \frac{2}{\Delta y_j^2}\Big(G^T_{yy,g,i,j}\phi_{g,i,j+1/2} - (G^{CT}_{yy,g,i,j} + G^{CB}_{yy,g,i,j})\phi_{g,i,j} + G^B_{yy,g,i,j}\phi_{g,i,j-1/2}\Big)\,, \quad (3.20b)$$

and the modified coefficients are defined in terms of the Eddington factors and consistency terms as

$$G^{CL}_{xx,g,i,j} = \frac{E_{xx,g,i,j} + \xi^{L-}_{g,i,j}}{\Sigma_{t,g,i,j}}\,, \quad G^{CR}_{xx,g,i,j} = \frac{E_{xx,g,i,j} + \xi^{R+}_{g,i,j}}{\Sigma_{t,g,i,j}}\,, \tag{3.21a}$$

$$G^{CB}_{yy,g,i,j} = \frac{E_{yy,g,i,j} + \xi^{B-}_{g,i,j}}{\Sigma_{t,g,i,j}}\,, \quad G^{CT}_{yy,g,i,j} = \frac{E_{yy,g,i,j} + \xi^{T+}_{g,i,j}}{\Sigma_{t,g,i,j}}\,, \tag{3.21b}$$

$$G^{L}_{xx,g,i,j} = \frac{E_{xx,g,i-1/2,j} + \xi^{L+}_{g,i,j}}{\Sigma_{t,g,i,j}}\,, \; G^{R}_{xx,g,i,j} = \frac{E_{xx,g,i+1/2,j} + \xi^{R-}_{g,i,j}}{\Sigma_{t,g,i,j}}\,, \tag{3.21c}$$

$$G^{B}_{yy,g,i,j} = \frac{E_{yy,g,i,j-1/2} + \xi^{B+}_{g,i,j}}{\Sigma_{t,g,i,j}}\,, \; G^{T}_{yy,g,i,j} = \frac{E_{yy,g,i,j+1/2} + \xi^{T-}_{g,i,j}}{\Sigma_{t,g,i,j}}\,. \tag{3.21d}$$

3.3 The Hierarchy of Low-Order Equations on Multiple Grids in Energy

A hierarchy of grids is defined as described in Sec. 2.1. The first energy grid in the low-order problem Λ^1_E is defined to be identical to the original energy grid of the transport problem. The low-order equations are successively averaged over groups on the set of grids in energy to derive a hierarchy of group low-order problems. The averaged cross sections and factors are defined for each grid to close exactly the multigrid system of group low-order equations. This procedure is applied directly to the spatially discretized low-order equations.

As a result we obtain a system of nonlinearly coupled multigrid low-order equations in which cross sections depend on solution on the previous grid. The multigrid system of low-order equations in the spatial (i,j) cell are defined by

$$\mathbb{L}^{\gamma}_{p}\phi^{\gamma}_{g,i,j} + \bar{\Sigma}^{\gamma}_{t,g,i,j}\phi^{\gamma}_{g,i,j} = \sum_{g'=1}^{G^\gamma} \bar{\Sigma}^{\gamma}_{s,g'\to g,i,j}\phi^{\gamma}_{g',i,j} + \frac{\bar{\chi}^{\gamma}_{g,i,j}}{k}\sum_{g'=1}^{G^\gamma}\overline{\nu\Sigma}^{\gamma}_{f,g',i,j}\phi^{\gamma}_{g',i,j}\,, \tag{3.22a}$$

$$g = 1,\ldots,G^\gamma\,, \quad \gamma = 1,\ldots,\Gamma-1,$$

$$\mathbb{L}^{\Gamma}_{1}\phi^{\Gamma}_{1,i,j} + \Big(\bar{\Sigma}^{\Gamma}_{a,1,i,j} - \frac{1}{k}\overline{\nu\Sigma}^{\Gamma}_{f,1,i,j}\Big)\phi^{\Gamma}_{1,i,j} = 0\,, \quad \gamma = \Gamma\,, \tag{3.22b}$$

where $\phi^{\gamma}_{g,i,j}$ is the cell-average group scalar flux, $J^{\gamma}_{x,g,i+1/2,j}$ and $J^{\gamma}_{y,g,i,j+1/2}$ are the face-average group currents on grid γ. The cross sections on the coarse energy grid Λ^{γ}_E are defined by the cross sections and solution on the grid $\Lambda^{\gamma-1}_E$ as follows as in Equations (2.7). For the NDA method the leakage operator $\mathbb{L}^{\gamma}_{p} = \mathbb{L}^{\gamma}_{p}[D^{\pm,\gamma}_{p}]$ and the modified diffusion coefficients are averaged as described by Equations (2.29). The coarse-group leakage operator $\mathbb{L}^{\gamma}_{p} = \mathbb{L}^{\gamma}_{p}[G^{*,\gamma}_{p}]$ and factors

for the QD method are defined by means of the solution on the previous energy grid as

$$\bar{G}^{CL,\gamma}_{xx,g,i,j} = \frac{\sum_{m\in\omega_g^\gamma} \bar{G}^{CL,\gamma-1}_{xx,m,i,j}\phi^{\gamma-1}_{m,i,j}}{\sum_{m\in\omega_g^\gamma}\phi^{\gamma-1}_{m,i,j}}, \quad \bar{G}^{CR,\gamma}_{xx,g,i,j} = \frac{\sum_{m\in\omega_g^\gamma} \bar{G}^{CR,\gamma-1}_{xx,m,i,j}\phi^{\gamma-1}_{m,i,j}}{\sum_{m\in\omega_g^\gamma}\phi^{\gamma-1}_{m,i,j}}, \tag{3.23a}$$

$$\bar{G}^{CB,\gamma}_{yy,g,i,j} = \frac{\sum_{m\in\omega_g^\gamma} \bar{G}^{CB,\gamma-1}_{yy,m,i,j}\phi^{\gamma-1}_{m,i,j}}{\sum_{m\in\omega_g^\gamma}\phi^{\gamma-1}_{m,i,j}}, \quad \bar{G}^{CT,\gamma}_{yy,g,i,j} = \frac{\sum_{m\in\omega_g^\gamma} \bar{G}^{CT,\gamma-1}_{yy,m,i,j}\phi^{\gamma-1}_{m,i,j}}{\sum_{m\in\omega_g^\gamma}\phi^{\gamma-1}_{m,i,j}}, \tag{3.23b}$$

$$\bar{G}^{L,\gamma}_{xx,g,i,j} = \frac{\sum_{m\in\omega_g^\gamma} \bar{G}^{L,\gamma-1}_{xx,m,i,j}\phi^{\gamma-1}_{m,i-1/2,j}}{\sum_{m\in\omega_g^\gamma}\phi^{\gamma-1}_{m,i-1/2,j}}, \quad \bar{G}^{R,\gamma}_{xx,g,i,j} = \frac{\sum_{m\in\omega_g^\gamma} \bar{G}^{R,\gamma-1}_{xx,m,i,j}\phi^{\gamma-1}_{m,i+1/2,j}}{\sum_{m\in\omega_g^\gamma}\phi^{\gamma-1}_{m,i+1/2,j}}, \tag{3.23c}$$

$$\bar{G}^{B,\gamma}_{yy,g,i,j} = \frac{\sum_{m\in\omega_g^\gamma} \bar{G}^{B,\gamma-1}_{yy,m,i,j}\phi^{\gamma-1}_{m,i,j-1/2}}{\sum_{m\in\omega_g^\gamma}\phi^{\gamma-1}_{m,i,j-1/2}}, \quad \bar{G}^{T,\gamma}_{yy,g,i,j} = \frac{\sum_{m\in\omega_g^\gamma} \bar{G}^{T,\gamma-1}_{yy,m,i,j}\phi^{\gamma-1}_{m,i,j-1/2}}{\sum_{m\in\omega_g^\gamma}\phi^{\gamma-1}_{m,i,j-1/2}}. \tag{3.23d}$$

3.4 Multigrid Algorithm

The hierarchy of multigrid equations (3.22a)-(3.22b) is solved sequentially employing some nested cycles between different grids that are similar to iterative cycles used in multigrid methods [50]. Each transport iteration begins with a single sweep over all energy groups and angles in the high-order problem.

$$\boldsymbol{\Omega}_m \cdot \boldsymbol{\nabla}\psi_{g,i,j,m} + \Sigma_{t,g,i,j}\psi_{g,i,j,m} = \frac{1}{4\pi}\sum_{g'=1}^{G}\Sigma_{s,g'\to g,i,j}\hat{\phi}^1_{g,i,j} + \frac{\chi_{g,i,j}}{4\pi k}\sum_{g'=1}^{G}\nu\Sigma_{f,g',i,j}\hat{\phi}^1_{g,i,j} \tag{3.24}$$

The right hand side of the equation is calculated from the most updated multigroup scalar flux $\hat{\phi}^1_{g,i,j}$ and k-eigenvalue from the one-group low-order problem. There are no within-group scattering iterations.

The algorithms starts from the given fine energy grid Λ^1_E and moves through the hierarchy of grids. On each grid Λ^γ_E were $\gamma < \Gamma$ the low-order equations are solved as a fixed-source multigroup problem

$$\mathbb{L}^\gamma_p\phi^\gamma_{g,i,j} + (\bar{\Sigma}^\gamma_{t,g,i,j} - \bar{\Sigma}^\gamma_{s,g\to g,i,j})\phi^\gamma_{g,i,j} + \sum_{g'=1}^{g-1}\bar{\Sigma}^\gamma_{s,g'\to g,i,j}\phi^\gamma_{g',i,j} = \sum_{g'=g+1}^{G^\gamma}\bar{\Sigma}^\gamma_{s,g'\to g,i,j}\hat{\phi}^\gamma_{g',i,j} + \frac{\bar{\chi}^\gamma_{g,i,j}}{k}\sum_{g'=1}^{G^\gamma}\overline{\nu\Sigma}^\gamma_{f,g',i,j}\hat{\phi}^\gamma_{g',i,j} \tag{3.25}$$

where the fission and up-scattering terms being calculated from the updated scalar flux $\hat{\phi}^\gamma_{g',i,j}$ and eigenvalue estimated on the previous multigrid cycle. The down scatter term is calculated from the new solution of the scalar flux by solving the group equations in sequence from

highest-energy to lowest-energy groups. This is essentially a single bock Gauss-Seidel iteration on the scattering matrix. Thus, there is only one relaxation step on each energy grid. To solve the diffusion equation in the spatial domain in each group we use BiCGSTAB with the LU preconditioner.

On the coarsest grid Λ_E^Γ the one-group low-order problem is solved for the eigenvalue and associated eigenfunction. The equations are formulated as a generalized eigenvalue problem and solved using a single Newton iteration. It can be cast as

$$\mathcal{F}(\mathbf{u}) = 0, \quad \mathbf{u} = (\phi_1^\Gamma, k), \tag{3.26}$$

$$\mathcal{F}(\mathbf{u}) = \begin{pmatrix} \mathcal{L}\mathbf{u} - \frac{1}{k}\mathcal{P}_f\mathbf{u} \\ \mathcal{B}\mathbf{u} \\ \mathcal{N}\mathbf{u} - \mathcal{C} \end{pmatrix}, \tag{3.27}$$

where $\mathcal{L}$, $\mathcal{P}_f$, and $\mathcal{B}$ are the loss, fission production, and boundary condition operators respectively. $\mathcal{N}$ is a operator that normalizes the solution to a constant $\mathcal{C}$. The obtained estimation of k is then used on all grids Λ_E^γ for $\gamma < \Gamma$ on the next multigrid cycle. On the first multigrid cycle we perform a Weilandt-Shift iteration on Λ_E^Γ as an initial guess in order to ensure the Newton iterations converge to the correct local minimum. A BiCGSTAB solver is also used to solve the Newton problem.

A prolongation operation is defined by factors based on solutions on two neighboring energy grids. The prolongation operator is based on a group-local factor associated with the coarse grid $\Lambda_E^{\gamma+1}$ that involves only one energy interval on this grid. It uses constant approximation of the solution over the energy interval $\delta\mathcal{E}_g^{\gamma+1}$ and is formulated as follows:

$$\mathfrak{f}_{ce,g}^{\gamma+1}(\mathbf{r}) = \frac{\hat{\phi}_g^{\gamma+1}(\mathbf{r})}{\sum_{g'\in\omega_g^\gamma}\phi_{g'}^\gamma(\mathbf{r})}, \quad g = 1,\ldots,G^{\gamma+1}. \tag{3.28}$$

This defines the operator $I_{ce}^{\gamma\leftarrow\gamma+1}$ that is referred to as the prolongation operator with constant approximation in energy. It can be shown that application of the factor (3.28) recursively according to Algorithm 3 is equivalent to the following factorization form of the operator $I_{ce}^{\gamma\leftarrow\gamma+1}$:

$$\hat{\phi}_g^\gamma = \phi_g^\gamma\,\tilde{\mathfrak{f}}_{ce,g'}^{\gamma+1}\,\tilde{\mathfrak{f}}_{ce,g''}^{\gamma+2}\cdots\tilde{\mathfrak{f}}_{ce,1}^{\Gamma} \quad \text{for } g\in\omega_{g'}^{\gamma+1},\ g'\in\omega_{g''}^{\gamma+2} \text{ etc}, \tag{3.29}$$

where

$$\tilde{\mathfrak{f}}_{ce,g}^{\gamma+1}(\mathbf{r}) = \frac{\phi_g^{\gamma+1}(\mathbf{r})}{\sum_{g'\in\omega_g^\gamma}\phi_{g'}^\gamma(\mathbf{r})}, \quad g = 1,\ldots,G^{\gamma+1}. \tag{3.30}$$

Thus, the group scalar flux on the grid Λ_E^γ is corrected by the product of the factors (3.30) computed by the solutions on coarser grids from the current multigrid cycle. The prolongation

operators with different definitions of correction factors are discussed in Sec. 2.3.

For cases with opposing reflective boundary conditions the low-order solution is used to update the incoming angular flux on the boundary in the following way:

$$\psi_{g,m}(\mathbf{r}) = \frac{\phi_g^1(\mathbf{r})}{2\tilde{\phi}_g^{out}(\mathbf{r})}\psi_{g,m*}(\mathbf{r}), \quad \text{for} \quad \mathbf{\Omega}_m \cdot \mathbf{n} < 0 \quad \text{and} \quad \mathbf{r} \in \partial D_{ref}\,, \tag{3.31}$$

where $\tilde{\phi}_g^{out} = \sum_{\mathbf{\Omega}_{m*}\cdot\hat{n}>0} w_{m*}\psi_{g,m*}$ is the high-order partial scalar flux, and $\mathbf{\Omega}_{m*}$ is the reflected angle of $\mathbf{\Omega}_m$.

The procedures for solving the system of equations is described in Algorithm 6 and 7 and illistrated in Figures 3.1 and 3.2. Here $\mathcal{T}$ is the transport sweep operator and $\mathcal{S}$ and $\mathcal{P}$ are the

Solve $\boldsymbol{\psi} = \mathcal{T}^{-1}\mathcal{S}\hat{\boldsymbol{\phi}}^1 + \frac{1}{k}\mathcal{T}^{-1}\mathcal{P}\hat{\boldsymbol{\phi}}^1$
Calculate QD/NDA factors and average the high-order equations over angle to form $\mathcal{A}_1$, $\mathcal{B}_1$, $\mathcal{C}_1$
for $\gamma \leftarrow 1$ *to* $\Gamma - 1$ **do**
  Solve $\boldsymbol{\phi}^\gamma = \mathcal{A}_\gamma^{-1}\mathcal{B}_\gamma\hat{\boldsymbol{\phi}}^\gamma + \frac{1}{k}\mathcal{A}_\gamma^{-1}\mathcal{C}_\gamma\hat{\boldsymbol{\phi}}^\gamma$
  Perform homogenization in energy to form $\mathcal{A}_{\gamma+1}$, $\mathcal{B}_{\gamma+1}$, $\mathcal{C}_{\gamma+1}$
end
Solve the eigenvalue problem $\mathcal{C}_\Gamma^{-1}\mathcal{A}_\Gamma\boldsymbol{\phi}^\Gamma = k\boldsymbol{\phi}^\Gamma$ to update k and $\boldsymbol{\phi}^\Gamma$
for $\gamma \leftarrow \Gamma - 1$ *to 1* **do**
  Perform prolongation $\hat{\boldsymbol{\phi}}^\gamma = I_\alpha^{\gamma\leftarrow\gamma+1}\boldsymbol{\phi}^{\gamma+1}$
end

Algorithm 6: pV-Γ. The multigrid algorithm with the partial V-cycle.

scattering and fission source operators. The operators $\mathcal{A}_\gamma$, $\mathcal{B}_\gamma$, and $\mathcal{C}_\gamma$ are the leakage, scattering, and fission terms respectively on each grid γ in the low-order problem.

In Section 2.2 the diffusion algorithm is described where the right hand side of the fixed source problems is calculated using the most recent solution from the previous grid. This can be implemented for the transport multigrid algorithms for coarser energy grids. On any grid $\gamma > 1$ the flux for the right hand side is calculated using the averaged flux from most recent solution the previous energy grid.

$$\phi_g^\gamma = \sum_{g'\in\omega_g^{\gamma-1}} \phi_{g'}^{\gamma-1}, \quad \text{for} \quad \gamma > 1 \tag{3.32}$$

This uses the most updated calculation of the flux on each grid. This version of the algorithm

Solve $\boldsymbol{\psi} = \mathcal{T}^{-1}\mathcal{S}\hat{\boldsymbol{\phi}}^1 + \frac{1}{k}\mathcal{T}^{-1}\mathcal{P}\hat{\boldsymbol{\phi}}^1$
Calculate QD/NDA factors and average the high-order equations over angle to form $\mathcal{A}_1$, $\mathcal{B}_1$, $\mathcal{C}_1$
for $\gamma \leftarrow 1$ *to* $\Gamma - 1$ **do**
  Solve $\boldsymbol{\phi}^\gamma = \mathcal{A}_\gamma^{-1}\mathcal{B}_\gamma\hat{\boldsymbol{\phi}}^\gamma + \frac{1}{k}\mathcal{A}_\gamma^{-1}\mathcal{C}_\gamma\hat{\boldsymbol{\phi}}^\gamma$
  Perform homogenization in energy to form $\mathcal{A}_{\gamma+1}$, $\mathcal{B}_{\gamma+1}$, $\mathcal{C}_{\gamma+1}$
end
Solve the eigenvalue problem $\mathcal{C}_\Gamma^{-1}\mathcal{A}_\Gamma\boldsymbol{\phi}^\Gamma = k\boldsymbol{\phi}^\Gamma$ to update k and $\boldsymbol{\phi}^\Gamma$
for $m \leftarrow 1$ *to* μ **do**
  for $\gamma \leftarrow \Gamma - 1$ *to* γ^* **do**
    Perform prolongation $\hat{\boldsymbol{\phi}}^\gamma = I_\alpha^{\gamma\leftarrow\gamma+1}\boldsymbol{\phi}^{\gamma+1}$
  end
  for $\gamma \leftarrow \gamma^*$ *to* $\Gamma - 1$ **do**
    Solve $\boldsymbol{\phi}^\gamma = \mathcal{A}_\gamma^{-1}\mathcal{B}_\gamma\hat{\boldsymbol{\phi}}^{\gamma-1} + \frac{1}{k}\mathcal{A}_\gamma^{-1}\mathcal{C}_\gamma\hat{\boldsymbol{\phi}}^{\gamma-1}$
    Perform homogenization in energy to form $\mathcal{A}_{\gamma+1}$, $\mathcal{B}_{\gamma+1}$, $\mathcal{C}_{\gamma+1}$
  end
  Solve the eigenvalue problem $\mathcal{C}_\Gamma^{-1}\mathcal{A}_\Gamma\boldsymbol{\phi}^\Gamma = k\boldsymbol{\phi}^\Gamma$ to update k and $\boldsymbol{\phi}^\Gamma$
end
for $\gamma \leftarrow \Gamma - 1$ *to 1* **do**
  Perform prolongation $\hat{\boldsymbol{\phi}}^\gamma = I_\alpha^{\gamma\leftarrow\gamma+1}\boldsymbol{\phi}^{\gamma+1}$
end

Algorithm 7: $pW\text{-}\Gamma(\gamma^*, \mu)$. The multigrid algorithm with the partial W-cycle.

is shown in 8. Note that in this algorithm the initial guess for the Newton's iterations to solve the eigen problem is also calculated using the solution from the previous grid.

Another way to calculate the right hand side of the low-order equations of the first grid Λ_E^1 is to use the high-order transport solution from the transport sweep. Thus, in this case $\phi_g^1 = \tilde{\phi}_g$. On the coarser grids the right hand side is calculated using the corrected flux from the previous cycle. This version of the cycle is described in Algorithm 9.

The Figure 3.1 illustrates the partial V-cycles, pV-Γ, for methods with $\Gamma = 2 - 4$ algorithm that solves the LO equations on each grid a single time without nested loops. The pV cycle can also be viewed as the multilevel method with \-cycle (backslash cycle) [50]. Figure 3.2 shows the partial W-cycles, pW-Γ(μ,γ) for $\Gamma = 3$ with nested loops on each grid. The symbol γ indicates upon which grid nested cycles are performed and μ indicates the number of loops on that grid.

The algorithms move from the coarsest grid Λ_E^Γ towards the finest grid Λ_E^1 without solving group diffusion equations on any grid. This is shown on the cycle graphs by open circles. The prolongation procedure between grids uses one of versions of the interpolation operator $I_\alpha^{\gamma\leftarrow\gamma+1}$ described in Sec. 2.3. The subscript α indicates the type of interpolation

Solve $\boldsymbol{\psi} = \mathcal{T}^{-1}\mathcal{S}\boldsymbol{\phi}^1 + \frac{1}{k}\mathcal{T}^{-1}\mathcal{P}\boldsymbol{\phi}^1$
Calculate QD/NDA factors and average the high-order equations over angle to form $\mathcal{A}_1$, $\mathcal{B}_1$, $\mathcal{C}_1$
for $\gamma \leftarrow 1$ *to* $\Gamma - 1$ **do**
  if $\gamma = 1$ **then**
    Solve $\boldsymbol{\phi}^\gamma = \mathcal{A}_\gamma^{-1}\mathcal{B}_\gamma\hat{\boldsymbol{\phi}}^\gamma + \frac{1}{k}\mathcal{A}_\gamma^{-1}\mathcal{C}_\gamma\hat{\boldsymbol{\phi}}^\gamma$
  else
    Solve $\boldsymbol{\phi}^\gamma = \mathcal{A}_\gamma^{-1}\mathcal{B}_\gamma\boldsymbol{\phi}^{\gamma-1} + \frac{1}{k}\mathcal{A}_\gamma^{-1}\mathcal{C}_\gamma\boldsymbol{\phi}^{\gamma-1}$
  end
  Perform homogenization in energy to form $\mathcal{A}_{\gamma+1}$, $\mathcal{B}_{\gamma+1}$, $\mathcal{C}_{\gamma+1}$
end
Solve the eigenvalue problem $\mathcal{C}_\Gamma^{-1}\mathcal{A}_\Gamma\boldsymbol{\phi}^\Gamma = k\boldsymbol{\phi}^\Gamma$ to update k and $\boldsymbol{\phi}^\Gamma$
for $\gamma \leftarrow \Gamma - 1$ *to 1* **do**
  Perform prolongation $\hat{\boldsymbol{\phi}}^\gamma = I_\alpha^{\gamma\leftarrow\gamma+1}\boldsymbol{\phi}^{\gamma+1}$
end

Algorithm 8: pV-Γ. The multigrid algorithm with the partial V-cycle with the RHS of the low-order equations on Λ_E^γ for $\gamma > 1$ calculated using most recent solution from the previous grid ($\phi^{\gamma-1}$ for $\gamma > 1$).

- $\alpha = ce$: the correction factor based on constant approximation in energy,
- $\alpha = le$: the correction factor based on linear approximation in energy,
- $\alpha = lef$: the correction factor based on linear approximation in energy with factorization.

An important characteristic of a multigrid algorithm is the total number of low-order solves (N_{lo}) which is the number per transport iterations multiplied by the number of transport iterations N_t. For the given numbers of cycles and groups in each grids, the total number of group-wise low-order solves can be calculated as

$$N_{lo} = N_t \sum_{\gamma=1}^{\Gamma} G^\gamma + 1 \tag{3.33}$$

for the pV-Γ algorithm and

$$N_{lo} = N_t\Big(\sum_{\gamma=1}^{\Gamma} G^\gamma + \mu \sum_{\gamma=\gamma^*}^{\Gamma} G^\gamma\Big) + 1 \tag{3.34}$$

for the pW-$\Gamma(\gamma^*, \mu)$ algorithm.

Solve $\boldsymbol{\psi} = \mathcal{T}^{-1}\mathcal{S}\boldsymbol{\phi}^1 + \frac{1}{k}\mathcal{T}^{-1}\mathcal{P}\boldsymbol{\phi}^1$
Calculate QD/NDA factors and average the high-order equations over angle to form $\mathcal{A}_1$, $\mathcal{B}_1$, $\mathcal{C}_1$
for $\gamma \leftarrow 1$ *to* $\Gamma - 1$ **do**
  if $\gamma = 1$ **then**
    Solve $\boldsymbol{\phi}^\gamma = \mathcal{A}_\gamma^{-1}\mathcal{B}_\gamma\boldsymbol{\psi} + \frac{1}{k}\mathcal{A}_\gamma^{-1}\mathcal{C}_\gamma\boldsymbol{\psi}$
  else
    Solve $\boldsymbol{\phi}^\gamma = \mathcal{A}_\gamma^{-1}\mathcal{B}_\gamma\hat{\boldsymbol{\phi}}^\gamma + \frac{1}{k}\mathcal{A}_\gamma^{-1}\mathcal{C}_\gamma\hat{\boldsymbol{\phi}}^\gamma$
  end
  Perform homogenization in energy to form $\mathcal{A}_{\gamma+1}$, $\mathcal{B}_{\gamma+1}$, $\mathcal{C}_{\gamma+1}$
end
Solve the eigenvalue problem $\mathcal{C}_\Gamma^{-1}\mathcal{A}_\Gamma\boldsymbol{\phi}^\Gamma = k\boldsymbol{\phi}^\Gamma$ to update k and $\boldsymbol{\phi}^\Gamma$
for $\gamma \leftarrow \Gamma - 1$ *to 1* **do**
  Perform prolongation $\hat{\boldsymbol{\phi}}^\gamma = I_\alpha^{\gamma\leftarrow\gamma+1}\boldsymbol{\phi}^{\gamma+1}$
end

Algorithm 9: pV-Γ. The multigrid algorithm with the partial V-cycle with the RHS of the low-order equations on Λ_E^1 is calculated from the high-order transport solution ($\tilde{\phi}_g$ for $\gamma = 1$).

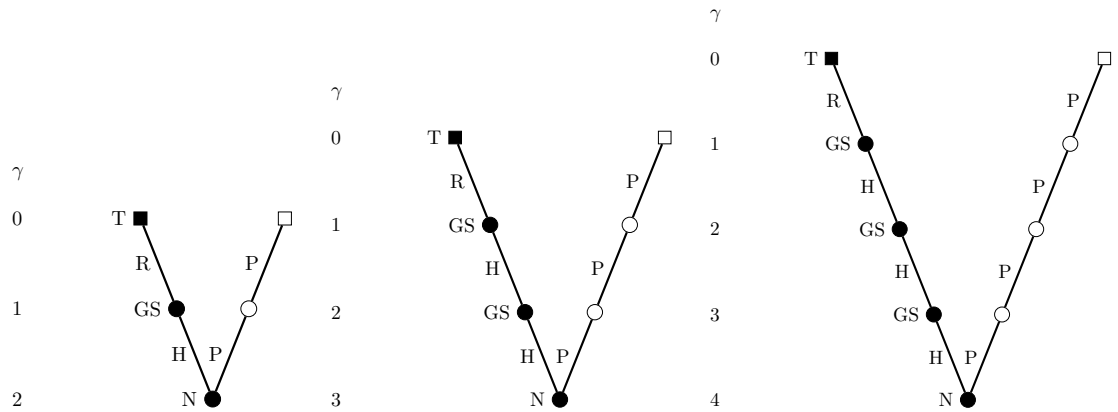

(a) pV-2 (b) pV-3 (c) pV-4

Figure 3.1: Multigrid pV cycles for grids with $\Gamma = 2 - 4$. GS - Gauss-Seidel iteration over groups on Λ_E^γ, R - projection over angle, H - homogenization over energy, N - Newton iteration, P - prolongation

3.5 Numerical Results

We now demonstrate performance of the developed methods in two test problems. Test A is a color-set problem defined by a checkerboard configuration of quarters of MOX and UO_2 diffined in Chapter 2. The geometry and dimensions are given in Figure 2.2. Test C consists of quarters

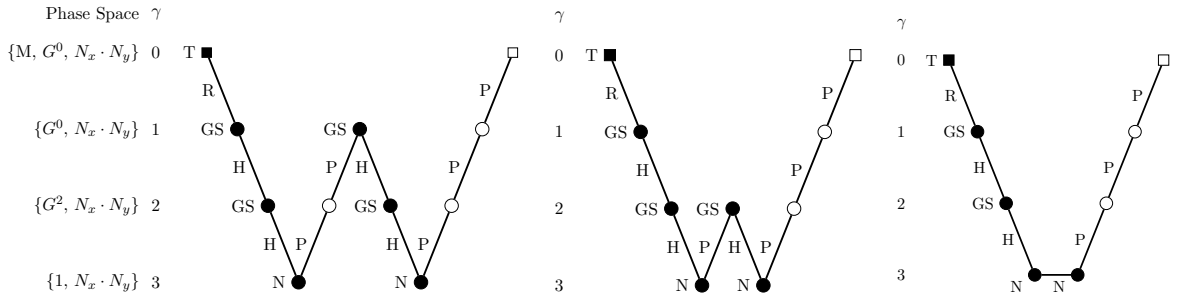

(a) pW-3(2,1) (b) pW-3(2,2) (c) pW-3(2,3)

Figure 3.2: Multigrid pW cycles for grids with $\Gamma = 3$. GS - Gauss-Seidel iteration over groups on Λ_E^γ, R - projection over angle, H - homogenization over energy, N - Newton iteration, P - prolongation

of MOX and UO_2 assemblies next to each other surrounded by water, demonstrated in Figure 3.3, with a 224×448 cell spatial mesh. The left boundary is reflective. The rest of boundaries are vacuum. The assembly design is the same as in Test A and the pin cell and discretization are illustrated in Figure 2.4. Test C has different physics with much more coupling between space and energy than Test A because of the large moderator regions.

We use quadruple-range angular quadrature set with 36 angles per octant (q461214) [27]. The transport stopping criteria of 10^{-6} is used. The transport equation is solved by the method short of characteristics with subcell balances [10]. The multigroup low-order equations and the transport equation are discretized on the same spatial mesh.

The performance of the method is evaluated by ability of the multigrid algorithm to accelerates transport iterations and to reduce computational work in solving the low-order equations. The fewest number of transport iterations expected to solve a test can be estimated by solving the original multigroup low-order equations until convergence on each transport iteration. Note that the iteration sequence begins with a diffusion initial guess which is found by solving low-order problems on a sequence of energy grids according to the given algorithm using the low-order factors calculated with isotropic angular flux.

In order to evaluate the performance of the methodology we look at two main indicators, the number of transport iterations and the number of low-order solves. The number of transport iterations N_t simply indicates the number of high-order sweeps performed. The number of low-order solves N_{lo} indicates the number of times the group-wise linear problems are solved on all the grids. The exact clock time to solve either the high- or low-order problem depends on the particular solvers and implementation in the code. Assuming the average clock time is T_t for the transport sweep and T_{lo} linear low-order solver than the total clock time approximately $T_{total} = T_t N_t + T_{lo} N_{lo}$. T_t changes with increase in number of angular directions involved

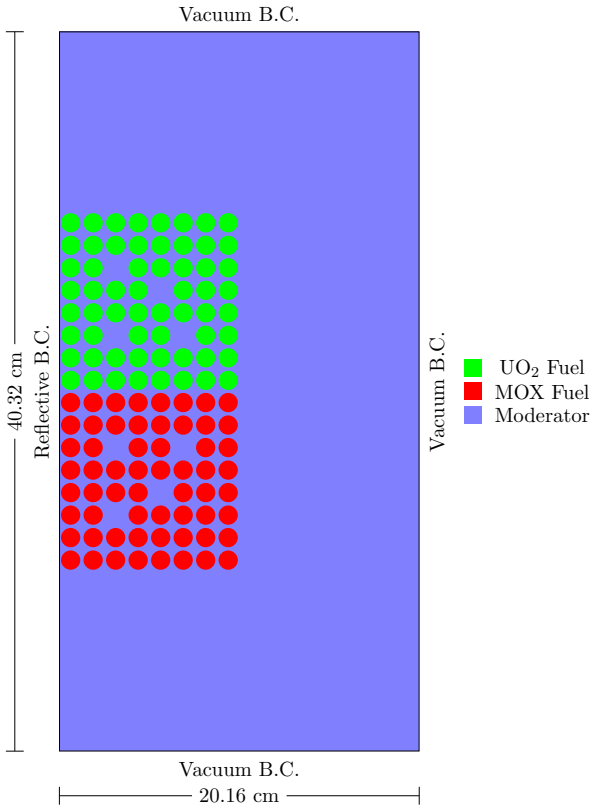

Figure 3.3: Test C geometry and configuration.

in solving the high-order transport equations. This part of the problem can be arbitrarily expensive. On the other hand N_t, and N_{lo} do not depend on the number of angular direction. They are mainly influenced by the physics of the problem. Minimizing the number of transport iterations should be one of highest priority. Minimizing the number of low-order solves can further improve the efficiency of the method. For implementations where the cost of the high-order and low-order solves are similar the importance of minimizing each of these numbers may change. Note that this analysis of the clock time does not include the overhead introduced by additional energy grids, however this overhead is not very significant compared to the high- and low-order solves and is easily parallelizable.

Within the system of low-order equations the dimensionality of the problem at each level is reduced by projection in energy. In contrast to traditional multi-grid methods, this homogenization is done by a nonlinear projection equations between levels. The results show that adding additional energy grids can make the transport iterations converge faster and reduce the work in the low order problem on each transport iteration. Once the number of grids is sufficient to get the fewest transport iterations with pV-cycle in the low-order problem, adding additional

grids will only increase the low-order work in each transport iteration without decreasing the number of transport iterations. The optimal number of grids depends on the choice of groups on each grid and the specific problem. Using more grids than this still accelerates the transport iterations very well, but it does not yield any futher reduction it the high-order work to justify the additional work in the low-order problem. The refinement on each energy grid effects behavior of the iterative methods. Performing multiple nested cycles on grids with few groups does not accelerate the convergence of the solution very much compared to multiple cycle on grids with many groups. A combination of grids behaves differently than separate sub sets of grids.

3.5.1 Analysis of Results with Multilevel QD Algorithms with Multigrid in Energy

The cross sections for these problems are obtained from the ENDF/B-V neutron group library [66]. This cross section library has 44 energy groups ($G = 44$) with 22 fast and 22 thermal groups. We present numerical results for several of the MLQD algorithms with different hierarchies of energy grids on which the LOQD equations are solved. The coarse energy grids used in these hierarchies are:

- $\Lambda_{E,22}$: 22 groups consisting of 11 fast and 11 thermal,
- $\Lambda_{E,8}$: 8 groups with 4 fast and 4 thermal,
- $\Lambda_{E,4}$: 4 groups with 2 fast and 2 thermal,
- $\Lambda_{E,2}$: 2 groups corresponding to fast and thermal energies.

The energy grids sequences are defined below. The energy bounds of these grids are discribed in Tables 2.3-2.5. The coarse groups are chosen to have approximately equal numbers of subgroups in each coarse group.

The results of the MLQD methods using different multigrid cycles are listed in Tables 3.1 and 3.2. These tables provide (i) the number of transport iterations (N_t), (ii) the total number low-order solves(N_{lo}), i.e. the number of times the groupwise LOQD equations were solved in each case. These results were found using the algorithm with the right hand side calculated using the corrected scalar flux. Note that one cycle of LO solves is performed before the transport iterations begin to generate an initial guess. The expected number of transport iterations to solve a problem can be determined, for example, by converging the solution of the multigroup LOQD equations on each transport iteration. The resulting number of transport iterations obtained this way for Test A is 11 and for Test C equals 9.

Table 3.1: Test A with 44 Group Cross Sections using MLQD with various prolongations.

Multigrid Algorithm	Prolongation Operator $I_{ce}^{\gamma\leftarrow\gamma+1}$			$I_{le}^{\gamma\leftarrow\gamma+1}$			$I_{lef}^{\gamma\leftarrow\gamma+1}$		
	N_t	N_{lo}	N_{lo}/G	N_t	N_{lo}	N_{lo}/G	N_t	N_{lo}	N_{lo}/G
Energy Grid Sequence {44,1}									
pV-2	21	991	22.5		N/A			N/A	
pW-2(1,2)	21	1013	23.0		N/A			N/A	
pW-2(2,1)	12	1171	26.6		N/A			N/A	
pW-2(3,1)	11	1486	33.8		N/A			N/A	
Energy Grid Sequence {44,2,1}									
pV-3	13	659	15.0	14	706	16.0		N/A	
pW-3(2,2)	13	701	15.9	14	751	17.1		N/A	
pW-3(2,1)	12	1176	26.7	13	1270	28.9		N/A	
pW-3(3,1)	11	1599	36.3	15	2069	47.0		N/A	
Energy Grid Sequence {44,8,1}									
pV-3	12	690	15.7	13	743	16.9		N/A	
pW-3(2,2)	12	869	19.8	13	869	19.8		N/A	
pW-3(2,1)	11	1273	28.9	11	1273	28.9		N/A	
Energy Grid Sequence {44,8,2,1}									
pV-4	12	716	16.3	14	826	18.8	15	881	20.0
pW-4(2,2)	12	859	19.5	13	925	21.0	13	925	21.0
pW-4(2,1)	11	1321	30.0	12	1431	32.5	13	1541	35.0

N/A - Not applicable on this grid sequence.

The advantage of the proposed multilevel methods is that computational work can be moved from the given fine energy grid to coarser ones minimizing the amount of calculations in solving multigroup low-order problems on a sequence of energy grids. The best MLQD method is one where the convergence is reached target number of transport iterations while also having the minimum number of LO solves per iteration. The presented numerical results for both tests show a significant reduction in low-order solves achieved by using multigrid algorithms.

The first two columns show results for methods with constant energy prolongations $I_{ce}^{\gamma\leftarrow\gamma+1}$. In order to get the target number of transport iterations for Test A with the two-grid method one needs the partial W-cycle pW-2(3,1) with three loops on the original energy grid on each transport iteration. This results in solving groupwise LOQD equations 1485 times, this however is an average of only 2.90 solves of the group LOQD problem per group per transport iteration. The pV-3 on the {44,2,1} energy grid sequence requires fewer transport iterations than the two-grid pV-2 which demonstrates that additional energy grids can accelerate the transport iterations. The {44,2,1} energy grid sequence still requires the algorithm pW-3(3,1) with 3 loops on the original energy grid on each transport iteration to get minimum number of transport

Table 3.2: Test C with 44 Group Cross Sections using MLQD with various prolongations.

Multigrid	Prolongation Operator								
	$I_{ce}^{\gamma \leftarrow \gamma+1}$			$I_{le}^{\gamma \leftarrow \gamma+1}$			$I_{lef}^{\gamma \leftarrow \gamma+1}$		
Algorithm	N_t	N_{lo}	N_{lo}/G	N_t	N_{lo}	N_{lo}/G	N_t	N_{lo}	N_{lo}/G
Energy Grid Sequence {44,1}									
pV-2	32	1486	33.8		N/A			N/A	
pW-2(2,2)	32	1519	34.5		N/A			N/A	
pW-2(2,1)	17	1621	36.8		N/A			N/A	
pW-2(3,1)	12	1666	37.9		N/A			N/A	
pW-2(4,1)	10	1711	38.9		N/A			N/A	
pW-2(5,1)	9	1936	44.0		N/A			N/A	
Energy Grid Sequence {44,2,1}									
pV-3	13	659	15.0	14	706	16.0		N/A	
pW-3(2,2)	13	701	15.9	14	751	17.0		N/A	
pW-3(2,1)	8	847	19.3	9	941	21.4		N/A	
Energy Grid Sequence {44,8,1}									
pV-3	20	1114	25.3	20	1114	25.3		N/A	
pW-3(2,2)	11	745	16.9	11	745	16.9		N/A	
pW-3(2,1)	11	1273	28.9	11	1273	28.9		N/A	
pW-3(3,1)	9	1485	33.8	9	1591	36.2		N/A	
Energy Grid Sequence {44,8,2,1}									
pV-4	9	551	12.5	10	606	13.8	10	606	13.8

N/A - Not applicable on this grid sequence.

iterations. This slightly increases the total number of low-order solves compared to the best two-grid method because of the additional grid with two groups. The three-grid method with grids {44,8,1} only requires 2 loops on the original energy grid on each transport iteration, i.e. pW-3(2,1). This results in a 17% reduction on low-order solves compared to the best two-grid method. The four-grid method pW-4(2,1) decreases the number of groupwise LO solves by only 14 % compared to the best two-grid method and does not improve over the best three-grid cycle. As a result pW-3(2,1) on the {44,8,1} has the minimum number of transport iterations and the fewest number LO solves.

In Test C the two-grid method needs the partial W-cycle pW-2(5,1) with 5 loops on the original groups on each transport iteration to achieve the target number of transport iterations solving groupwise LOQD equations 1936 times. The three-grid method pW-3(2,1) on the {44,2,1} energy grid sequence reduces this amount of LO solves by 51 %. The {44,8,1} three-grid methods require more low-order solves and showed no advantage over the {44,2,1} three-grid methods. The four-grid method decreases further the computational work in low-order equations and only requires a simple pV-4 cycle. The cycle pV-4 yields the target number

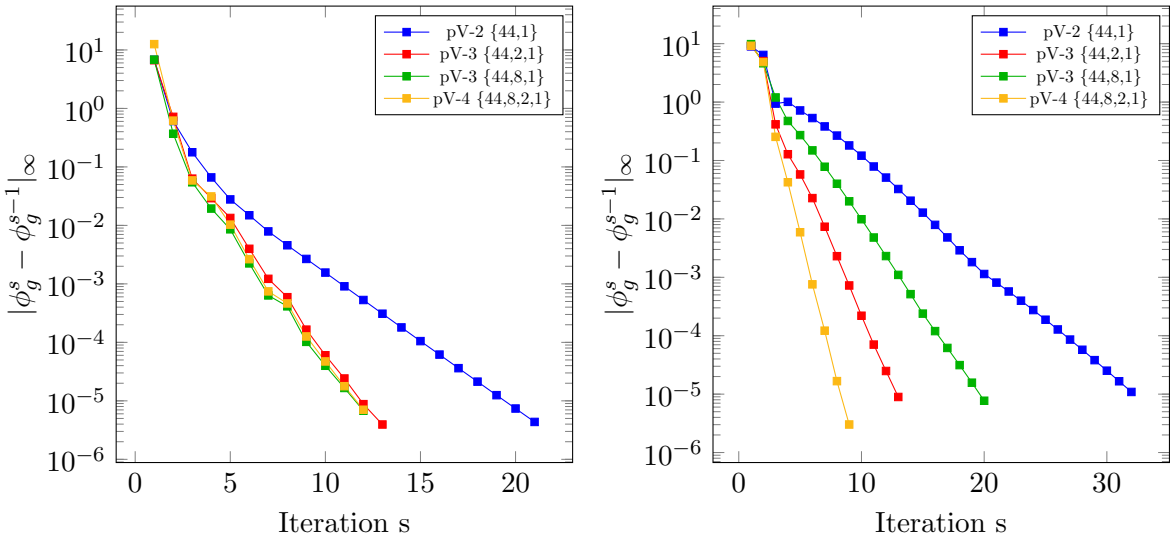

(a) Test A (b) Test C

Figure 3.4: Convergence histories of transport iterations of the MLQD method with pV-cycles on hierarchies of grids with different number of levels and constant energy prolongation.

of transport iterations with a 42 % reduction of low-order solves compared to the best {44,2,1} energy grid cycle and 72 % reduction compared to the best two-grid method. We also notice that in this test pW-3(2,1) on grids {44,2,1} converged in 8 transport iterations rather than the 9 achieved if the multigroup LOQD equations are converged on each transport iterations. This is an illustration of a case in which the multilevel algorithms are capable in further reduction of transport iterations.

For the three-grid methods in Test A is can be seen that the sequence with more groups in the second grid ({44,8,1}) yielded fewer low-order solves. However for the three-grid methods in Test C the results show that fewer groups in the second grid ({44,2,1}) required less work in the low-order problem. This demonstrates that for different types of problems various sets of grids can behave differently.

The last four columns show results for methods with linear in energy prolongations $I_{le}^{\gamma \leftarrow \gamma+1}$ and linear in energy prolongations with factorization $I_{lef}^{\gamma \leftarrow \gamma+1}$. The results with these prolongation operators do not show any reduction in number of transport iterations or low-order solves compared to the constant energy prolongations.

Figures 3.4a and 3.4b show the convergence of the scalar flux for various energy grids with pV cycles with constant energy prolongations. These plots show that more energy grids can increase the rate of convergence. For Test A the methods with three or four grids all converge similarly. For Test C there is a significant difference in the convergence rate for each set of grids. Figures

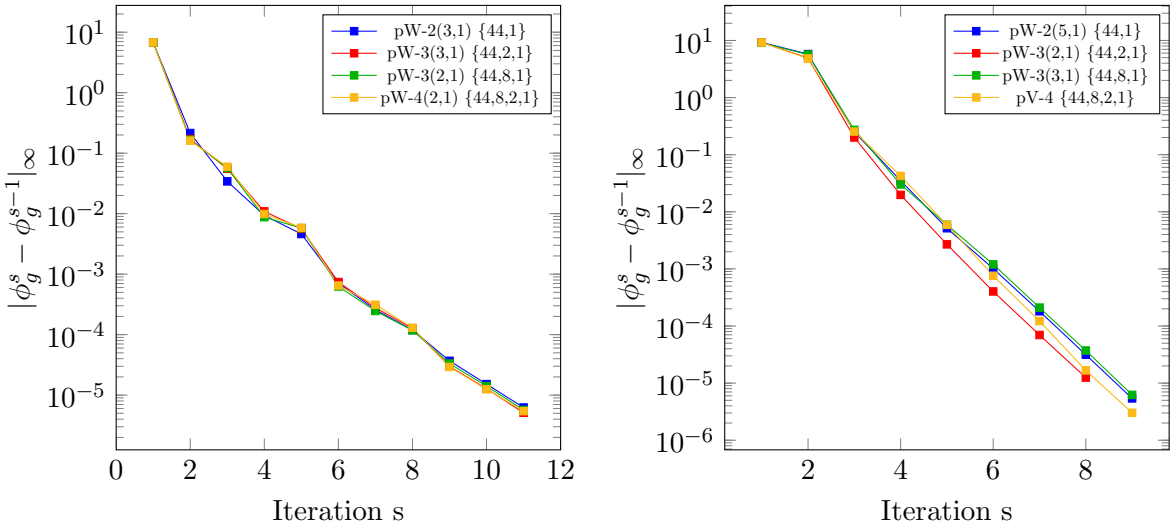

(a) Test A (b) Test C

Figure 3.5: Convergence histories of transport iterations of the MLQD method with pW-cycles on hierarchies of grids with different number of levels and constant energy prolongation.

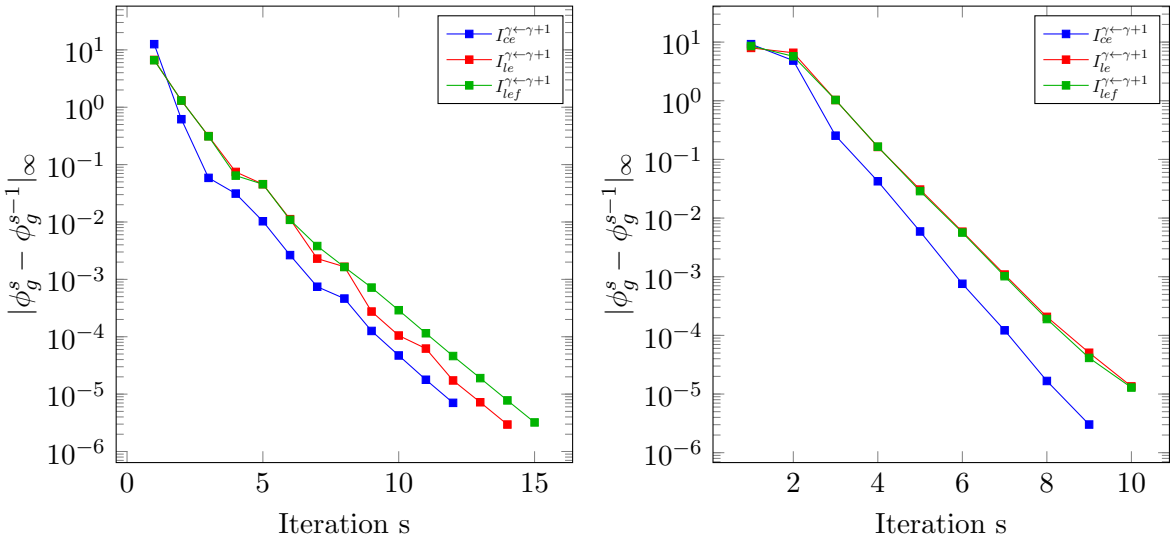

(a) Test A (b) Test C

Figure 3.6: Convergence histories of transport iterations of the MLQD method with pV-4 cycle on {44,8,2,1} with different prolongation operators.

3.5a and 3.5b show the convergence of the scalar flux for various energy grids with the cycle that results in the fewest transport iterations and with constant energy prolongations. These figures both show that the fastest converging cycle on each set of grids behave very similarly. Figures 3.6a and 3.6b demonstrate the convergence of the pV cycle on 4 grids with different prolongation operators. These results show that the linear in energy prolongation operators do not have a significant advantage over the constant energy prolongations.

3.5.2 Analysis of Results with Multilevel NDA Algorithms with Multigrid in Energy

The multilevel NDA (MLNDA) method is evaluated using the same test problems described previously and shown in Figure 2.2 and Figure 3.3.

Tests with 44 Energy Groups

The first set of problems use the same 44-group ENDF/B-V cross-sections. These tests are solved with algorithms based on three different energy-grid sequences.

The obtained results with different prolongation operators are summarized in Tables 3.3 and 3.4. These results were found using the algorithm with the right hand side calculated using the corrected scalar flux. The least number of transport iterations for these problems is 11 for Test A and 9 for Test C. The presented results demonstrate that algorithms with a pV cycle improve the rate of convergence of transport iterations if we add extra coarse grids (see the results for pV-2, pV-3, and pV-4). However none of these algorithms has the target number of transport iterations. The performance of multigrid algorithms can be improved by using different cycles. Table 3.3 shows that for Test A the algorithms with the minimum number of transport iterations are pW-2(3,1), pW-3(3,1), pW-3(2,1), and pW-4(2,1) for the grid structures {44,1}, {44,2,1}, {44,8,1}, and {44,8,2,1}, respectively. Of these the most efficient algorithm is pW-3(2,1) on the grid structure {44,8,1} which requires 17% fewer LO solves than pW-2(3,1), 20% fewer that pW-3(3,1) on grids {44,2,1} and 4% fewer than pW-4(2,1). The four-grid algorithm pW-4(2,1) is better than the two-grid algorithm pW-2(3,1) and the three grid algorithm pW-3(3,1) on grid structure {44,2,1}. However the additional grid does not give pW-4(2,1) any advantage over the best three-grid method and instead increases the total number of LO solves slightly. For Test C pW-2(4,1), pW-3(2,1), pW-3(3,2), and pW-4(2,4) demonstrate fastest convergence of transport iterations for grids {44,1}, {44,2,1}, {44,8,1}, and {44,8,2,1} respectively. The four-grid cycle, pW-4(2,4), is the most efficient requiring 65% fewer LO solves than pW-2(5,1) and 20% fewer than the second best cycle pW-3(3,2) on grids {44,8,1}.

Results for different ways of calculating the right hand side (RHS) are summarized in Tables 3.5 and 3.6. The first three columns of data show results with the RHS calculated from the

Table 3.3: Test A with 44 Group Cross Sections using MLNDA with various prolongations.

Multigrid Algorithm	Prolongation Operator								
	$I_{ce}^{\gamma \leftarrow \gamma+1}$			$I_{le}^{\gamma \leftarrow \gamma+1}$			$I_{lef}^{\gamma \leftarrow \gamma+1}$		
	N_t	N_{lo}	N_{lo}/G	N_t	N_{lo}	N_{lo}/G	N_t	N_{lo}	N_{lo}/G
2 Energy Grid Sequence {44,1}									
pV-2	21	991	22.5		N/A			N/A	
pW-2(2,2)	21	1013	23.0		N/A			N/A	
pW-2(2,1)	12	1171	26.6		N/A			N/A	
pW-2(3,1)	11	1531	34.8		N/A			N/A	
3 Energy Grid Sequence {44,2,1}									
pV-3	13	659	15.0	14	706	16.0		N/A	
pW-3(2,2)	13	701	15.9	14	751	17.0		N/A	
pW-3(2,1)	12	1176	26.7	13	1270	28.9		N/A	
pW-3(3,1)	11	1599	36.3	15	2069	47.0		N/A	
3 Energy Grid Sequence {44,8,1}									
pV-3	12	690	15.7	13	743	16.9		N/A	
pW-3(2,2)	13	869	19.8	13	869	19.8		N/A	
pW-3(2,1)	11	1273	28.9	11	1273	28.9		N/A	
4 Energy Grid Sequence {44,8,2,1}									
pV-4	12	716	16.3	14	826	18.8	15	881	20.0
pW-4(2,2)	13	925	21.0	13	925	21.0	13	925	21.0
pW-4(2,1)	11	1321	30.0	12	1431	32.5	13	1541	35.0

N/A - Not applicable on this grid sequence.

Table 3.4: Test C with 44 Group Cross Sections using MLNDA with various prolongations.

Multigrid	Prolongation Operator								
	$I_{ce}^{\gamma\leftarrow\gamma+1}$			$I_{le}^{\gamma\leftarrow\gamma+1}$			$I_{lef}^{\gamma\leftarrow\gamma+1}$		
Algorithm	N_t	N_{lo}	N_{lo}/G	N_t	N_{lo}	N_{lo}/G	N_t	N_{lo}	N_{lo}/G
2 Energy Grid Sequence {44,1}									
pV-2	31	1441	32.8		N/A			N/A	
pW-2(2,2)	31	1473	33.5		N/A			N/A	
pW-2(2,1)	16	1531	34.8		N/A			N/A	
pW-2(3,1)	11	1576	35.8		N/A			N/A	
pW-2(4,1)	9	1621	36.8		N/A			N/A	
3 Energy Grid Sequence {44,2,1}									
pV-3	13	659	15.0	14	706	16.0		N/A	
pW-3(2,2)	13	701	15.9	14	751	17.1		N/A	
pW-3(2,1)	9	894	20.3	9	1317	29.9		N/A	
3 Energy Grid Sequence {44,8,1}									
pV-3	19	1061	24.1	19	1061	24.1		N/A	
pW-3(2,2)	10	683	15.5	11	745	16.9		N/A	
pW-3(3,2)	9	702	16.0	11	835	19.0		N/A	
4 Energy Grid Sequence {44,8,2,1}									
pV-4	10	606	13.8	12	716	16.3	12	716	16.3
pW-4(2,4)	9	561	12.8	11	673	15.3	11	673	15.3

N/A - Not applicable on this grid sequence.

corrected flux on the previous cycle ($\hat{\phi}^{\gamma}$). The second set of results in the next three columns show the variant where the RHS on the first grid is calculated using the corrected flux ($\tilde{\phi}$ for $\gamma = 1$) and for the coarser grids the RHS is calculated from the most recent solution on the previous grid ($\phi^{\gamma-1}$ for $\gamma > 1$). The last set of results show results where the RHS is calculated using the high-order flux on the first grid ($\tilde{\phi}$ for $\gamma = 1$) and the corrected flux used for the coarser grids ($\hat{\phi}^{\gamma}$ for $\gamma > 1$).

In Test A the different methods for calculating the RHS behave the same for most of the sets of cycles and grids with only a few exceptions. The RHS calculated from $\phi^{\gamma-1}$ behaved the same as the corrected RHS except for the grids {44,2,1} where the pV-3 cycle took one less transport iteration and the pW-3(3,1) cycle took three more transport iterations. The RHS calculated from $\tilde{\phi}$ took four fewer iterations for cycle pV-2 on {44,1} and two more iterations for cycle pW-3(2,1) on {44,8,1}. In Test C the RHS calculated from $\phi^{\gamma-1}$ consistently took more transport iterations than the corrected RHS. For some of the grids this is a very significant number of iterations. The transport RHS took fewer iterations than the corrected RHS for cycles pV-2 and pW-2(2,1) on {44,1} and cycle pV-3 on {44,2,1}. These results demonstrate that neither the RHS calculated from $\phi^{\gamma-1}$ nor the RHS calculated from $\tilde{\phi}$ reduce the work

Table 3.5: Test A with 44 Group Cross Sections using MLNDA with various RHS calculations.

Multigrid	Right Hand Side Source								
	$\hat{\phi}^{\gamma}$			$\phi^{\gamma-1}$ for $\gamma > 1$			$\tilde{\phi}$ for $\gamma = 1$		
Algorithm	N_t	N_{lo}	N_{lo}/G	N_t	N_{lo}	N_{lo}/G	N_t	N_{lo}	N_{lo}/G
2 Energy Grid Sequence {44,1}									
pV-2	21	991	22.5	21	991	22.5	17	811	18.4
pW-2(2,1)	12	1171	26.6	12	1171	26.6	12	1171	26.6
pW-2(3,1)	11	1531	34.8	11	1621	36.8	11	1621	36.8
3 Energy Grid Sequence {44,2,1}									
pV-3	13	659	15.0	12	612	13.9	13	659	15.0
pW-3(2,1)	12	1176	26.7	12	1223	27.8	12	1223	27.8
pW-3(3,1)	11	1599	36.3	14	1975	44.9	11	1693	38.5
3 Energy Grid Sequence {44,8,1}									
pV-3	12	690	15.7	12	690	15.7	12	690	15.7
pW-3(2,1)	11	1273	28.9	11	1273	28.9	13	1379	31.3
4 Energy Grid Sequence {44,8,2,1}									
pV-4	12	716	16.3	12	716	16.3	12	716	16.3
pW-4(2,1)	11	1321	30.0	11	1321	30.0	11	1321	30.0

Table 3.6: Test C with 44 Group Cross Sections using MLNDA with various RHS calculations.

Multigrid	Right Hand Side Source								
	$\hat{\phi}^{\gamma}$			$\phi^{\gamma-1}$ for $\gamma > 1$			$\tilde{\phi}$ for $\gamma = 1$		
Algorithm	N_t	N_{lo}	N_{lo}/G	N_t	N_{lo}	N_{lo}/G	N_t	N_{lo}	N_{lo}/G
2 Energy Grid Sequence {44,1}									
pV-2	31	1441	32.8	31	1441	32.8	27	1261	28.7
pW-2(2,1)	16	1531	34.8	18	1711	38.9	15	1396	31.7
pW-2(3,1)	11	1576	35.8	12	1711	38.9	11	1486	33.8
pW-2(4,1)	9	1621	36.8	11	2161	49.1	9	1621	36.8
3 Energy Grid Sequence {44,2,1}									
pV-3	13	659	15.0	52	2492	56.6	11	565	12.8
pW-3(2,1)	9	894	20.3	40	3855	87.6	9	894	20.3
3 Energy Grid Sequence {44,8,1}									
pV-3	19	1061	24.1	30	1644	37.4	19	1061	24.1
pW-3(2,2)	10	683	15.5	20	1303	29.6	10	683	15.5
pW-3(3,2)	9	702	16.0	11	853	19.4	9	702	16.0
4 Energy Grid Sequence {44,8,2,1}									
pV-4	10	606	13.8	49	2751	62.5	10	606	13.8
pW-4(2,4)	9	561	12.8	9	571	13.0	9	561	12.8

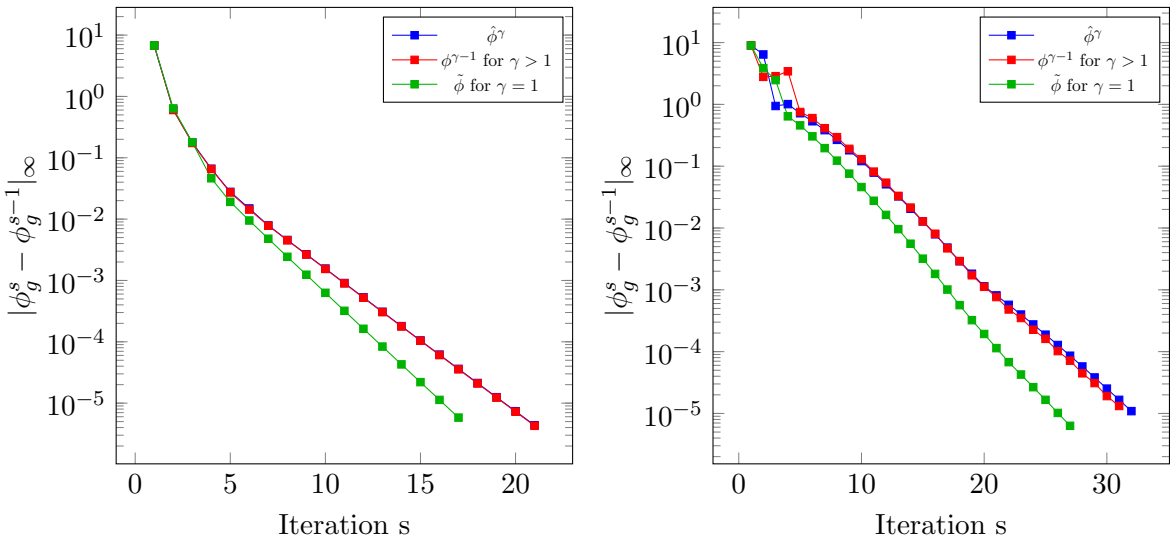

(a) Test A (b) Test C

Figure 3.7: Convergence histories of transport iterations of the MLNDA method with pV-2 cycle on {44,1} with different right hand sides.

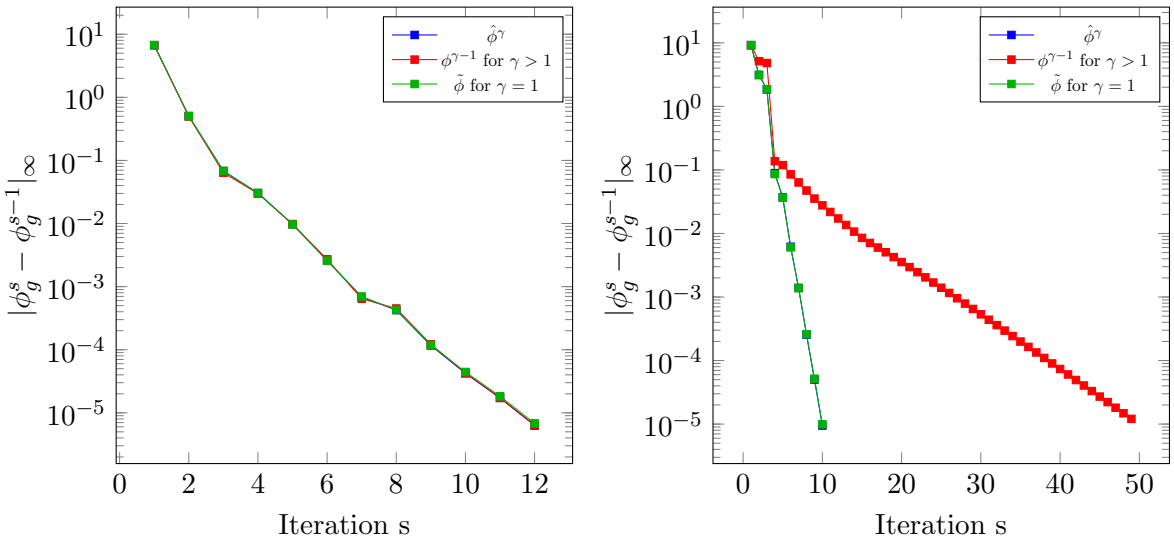

(a) Test A (b) Test C

Figure 3.8: Convergence histories of transport iterations of the MLNDA method with pV-4 cycle on {44,8,2,1} with different right hand sides.

in the high-order or low-order problem for the fastest converging algorithms. Additionally the RHS calculated from $\phi^{\gamma-1}$ can significantly slow the convergence of some test problems.

The convergence of the transport solution for the three variants of calculating the RHS are illustrated in Figures 3.7 and 3.8. Figure 3.7 shows the convergence for the pV-2 cycle on grids {44,1} for Test A and C. These figures show that the RHS calculated from $\tilde{\phi}$ converges faster than the corrected RHS. The RHS calculated from $\phi^{\gamma-1}$ converges very similarity to the corrected RHS. Figure 3.8 shows the convergence for the pV-4 cycle on grids {44,8,2,1} for Test A and C. For Test A all three versions converge with the same behavior. In Test C the RHS calculated from $\phi^{\gamma-1}$ converges much slower than the other methods and the convergence of the corrected RHS and RHS calculated from $\tilde{\phi}$ is almost indistinguishable.

Tests with 238 Energy Groups

The same test problems were defined using the 238-group cross sections from the ENDF/B-VII cross section libraries with 148 fast and 90 thermal groups. The tests with 238 groups are solved with algorithms that use from 2 to 5 energy grids. The coarse energy grids used in the multilevel hierarchies are:

- $\Lambda_{E,44}$: 44 groups consisting of 22 fast and 22 thermal, corresponding to the ENDF/B 44-group cross section library
- $\Lambda_{E,22}$: 22 groups consisting of 11 fast and 11 thermal,
- $\Lambda_{E,8}$: 8 groups with 4 fast and 4 thermal,
- $\Lambda_{E,4}$: 4 groups with 2 fast and 2 thermal,
- $\Lambda_{E,2}$: 2 groups corresponding to fast and thermal energies.

These results were found using the algorithm with the right hand side calculated using the corrected scalar flux.

Test A can be solved with a minimum of 12 transport iterations while Test C requires at least 9 transport iterations. The results for various multigrid algorithms are shown in Tables 3.7a and 3.7b. The most efficient algorithm in Test A is pV-4 on the energy grid structure {238,8,2,1}. This algorithm requires 3% fewer LO solves than the next best algorithm pW-3(2,2) on grids {238,8,1}, 15% fewer than the five-grid method pV-5, and 71% fewer than the best two-grid method pW-2(4,1). In Test C the best algorithm is pW-5(2,5) on grids {238,44,8,2,1}. It requires 67% fewer LO solves than MA-2(4,1), 35% fewer than pW-3(2,1) on grids {238,2,1}, 11% fewer than pW-4(2,2) on grids {238,44,2,1}.

Tables 3.8 and 3.9 summarize the results for the methods applied to solve the test problems defined with different numbers of original energy groups and hence different levels of resolution of

Table 3.7: Results with 238 Group Cross Sections using MLNDA.

(a) Test A

Multigrid Algorithm	Prolongation Operator $I_{ce}^{\gamma \leftarrow \gamma+1}$		
	N_t	N_{lo}	N_{lo}/G
2 Energy Grid Sequence {238,1}			
pV-2	25	6215	26.1
pW-2(2,2)	25	6241	26.2
pW-2(2,1)	14	7171	30.1
pW-2(3,1)	13	9083	38.2
pW-2(4,1)	12	11234	47.2
3 Energy Grid Sequence {238,2,1}			
pV-3	15	3857	16.2
pW-3(2,2)	15	3905	16.4
pW-3(2,1)	12	6267	26.3
3 Energy Grid Sequence {238,8,1}			
pV-3	13	3459	14.5
pW-3(2,3)	13	3473	14.6
pW-3(2,2)	12	3329	14.0
4 Energy Grid Sequence {238,8,2,1}			
pV-4	12	3238	13.6
4 Energy Grid Sequence {238,44,2,1}			
pV-4	13	3991	16.8
pW-4(2,3)	13	4033	16.9
pW-4(2,2)	12	4317	18.1
5 Energy Grid Sequence {238,44,8,2,1}			
pV-5	12	3810	16.0

(b) Test C

Multigrid Algorithm	Prolongation Operator $I_{ce}^{\gamma \leftarrow \gamma+1}$		
	N_t	N_{lo}	N_{lo}/G
2 Energy Grid Sequence {238,1}			
pV-2	33	8127	34.1
pW-2(2,2)	33	8161	34.1
pW-2(2,1)	18	8844	37.2
pW-2(3,1)	12	8605	36.2
pW-2(4,1)	9	8844	37.2
3 Energy Grid Sequence {238,2,1}			
pV-3	15	3857	16.2
pW-3(2,2)	15	3905	16.4
pW-3(2,1)	9	4580	19.2
3 Energy Grid Sequence {238,8,1}			
pV-3	20	5188	21.8
pW-3(2,2)	11	3073	12.9
pW-3(3,2)	10	2907	12.2
pW-3(2,1)	11	5682	23.9
pW-3(3,1)	9	6917	29.0
4 Energy Grid Sequence {238,8,2,1}			
pV-4	10	2740	11.5
pW-4(2,2)	10	2861	12.0
pW-4(2,1)	9	4732	19.9
4 Energy Grid Sequence {238,44,2,1}			
pV-4	13	3991	16.8
pW-4(2,3)	13	4033	16.9
pW-4(2,2)	9	3321	14.0
5 Energy Grid Sequence {238,44,8,2,1}			
pV-5	10	3224	13.5
pW-5(2,5)	9	2941	12.4

Table 3.8: Comparison of Test A using MLNDA based algorithms

Multigrid Algorithm	Test with 44 Groups		Test with 238 Groups	
	N_t	N_{lo}/G	N_t	N_{lo}/G
	Energy Grid Sequence {44,1}		Energy Grid Sequence {238,1}	
pV-2	21	22.5	25	26.1
pW-2(2,1)	12	26.6	14	30.1
pW-2(3,1)	11	34.8	13	38.2
	Energy Grid Sequence {44,2,1}		Energy Grid Sequence {238,2,1}	
pV-3	13	15.0	15	16.2
pW-3(2,2)	13	15.9	15	16.4
pW-3(2,1)	12	26.7	12	26.3
	Energy Grid Sequence {44,8,1}		Energy Grid Sequence {238,8,1}	
pV-3	12	15.7	13	14.5
pW-3(2,2)	13	19.8	12	14.0
	Energy Grid Sequence {44,8,2,1}		Energy Grid Sequence {238,8,2,1}	
pV-4	12	16.3	12	16.0

Table 3.9: Comparison of Test C using MLNDA based algorithms

Multigrid Algorithm	Test with 44 Groups		Test with 238 Groups	
	N_t	N_{lo}/G	N_t	N_{lo}/G
	Energy Grid Sequence {44,1}		Energy Grid Sequence {238,1}	
pV-2	31	32.8	33	34.1
pW-2(2,1)	16	34.8	18	37.2
pW-2(3,1)	11	35.8	12	36.2
pW-2(4,1)	9	36.8	9	37.2
	Energy Grid Sequence {44,2,1}		Energy Grid Sequence {238,2,1}	
pV-3	13	15.0	15	16.2
pW-3(2,1)	9	20.3	9	19.2
	Energy Grid Sequence {44,8,1}		Energy Grid Sequence {238,8,1}	
pV-3	19	24.1	15	16.2
pW-3(2,2)	10	15.5	11	12.9
pW-3(3,2)	9	16.0	10	12.2
	Energy Grid Sequence {44,8,2,1}		Energy Grid Sequence {238,8,2,1}	
pV-4	10	13.8	10	11.5

Table 3.10: Hybrid Cycles with 44 Group Cross Sections using MLQD based algorithms.

(a) Test A

Multigrid Algorithm	N_t	N_{lo}	N_{lo}/G
Energy Grid Sequence {44,1}			
pW-2(3,1) x12	11	1531	34.80
pW-2(3,1) x6 - pV-2 x6	11	1081	24.57
Energy Grid Sequence {44,2,1}			
pW-3(3,1) x12	11	1599	36.34
pW-3(3,1) x2 - pV-3 x10	11	753	17.11
Energy Grid Sequence {44,8,1}			
pW-3(2,1) x12	11	1273	28.93
pW-3(2,1) x2 - pV-3 x10	11	743	16.89
Energy Grid Sequence {44,8,2,1}			
pW-4(2,1) x12	11	1321	30.02
pW-4(2,1) x2 - pV-4 x10	11	771	17.52

(b) Test C

Multigrid Algorithm	N_t	N_{lo}	N_{lo}/G
Energy Grid Sequence {44,1}			
pW-2(5,1) x10	9	1936	44.00
pW-2(5,1) x6 - pV-2 x4	9	1531	34.80
Energy Grid Sequence {44,2,1}			
pW-3(2,1) x9	8	847	19.25
pW-3(2,1) x4 - pV-3 x5	9	659	14.98
Energy Grid Sequence {44,8,1}			
pW-3(3,1) x10	9	1485	33.75
pW-3(3,1) x6 - pV-3 x3	9	1167	26.52

neutron transport physics. These data allow comparing performance of individual algorithms in the same reactor-physics problem with significantly different number of groups. The results show that each algorithm has almost the same numbers of transport iterations in both cases and close values of such average performance parameters as the number of LO solves per group (N_{lo}/G). This demonstrates that the effectiveness of this multigrid methodology is almost independent of numbers of energy groups.

3.5.3 Analysis of Results with Hybrid Cycle with MLQD

Analysis of convergence histories of the proposed methods showed that in some cases different multigrid algorithms have close convergence rates during second half of transport iterations. The main differences in convergence occur on the first couple transport iterations. This suggests that it is possible to further improve efficiency of the methods by taking advantage of algorithms with hybrid multigrid cycles. For thee first few transport iterations the hybrid multilevel methods use however many nested cycles are necessary to ensure the fastest convergence of those iterations. For the rest of the transport transport iterations the cheapest cycle, a pV cycle, is used.

Table 3.10 shows the results for some hybrid cycles compared to the best method for each particular energy grid sequence. They show that using certain hybrid cycles improved further performance of these multilevel methods. We notice that in Test A the hybrid algorithm on grids {44,2,1} requires the smallest numbers of transport iterations and of total LO solves that is equal to 743. This is a 41% reduction in the total number of LO solves compared to pW-3(2,1)

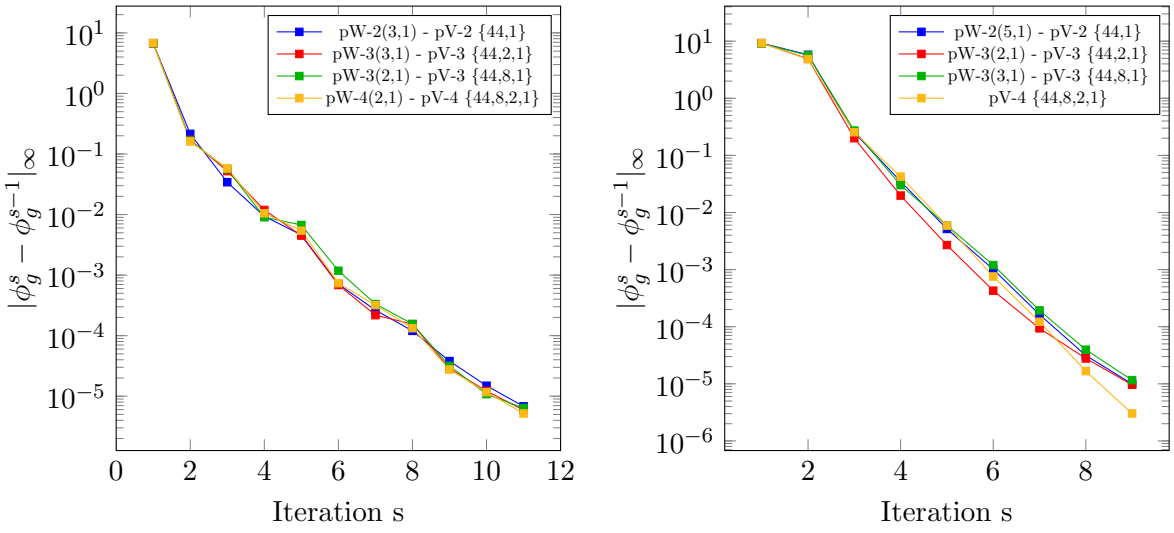

(a) Test A Hybrid Cycles

(b) Test C Hybrid Cycles

Figure 3.9: Convergence histories of transport iterations of the MLQD method on hierarchies of grids with different number of levels.

algorithm on the same grids. The hybrid cycles also demonstrate reduction in LO solves for each of the other sequences of energy grids. In Test C the best cycle is the four-grid cycle pV-4 which is already the cheapest cycle so there is no need to use hybrid cycles.

Figures 3.9a and 3.9b show the convergence of the scalar flux for hybrid cycles with different sets of energy grids. These hybrid cycles converge very similar to the pW cycles in Figures 3.5a and 3.5b even for the iterations were a pV cycle is used.

3.6 Coarse Grid Multilevel NDA and QD

In the presented above NDA and QD methods, the first energy grid (Λ_E^1) on which the low-order equations are formulated is the original energy grid Λ_E of the given transport problem. We now present a version of the proposed multilevel methodology such that the first energy grid has multiple groups and is coarser than the original transport energy grid $G^1 < G$. The first low-order energy grid is defined by sets of groups from the original transport grid ω_p^1. This yields a set of low-order equations which have reduced dimensionality on every grid.

This set of equations is solved using the multigrid algorithm described in Section 3.4. Figure 3.10 demonstrates a pV-3 cycle for the coarse grid method. It also shows that the dimensionality of the energy grid is different between the grids $\gamma = 0$ and $\gamma = 1$. The distinguishing feature of the algorithm shown in Figure 3.10 is that the projection step R is a projection in angle and

homogenization over energy.

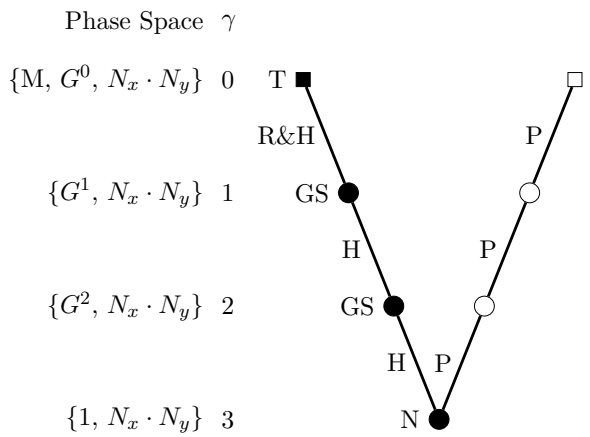

Figure 3.10: Multigrid pV-3 cycle with coarse energy grids. GS - Gauss-Seidel iteration over groups on Ω_E^γ, R - projection over angle, H - homogenization over energy, N - Newton iteration, P - prolongation

The set of NDA equations in this coarser energy space are identical to the equations (3.11) except the cross sections and coefficients on the first level $\gamma = 1$ are derived by averaging with high-order transport scalar flux $\tilde{\phi}_g$. The cross sections have the following form:

$$\bar{\chi}^1_{g,i,j} = \sum_{g\in\omega^1_p} \chi_{g,i,j}\,, \quad \bar{\Sigma}^1_{s,g'\to g,i,j} = \frac{\sum_{g'\in\omega^1_{g'}} \left(\sum_{g\in\omega^1_p} \Sigma_{s,g'\to g,i,j}\right) \tilde{\phi}_{g',i,j}}{\sum_{g'\in\omega^1_{g'}} \tilde{\phi}_{g',i,j}}\,, \tag{3.35a}$$

$$\bar{\Sigma}^1_{t,g,i,j} = \frac{\sum_{g\in\omega^1_p} \Sigma_{t,g,i,j}\tilde{\phi}_{g,i,j}}{\sum_{g\in\omega^1_p} \tilde{\phi}_{g,i,j}}\,, \quad \overline{\nu\Sigma}^1_{f,g,i,j} = \frac{\sum_{g\in\omega^1_p} \nu\Sigma_{f,g,i,j}\tilde{\phi}_{g,i,j}}{\sum_{g\in\omega^1_p} \tilde{\phi}_{g,i,j}}\,. \tag{3.35b}$$

The leakage operator $\mathbb{L}^1_p = \mathbb{L}^1_p[D^{\pm,1}_p]$ and the modified diffusion coefficients are

$$\bar{D}^{+,1}_{g,i+1/2,j} = \frac{\sum_{g\in\omega^1_p} D^+_{g,i+1/2,j}\tilde{\phi}_{g,i+1,j}}{\sum_{g\in\omega^1_p} \tilde{\phi}_{g,i+1,j}}\,, \quad \bar{D}^{-,1}_{g,i+1/2,j} = \frac{\sum_{g\in\omega^1_p} D^-_{g,i+1/2,j}\tilde{\phi}_{g,i,j}}{\sum_{g\in\omega^1_p} \tilde{\phi}_{g,i,j}}\,, \tag{3.36a}$$

$$\bar{D}^{+,1}_{g,i,j+1/2} = \frac{\sum_{g\in\omega^1_p} D^+_{g,i,j+1/2}\tilde{\phi}_{g,i,j+1}}{\sum_{g\in\omega^1_p} \tilde{\phi}_{g,i,j+1}}\,, \quad \bar{D}^{-,1}_{g,i,j+1/2} = \frac{\sum_{g\in\omega^1_p} D^-_{g,i,j+1/2}\tilde{\phi}_{g,i,j}}{\sum_{g\in\omega^1_p} \phi_{g,i,j}}\,. \tag{3.36b}$$

Correction factors similar to those used bewtween energy grids in the low-order problem are

calculated

$$\mathfrak{f}_g^1(\mathbf{r}) = \frac{\hat{\phi}_g^1(\mathbf{r})}{\sum_{g\in\omega_g^1}\tilde{\phi}_g(\mathbf{r})}\,, \quad g = 1,\ldots,G^1 \tag{3.37}$$

and are used to update the solution on the same grid as the transport problem

$$\hat{\phi}_g = \tilde{\phi}_g\,\mathfrak{f}_g^1 \quad \text{for } g \in \omega_g^1. \tag{3.38}$$

The multilevel QD equations in a coarse energy space are the same as (4.8) except the cross sections and coefficients on the first energy grid for the low-order equations. The coarse-group leakage operator $\mathbb{L}_p^1 = \mathbb{L}_p^\gamma[G_p^{*,1}]$ and factors for the QD method are defined by means of the high-order transport solution as

$$\bar{G}^{CL,1}_{xx,g,i,j} = \frac{\sum_{g\in\omega_g^1} G^{CL}_{xx,g,i,j}\tilde{\phi}_{g,i,j}}{\sum_{g\in\omega_g^1}\phi_{g,i,j}}\,, \quad \bar{G}^{CR,1}_{xx,g,i,j} = \frac{\sum_{g\in\omega_g^1} G^{CR}_{xx,g,i,j}\tilde{\phi}_{g,i,j}}{\sum_{g\in\omega_g^1}\tilde{\phi}_{g,i,j}}\,, \tag{3.39a}$$

$$\bar{G}^{CB,1}_{yy,g,i,j} = \frac{\sum_{g\in\omega_g^1} G^{CB}_{yy,g,i,j}\tilde{\phi}_{g,i,j}}{\sum_{g\in\omega_g^1}\tilde{\phi}_{g,i,j}}\,, \quad \bar{G}^{CT,1}_{yy,g,i,j} = \frac{\sum_{g\in\omega_g^1} G^{CT}_{yy,g,i,j}\tilde{\phi}_{g,i,j}}{\sum_{g\in\omega_g^1}\tilde{\phi}_{g,i,j}}\,, \tag{3.39b}$$

$$\bar{G}^{L,1}_{xx,g,i,j} = \frac{\sum_{g\in\omega_g^1} G^{L}_{xx,g,i,j}\tilde{\phi}_{g,i-1/2,j}}{\sum_{g\in\omega_g^1}\tilde{\phi}_{g,i-1/2,j}}\,, \quad \bar{G}^{R,1}_{xx,g,i,j} = \frac{\sum_{g\in\omega_g^1} G^{R}_{xx,g,i,j}\tilde{\phi}_{g,i+1/2,j}}{\sum_{g\in\omega_g^1}\tilde{\phi}_{g,i+1/2,j}}\,, \tag{3.39c}$$

$$\bar{G}^{B,1}_{yy,g,i,j} = \frac{\sum_{g\in\omega_g^1} G^{B}_{yy,g,i,j}\tilde{\phi}_{g,i,j-1/2}}{\sum_{g\in\omega_g^1}\tilde{\phi}_{g,i,j-1/2}}\,, \quad \bar{G}^{T,1}_{yy,g,i,j} = \frac{\sum_{g\in\omega_g^1} G^{T}_{yy,g,i,j}\tilde{\phi}_{g,i,j-1/2}}{\sum_{g\in\omega_g^1}\tilde{\phi}_{g,i,j-1/2}}\,. \tag{3.39d}$$

The factors (3.37) are used to update the high-order solution (3.38).

3.6.1 Analysis of Results with Coarse Grid MLNDA

Tables 3.11a and 3.11b show the results of the coarse energy MLNDA methods for Tests A and B. The grid sets $\{G^1,...,G^\Gamma\}$ show the number of groups and energy grids for the low-order equations. The boundaries in each of these coarse energy groups are defined in Tables 2.3, 2.4, and 2.5. These results demonstrate that a coarsening by a factor of two in the low-order problem space increases the number of transport iterations compared to forming the low-order problem on the same energy space. Further coarsening the first low-order energy grid increases the number of transport iterations. Some combinations of coarser energy grids can reduce the number of transport iterations slightly. However these coarse grids all result in more transport iterations than the target number of iterations with the low-order problem on the original groups. This increase in the number of transport iterations makes this selection of coarse low-order problems inefficient for accelerating the transport iterations.

Table 3.11: Results with 44 Group Cross Sections using MLNDA

(a) Test A

Multigrid Algorithm	Grids	N_t	N_{lo}	N_{lo}/G
pV-2	{22,1}	27	645	14.7
pW-2(2,1)	{22,1}	27	1289	29.3
pV-2	{8,1}	41	379	8.6
pV-2	{4,1}	60	306	7.0
pV-2	{2,1}	111	337	7.7
pV-3	{22,2,1}	23	601	13.7
pV-5	{22,8,4,2,1}	27	1037	23.6

(b) Test B

Multigrid Algorithm	Grids	N_t	N_{lo}	N_{lo}/G
pV-2	{22,1}	25	599	13.6
pW-2(2,1)	{22,1}	23	1105	25.1
pV-2	{8,1}	38	352	8.0
pV-2	{4,1}	57	291	6.6
pV-2	{2,1}	104	106	2.4
pV-3	{22,2,1}	23	601	13.7
pV-5	{22,8,4,2,1}	23	889	20.2

Tables 3.17a and 3.17b show results for the coarse energy MLNDA with agglomeration for Tests A and B. These grids use a fine energy structure, identical to the original energy structure, for the fast groups and a coarse grid structure in the thermal groups. The grids are

- $\Lambda_{E,33}$: 33 groups consisting of 22 fast and 11 thermal,
- $\Lambda_{E,26}$: 26 groups consisting of 22 fast and 4 thermal,
- $\Lambda_{E,24}$: 24 groups with 22 fast and 2 thermal,
- $\Lambda_{E,23}$: 23 groups with 22 fast and 1 thermal,
- $\Lambda_{E,5}$: 5 groups corresponding to 1 fast and 4 thermal groups,
- $\Lambda_{E,3}$: 3 groups corresponding to 1 fast and 2 thermal groups.

The energy group boundaries are listed in Tables 3.12, 3.13, 3.14, 3.15, and 3.16.

These results show that preserving the energy groups in the fast region reduces the number of transport iterations compared to coarsening over all groups. Performing additional cycles on the finest low-order grid or adding energy grids also reduces the number of transport iterations. With the 33 group first energy grid in the low-order problem, consisting in 22 fast and 11 thermal groups, it is possible to get within 1 transport iteration of the target number of iterations for the multilevel method on the 44 group first low-order grid. Coarsening the thermal groups more than by a factor of two increases the number of transport iterations. In the sequence {33,5,1} the first grid $\Lambda_E^1 = \Lambda_{E,33}$ has fewer groups in the thermal energies and the second grid $\Lambda_E^2 = \Lambda_{E,5}$ and fewer groups in the fast region. This sequence performed similarly to the sequence {33,8,1}. These results indicate that preserving the detail in the fast groups is important, but that it is possible to reduce the work in the low-order problem by coarsening the first low-order grid with

Table 3.12: Boundaries of energy intervals E_g in eV of the 33-group grid.

$i\backslash j^*$	0	1	2	3	4	5	6	7	8	9
0	$2.\times10^{7}$	8.1873×10^{6}	6.434×10^{6}	4.8×10^{6}	$3.\times10^{6}$	2.479×10^{6}	2.354×10^{6}	1.85×10^{6}	1.4×10^{6}	$9.\times10^{5}$
10	$4.\times10^{5}$	$1.\times10^{5}$	2.5×10^{4}	1.7×10^{4}	$3.\times10^{3}$	5.5×10^{2}	$1.\times10^{2}$	$3.\times10^{1}$	$1.\times10^{1}$	8.1
20	6.	4.75	3.	1.	$4.\times10^{-1}$	3.5×10^{-1}	2.75×10^{-1}	2.25×10^{-1}	1.5×10^{-1}	$7.\times10^{-2}$
30	$4.\times10^{-2}$	2.53×10^{-2}	7.5×10^{-3}	$1.\times10^{-5}$						

$^*g = i + j$

Table 3.13: Boundaries of energy intervals E_g in eV of the 26-group energy grid $\Lambda_{E,26}$.

$i\backslash j^*$	0	1	2	3	4	5	6	7	8	9
0	$2.\times10^{7}$	8.1873×10^{6}	6.434×10^{6}	4.8×10^{6}	$3.\times10^{6}$	2.479×10^{6}	2.354×10^{6}	1.85×10^{6}	1.4×10^{6}	$9.\times10^{5}$
10	$4.\times10^{5}$	$1.\times10^{5}$	2.5×10^{4}	1.7×10^{4}	$3.\times10^{3}$	5.5×10^{2}	$1.\times10^{2}$	$3.\times10^{1}$	$1.\times10^{1}$	8.1
20	6.	4.75	3.	$4.\times10^{-1}$	2.25×10^{-1}	$4.\times10^{-2}$	$1.\times10^{-5}$			

$^*g = i + j$

Table 3.14: Boundaries of energy intervals E_g in eV of the 24-group energy grid $\Lambda_{E,24}$.

$i\backslash j^*$	0	1	2	3	4	5	6	7	8	9
0	$2.\times10^{7}$	8.1873×10^{6}	6.434×10^{6}	4.8×10^{6}	$3.\times10^{6}$	2.479×10^{6}	2.354×10^{6}	1.85×10^{6}	1.4×10^{6}	$9.\times10^{5}$
10	$4.\times10^{5}$	$1.\times10^{5}$	2.5×10^{4}	1.7×10^{4}	$3.\times10^{3}$	5.5×10^{2}	$1.\times10^{2}$	$3.\times10^{1}$	$1.\times10^{1}$	8.1
20	6.	4.75	3.	2.25×10^{-1}	$1.\times10^{-5}$					

$^*g = i + j$

Table 3.15: Boundaries of energy intervals E_g in eV of the 23-group energy grid $\Lambda_{E,23}$.

$i\backslash j^*$	0	1	2	3	4	5	6	7	8	9
0	$2.\times10^{7}$	8.1873×10^{6}	6.434×10^{6}	4.8×10^{6}	$3.\times10^{6}$	2.479×10^{6}	2.354×10^{6}	1.85×10^{6}	1.4×10^{6}	$9.\times10^{5}$
10	$4.\times10^{5}$	$1.\times10^{5}$	2.5×10^{4}	1.7×10^{4}	$3.\times10^{3}$	5.5×10^{2}	$1.\times10^{2}$	$3.\times10^{1}$	$1.\times10^{1}$	8.1
20	6.	4.75	3.	$1.\times10^{-5}$						

$^*g = i + j$

Table 3.16: Boundaries of energy intervals E_g in eV of the nested energy grid $\Lambda_{E,5}$.

g	0	1	2	3	4	5
$\Lambda_{E,5}$	$2.\times10^{7}$	3.	$4.\times10^{-1}$	2.25×10^{-1}	$4.\times10^{-2}$	$1.\times10^{-5}$
$\Lambda_{E,3}$	$2.\times10^{7}$	3.	2.25×10^{-1}	$1.\times10^{-5}$		

agglomeration in thermal groups. This can be combined in a sequence with coarser grids with agglomeration in the fast groups.

3.6.2 Analysis of Results with Coarse Grid MLQD

Tables 3.18a and 3.18b demonstrate the results of the coarse energy MLQD methods for Tests A and B. These results again demonstrate that a coarsening energy space increases the number of transport iterations compared to forming the low-order problem on the same energy space.

Tables 3.19a and 3.19b demonstrate results for the coarse energy MLQD with agglomeration for Tests A and B. These grids use a fine energy structure, identical to the original energy

Table 3.17: Results with 44 Groups using MLNDA with agglomeration.

(a) Test A

Multigrid Algorithm	Grids	N_t	N_{lo}	N_{lo}/G
pV-2	{33,1}	18	647	14.7
pW-2(2,1)	{33,1}	12	885	20.1
pV-2	{26,1}	19	541	12.3
pW-2(2,1)	{26,1}	19	1081	24.6
pV-2	{24,1}	26	676	15.4
pV-2	{23,1}	33	817	18.6
pV-3	{33,2,1}	13	505	11.5
pV-3	{33,5,1}	13	547	12.4
pW-3(2,1)	{33,5,1}	12	1015	23.1
pV-3	{33,8,1}	12	547	12.4
pV-5	{33,8,4,2,1}	13	673	15.3
pW-5(2,1)	{33,8,4,2,1}	12	1249	28.4
pV-5	{33,5,3,2,1}	13	617	14.0
pW-5(2,1)	{33,5,3,2,1}	12	1145	26.0

(b) Test B

Multigrid Algorithm	Grids	N_t	N_{lo}	N_{lo}/G
pV-2	{33,1}	25	885	20.1
pW-2(2,1)	{33,1}	14	987	22.4
pW-2(3,1)	{33,1}	10	1297	29.5
pV-2	{26,1}	18	514	11.7
pW-2(2,1)	{26,1}	15	865	19.7
pV-2	{24,1}	23	601	13.7
pV-2	{23,1}	29	721	16.4
pV-3	{33,2,1}	12	469	10.7
pW-3(2,1)	{33,2,1}	10	793	18.0
pV-3	{33,5,1}	18	742	16.9
pW-3(2,1)	{33,5,1}	10	859	19.5
pV-3	{33,8,1}	18	799	18.2
pW-3(2,1)	{33,8,1}	10	925	21.0
pV-5	{33,8,4,2,1}	10	529	12.0
pV-5	{33,5,3,2,1}	10	485	11.0

Table 3.18: Results with 44 Group Cross Sections using MLQD

(a) Test A

Multigrid Algorithm	Grids	N_t	N_{lo}	N_{lo}/G
pV-2	{22,1}	27	645	14.7
pW-2(2,1)	{22,1}	27	1289	29.3
pV-3	{22,2,1}	27	701	15.9
pV-5	{22,8,4,2,1}	27	1037	23.6

(b) Test B

Multigrid Algorithm	Grids	N_t	N_{lo}	N_{lo}/G
pV-2	{22,1}	25	599	13.6
pW-2(2,1)	{22,1}	23	1105	25.1
pV-3	{22,2,1}	23	601	13.7
pV-5	{22,8,4,2,1}	23	889	20.2

Table 3.19: Test A with 44 Group Cross Sections using MLQD

(a) Test A

Multigrid Algorithm	Grids	N_t	N_{lo}	N_{lo}/G
pV-2	{33,1}	18	647	14.7
pW-2(2,1)	{33,1}	12	885	20.1
pV-3	{33,2,1}	13	505	11.5
pV-3	{33,5,1}	13	547	12.4
pW-3(2,1)	{33,5,1}	12	1015	23.1
pV-5	{33,8,4,2,1}	12	625	14.2

(b) Test B

Multigrid Algorithm	Grids	N_t	N_{lo}	N_{lo}/G
pV-2	{33,1}	26	919	20.9
pW-2(2,1)	{33,1}	14	987	22.4
pW-2(3,1)	{33,1}	10	1123	25.5
pV-3	{33,2,1}	12	469	10.7
pV-3	{33,5,1}	19	781	17.8
pV-5	{33,8,4,2,1}	10	529	12.0

structure, for the fast groups and a coarse grid structure in the thermal groups. These results also demonstrate the coarsening the thermal groups in the low-order problem can be used to reduce the work in the low-order problem without a significant increase in the number of transport iterations.

3.7 Summary

This chapter describes a new set of multilevel methods with multigrid in energy for multigroup k-eigenvalue transport problems in 2-D geometry. The proposed methodology is based on the NDA and QD equations. These methods formulate the low-order problem on a set of successively coarsened energy grids that form a hierarchy of low-order problems in energy. The low-order equations on coarser energy grids are used to accelerate transport iteration and reduce work in the low-order problem. The eigenvalue problem is solved on the grid with one group where the dimensionality is the smallest. These multilevel methods can be viewed as nonlinear multigrid algorithms for solving multigroup transport problems. The system of nonlinear multigrid low-order equations is solved using partial V-cycles and partial W-cycles.

The numerical results presented show the efficiency of the formulated multigrid schemes. They demonstrate that proposed algorithms on a set of coarse energy grids accelerate transport iterations and reduce computational costs of solving the multigroup low-order equations. Involving additional coarse energy grids can decrease the number of cycles on the original energy grid shifting the computational work to coarser energy grids. The advantage of the presented methodology is that the computational costs associated with solving a set of low-order problems on coarse energy grids do not scale when one increases the number of angular directions for solving the high-order transport equations. Results with linear in energy recursive correction factors and linear in energy with factorization were demonstrated. These prolongations did not show any improvement over the best cases with the constant energy correction factors. Using hybrid cycles can further improve the efficiency of the method by reducing the amount of unnecessary work when approaching the solution.

Coarse energy MLNDA and MLQD methods were presented that form the low-order problem on the first energy grid with a coarser structure compared to the energy grid of the given transport problem. This can reduce the dimensionality of the low-order problem, but can also increase the number of transport solution. Coarsening in the thermal groups with agglomeration and maintaining the fine groups structure in the fast region was found to be effective in accelerating the transport iterations and reducing the number of low-order solves. Agglomeration in the fast groups can be done on subsequent grids to further reduce the work in the low-order problem.

Chapter 4

Multilevel Transport Method with Multigrid in Space and Energy

Some NPI methods, notably CMFD [38], formulate the low-order equations on a coarser spatial mesh than the transport problem. This can further reduce the dimensionality of the problem and provide acceleration of transport iterations. In this chapter multilevel methods are presented where the low-order equations are formulated on a coarse spatial mesh and sequence of coarsening energy grids. These methods are based on both the NDA/CMFD equations and the QD equations. A similar multilevel method is also developed using the partial current based NDA/CMFD (pNDA/pCMFD) equations which have certain advantages for coarser spatial meshes.

The CMFD equations are described in Sec. 4.1. The coarse mesh QD (CMQD) equations are defined in Sec. 4.2. Sec. 4.3 presents the pCMFD equations. The multilevel hierarchy of these equations and the muligrid algorithms for solving them are demonstrated in Sec. 4.4. Sec. 4.5 contains results of the performance of the multilevel methods based on the CMFD, CMQD, and pCMFD equaitons.

4.1 Formulation of the Low-order CMFD Equations

The Coarse Mesh Finite Difference (CMFD) method is defined by Eqs. (1.4)-(1.9) as well as the NDA method. The difference from the NDA method is that the low-order equations (1.9) are approximated on a coarser spatial mesh compared to the given spatial mesh of the transport problem. Forming the low-order problem on a coarser can effect the number of transport iterations, however, it can also significantly reduce the work in the low-order problem.

For these methods a projection in space is performed from the mesh on which the high-order transport problem is defined. We can define the mesh for the high-order problem as

$M = \{(i'h_x, j'h_y) : i', j' \in \mathbb{I}\}$ where h_x and h_y are the size of the cells in the x and y directions respectively. The coarse mesh for each level is defined as a sub set of the points on the original mesh $M^\gamma = \{(in_x^\gamma h_x, jn_y^\gamma h_y) : i, j \in \mathbb{I}\}$ where n_x^γ and n_x^γ is the magnitude of coarsening in each direction. For this method the same spatial mesh is used on each level of the low-order problem so $M^1 = ... = M^\gamma = ... = M^\Gamma$. The sets of indices of fine cells in each coarse cell is defined in each direction as $\eta_i = \{i' : x_i < (x_{i'} + x_{i'+1})/2 < x_{i+1}\}$ and $\eta_j = \{j' : y_j < (y_{j'} + y_{j'+1})/2 < y_{j+1}\}$. The coarse mesh versions of the low-order equations is same as before, except the low-order factors are calculated using numerical integrals of the high-order transport solution in the sub integrals and cross sections are averaged using the transport solution.

The low-order equations are discretized on this coarse mesh just like the NDA equations in Section 3.1 except integrated transport solution and averaged cross section are used. These are found as

$$\bar{\phi}_{g,i,j} = \sum_{i' \in \eta_i} \sum_{j' \in \eta_j} \Delta x_{i'} \Delta y_{j'} \tilde{\phi}_{g,i',j'}, \tag{4.1a}$$

$$\bar{J}_{x,g,i+1/2,j} = \sum_{j' \in \eta_j} \Delta y_{j'} \tilde{J}_{x,g,n_x(i-1)+1/2,j'}, \tag{4.1b}$$

$$\bar{J}_{y,g,i,j+1/2} = \sum_{i' \in \eta_i} \Delta x_{i'} \tilde{J}_{y,g,i',n_y(j-1)+1/2}, \tag{4.1c}$$

and

$$\bar{\chi}_{g,i,j} = \sum_{i' \in \eta_i} \sum_{j' \in \eta_j} \Delta x_{i'} \Delta y_{j'} \chi_{g,i',j'}\,, \tag{4.2a}$$

$$\bar{\Sigma}_{s,g' \to g,i,j} = \frac{\sum_{i' \in \eta_i} \sum_{j' \in \eta_j} \Delta x_{i'} \Delta y_{j'} \Sigma_{s,g' \to g,i',j'} \tilde{\phi}_{g',i,j}}{\bar{\phi}_{g,i,j}}\,, \tag{4.2b}$$

$$\bar{\Sigma}_{t,g,i,j} = \frac{\sum_{i' \in \eta_i} \sum_{j' \in \eta_j} \Delta x_{i'} \Delta y_{j'} \Sigma_{t,g,i',j'} \tilde{\phi}_{g,i',j'}}{\bar{\phi}_{g,i,j}}\,, \tag{4.2c}$$

$$\overline{\nu\Sigma}_{f,g,i,j} = \frac{\sum_{i' \in \eta_i} \sum_{j' \in \eta_j} \Delta x_{i'} \Delta y_{j'} \nu\Sigma_{f,g,i',j'} \tilde{\phi}_{g,i',j'}}{\bar{\phi}_{g,i,j}}\,. \tag{4.2d}$$

The lwo-order equations then become

$$\mathbb{L}_g[\bar{D}_g^\pm]\phi_{g,i,j} + \bar{\Sigma}_{t,g,i,j} A_{i,j} \phi_{g,i,j} = A_{i,j} \sum_{g'=1}^{G} \bar{\Sigma}_{s,g' \to g,i,j} \phi_{g',i,j} + \frac{1}{k} A_{i,j} \bar{\chi}_{g,i,j} \sum_{g'=1}^{G} \overline{\nu\Sigma}_{f,g',i,j} \phi_{g',i,j} \tag{4.3a}$$

$$\mathbb{L}_g[D_g^{\pm}]\phi_{g,i,j} =$$
$$-\left[\frac{(D^+_{g,i+1/2,j}\phi_{g,i+1,j} - D^-_{g,i+1/2,j}\phi_{g,i,j})}{\Delta x_{i+1/2}} - \frac{(D^+_{g,i-1/2,j}\phi_{g,i,j} - D^-_{g,i-1/2,j}\phi_{g,i-1,j})}{\Delta x_{i-1/2}}\right]\Delta y_j$$
$$-\left[\frac{(D^+_{g,i,j+1/2}\phi_{g,i,j+1} - D^-_{g,i,j+1/2}\phi_{g,i,j})}{\Delta y_{j+1/2}} - \frac{(D^+_{g,i,j-1/2}\phi_{g,i,j} - D^-_{g,i,j-1/2}\phi_{g,i,j-1})}{\Delta y_{j-1/2}}\right]\Delta x_i\,. \quad (4.3b)$$

Here the modified diffusion coefficients are

$$D^{\pm}_{g,i+1/2,j} = D_{g,i+1/2,j} \mp \frac{1}{2}\bar{D}_{x,g,i+1/2,j}\Delta x_{i+1/2}\,, \quad (4.4a)$$

$$D^{\pm}_{g,i,j+1/2} = D_{g,i,j+1/2} \mp \frac{1}{2}\bar{D}_{y,g,i,j+1/2}\Delta y_{j+1/2} \quad (4.4b)$$

and

$$\bar{D}_{g,i+1/2,j} = \frac{\bar{J}_{x,g,i+1/2,j} + \frac{1}{\Delta x_{i+1/2}}D_{g,i+1/2,j}(\bar{\phi}_{g,i+1,j} - \bar{\phi}_{g,i,j})}{0.5(\bar{\phi}_{g,i+1,j} + \bar{\phi}_{g,i,j})}\,, \quad (4.5a)$$

$$\bar{D}_{g,i,j+1/2} = \frac{\bar{J}_{x,g,i,j+1/2} + \frac{1}{\Delta y_{j+1/2}}D_{g,i,j+1/2}(\bar{\phi}_{g,i,j+1} - \bar{\phi}_{g,i,j})}{0.5(\bar{\phi}_{g,i,j+1} + \bar{\phi}_{g,i,j})}\,, \quad (4.5b)$$

where $\bar{\phi}_g$ and $\bar{J}_{\alpha,g}$ are the integrated solution of the high-order transport problem defined above.

4.2 Formulation of the Low-order CMQD Equations

The QD discretization presented in the previous chapter can be applied to formulate the low-order equations on a coarser spatial mesh. Hereafter it is referred to as coarse mesh QD (CMQD). In this section we formulate the low-order CMQD equations.

The coarse mesh for each level of the low-order CMQD equations can be described as before. The transport solution is integrated over each coarse cell as (4.1) for the cell average flux and face average current, and

$$\bar{\phi}_{g,i+1/2,j} = \sum_{j'\in\eta_j}\Delta y_{j'}\tilde{\phi}_{g,n_x(i-1)+1/2,j'}, \quad \bar{\phi}_{g,i,j+1/2} = \sum_{i'\in\eta_i}\Delta x_{i'}\tilde{\phi}_{g,i',n_y(j-1)+1/2}, \quad (4.6)$$

for the face average scalar flux. The CMQD factors are defined by averaging the factors on the fine mesh over the scalar flux as

$$\bar{E}_{\alpha\alpha,g,i,j} = \frac{\sum_{i'\in\eta_i}\sum_{j'\in\eta_j}\Delta x_{i'}\Delta y_{j'}\tilde{\phi}_{g,i',j'}E_{\alpha\beta,g,i',j'}}{\bar{\phi}_{g,i,j}}, \quad (4.7a)$$

$$\bar{E}_{\alpha\beta,g,i+1/2,j} = \frac{\sum_{j'\in\eta_j} \Delta y_{j'} \tilde{\phi}_{g,n_x(i-1)+1/2,j'} E_{\alpha\beta,g,n_x(i-1)+1/2,j'}}{\bar{\phi}_{g,i+1/2,j}}, \tag{4.7b}$$

$$\bar{E}_{\alpha\beta,g,i,j+1/2} = \frac{\sum_{i'\in\eta_i} \Delta x_{i'} \tilde{\phi}_{g,i',n_y(j-1)+1/2} E_{\alpha\beta,g,i',n_y(j-1)+1/2}}{\bar{\phi}_{g,i,j+1/2}}, \tag{4.7c}$$

$$\text{for} \quad \alpha,\beta = x,y.$$

The low-order CMQD equations are discretized the same as the QD equations and can be written as

$$\mathbb{L}_g[G_g^*]\phi_{g,i,j} + \Sigma_{t,g,i,j}\phi_{g,i,j} = \sum_{g'=1}^{G} \Sigma_{s,g'\to g,i,j}\phi_{g',i,j} + \frac{\chi_{g,i,j}}{k}\sum_{g'=1}^{G} \nu_{f,g',i,j}\Sigma_{f,g',i,j}\phi_{g',i,j}\,, \tag{4.8a}$$

where the leakage operator is

$$\begin{aligned}\mathbb{L}_g[G_g^*]\phi_{g,i,j} = &-\frac{2}{\Delta x_i^2}\Big(G^R_{xx,g,i,j}\phi_{g,i+1/2,j} - (G^{CR}_{xx,g,i,j} + G^{CL}_{xx,g,i,j})\phi_{g,i,j} + G^L_{xx,g,i,j}\phi_{g,i-1/2,j}\Big) \\ &- \frac{2}{\Delta y_j^2}\Big(G^T_{yy,g,i,j}\phi_{g,i,j+1/2} - (G^{CT}_{yy,g,i,j} + G^{CB}_{yy,g,i,j})\phi_{g,i,j} + G^B_{yy,g,i,j}\phi_{g,i,j-1/2}\Big)\,,\end{aligned} \tag{4.8b}$$

and the modified coefficients are defined in terms of the QD factors and consistency terms as

$$G^{CL}_{xx,g,i,j} = \frac{\bar{E}_{xx,g,i,j} + \xi^{L-}_{g,i,j}}{\bar{\Sigma}_{t,g,i,j}}\,, \quad G^{CR}_{xx,g,i,j} = \frac{\bar{E}_{xx,g,i,j} + \xi^{R+}_{g,i,j}}{\bar{\Sigma}_{t,g,i,j}}\,, \tag{4.9a}$$

$$G^{CB}_{yy,g,i,j} = \frac{\bar{E}_{yy,g,i,j} + \bar{\xi}^{B-}_{g,i,j}}{\bar{\Sigma}_{t,g,i,j}}\,, \quad G^{CT}_{yy,g,i,j} = \frac{E_{yy,g,i,j} + \bar{\xi}^{T+}_{g,i,j}}{\bar{\Sigma}_{t,g,i,j}}\,, \tag{4.9b}$$

$$G^{L}_{xx,g,i,j} = \frac{\bar{E}_{xx,g,i-1/2,j} + \bar{\xi}^{L+}_{g,i,j}}{\bar{\Sigma}_{t,g,i,j}}\,, \quad G^{R}_{xx,g,i,j} = \frac{\bar{E}_{xx,g,i+1/2,j} + \bar{\xi}^{R-}_{g,i,j}}{\bar{\Sigma}_{t,g,i,j}}\,, \tag{4.9c}$$

$$G^{B}_{yy,g,i,j} = \frac{\bar{E}_{yy,g,i,j-1/2} + \bar{\xi}^{B+}_{g,i,j}}{\bar{\Sigma}_{t,g,i,j}}\,, \quad G^{T}_{yy,g,i,j} = \frac{\bar{E}_{yy,g,i,j+1/2} + \bar{\xi}^{T-}_{g,i,j}}{\bar{\Sigma}_{t,g,i,j}}\,. \tag{4.9d}$$

and

$$\bar{\xi}^{L-}_{x,g,i,j} = \begin{cases} -\frac{\bar{\gamma}^L_{x,g,i,j}}{\bar{\phi}_{g,i,j}\Delta y_j}, & \text{if } \bar{\gamma}^L_{x,g,i,j} \le 0, \\ 0, & \text{if } \bar{\gamma}^L_{x,g,i,j} > 0, \end{cases} \quad \bar{\xi}^{L+}_{x,g,i,j} = \begin{cases} 0, & \text{if } \bar{\gamma}^L_{x,g,i,j} \le 0, \\ \frac{\bar{\gamma}^L_{x,g,i,j}}{\bar{\phi}_{g,i-1/2,j}\Delta y_j}, & \text{if } \bar{\gamma}^L_{x,g,i,j} > 0, \end{cases} \tag{4.9e}$$

$$\bar{\xi}^{R-}_{x,g,i,j} = \begin{cases} -\frac{\bar{\gamma}^R_{x,g,i,j}}{\bar{\phi}_{g,i+1/2,j}\Delta y_j}, & \text{if } \bar{\gamma}^R_{x,g,i,j} \le 0, \\ 0, & \text{if } \bar{\gamma}^R_{x,g,i,j} > 0, \end{cases} \quad \bar{\xi}^{R+}_{x,g,i,j} = \begin{cases} 0, & \text{if } \bar{\gamma}^R_{x,g,i,j} \le 0, \\ \frac{\bar{\gamma}^R_{x,g,i,j}}{\bar{\phi}_{g,i,j}\Delta y_j}, & \text{if } \bar{\gamma}^R_{x,g,i,j} > 0, \end{cases} \tag{4.9f}$$

$$\bar{\gamma}^{L}_{x,g,i,j} = \Big(\bar{E}_{xx,g,i,j}\bar{\phi}_{g,i,j} - E_{xx,g,i-1/2,j}\bar{\phi}_{g,i-1/2,j}\Big)\Delta y_j + \Big(\bar{E}_{xy,g,i,j+1/2}\bar{\phi}_{g,i,j+1/2} - \bar{E}_{xy,g,i,j-1/2}\bar{\phi}_{g,i,j-1/2}\Big)\frac{\Delta x_i}{2} + \frac{1}{2}\bar{\Sigma}_{t,g,i,j}A_{i,j}\bar{J}_{x,g,i-1/2,j}\,, \quad (4.9g)$$

$$\bar{\gamma}^{R}_{x,g,i,j} = \Big(\bar{E}_{xx,g,i+1/2,j}\bar{\phi}_{g,i+1/2,j} - \bar{E}_{xx,g,i,j}\bar{\phi}_{g,i,j}\Big)\Delta y_j + \Big(\bar{E}_{xy,g,i,j+1/2}\bar{\phi}_{g,i,j+1/2} - \bar{E}_{xy,g,i,j-1/2}\bar{\phi}_{g,i,j-1/2}\Big)\frac{\Delta x_i}{2} + \frac{1}{2}\bar{\Sigma}_{t,g,i,j}A_{i,j}\bar{J}_{x,g,i-1/2,j}\,. \quad (4.9h)$$

The hierarchy of low-order CMQD equations are formulated and solved as described in Chapter 3.

4.3 Formulation of the Low-order Partial Current Based CMFD Equations

The low-order pCMFD equations (1.11)-(1.18) can be derived for a rectangular spatial mesh $G = \{0 \le x \le X, 0 \le y \le Y\}$ with rectangular spatial grids $\{x_{i-1/2}, i = 1, \ldots, N_x,\ y_{j-1/2}, j = 1, \ldots, N_y\}$. To derive the low-order pCMFD equations we apply classical formulation by means of a finite-volume scheme for the P_1 equations. For the cell (i, j) the system of low-order pCMFD equations consists of the balance equation

$$(J_{x,g,i+1/2,j} - J_{x,g,i-1/2,j})\Delta y_j + (J_{y,g,i,j+1/2} - J_{y,g,i,j-1/2})\Delta x_i + \Sigma_{t,g,i,j}A_{i,j}\phi_{g,i,j} = A_{i,j}\sum_{g'=1}^{G}\Sigma_{s,g'\to g,i,j}\phi_{g',i,j} + \frac{1}{k}A_{i,j}\chi_{g,i,j}\sum_{g'=1}^{G}\nu\Sigma_{f,g',i,j}\phi_{g',i,j} \quad (4.10a)$$

and the first-moment equations of the following form:

$$J_{x,g,i+1/2,j} = -\frac{D_{g,i+1/2,j}(\phi_{g,i+1,j} - \phi_{g,i,j})}{\Delta x_{i+1/2}} - \tilde{D}^{-}_{g,i+1/2,j}\phi_{g,i+1,j} + \tilde{D}^{+}_{g,i+1/2,j}\phi_{g,i,j}\,, \quad (4.10b)$$

$$J_{y,g,i,j+1/2} = -\frac{D_{g,i,j+1/2}(\phi_{g,i,j+1} - \phi_{g,i,j})}{\Delta y_{j+1/2}} - \tilde{D}^{-}_{g,i,j+1/2}\phi_{g,i,j+1} + \tilde{D}^{+}_{g,i,j+1/2}\phi_{g,i,j}\,. \quad (4.10c)$$

The compensation factors are formulated to make the high-order and low-order equations consistent. They are given by

$$\bar{D}^{-}_{g,i+1/2,j} = \frac{-\bar{J}^{-}_{x,g,i+1/2,j} - \frac{1}{2\Delta x_{i+1/2}}D_{g,i+1/2,j}(\bar{\phi}_{g,i+1,j} - \bar{\phi}_{g,i,j})}{\bar{\phi}_{g,i+1,j}}\,, \quad (4.11a)$$

$$\bar{D}^{+}_{g,i+1/2,j} = \frac{\bar{J}^{+}_{x,g,i+1/2,j} + \frac{1}{2\Delta x_{i+1/2}} D_{g,i+1/2,j}(\bar{\phi}_{g,i+1,j} - \bar{\phi}_{g,i,j})}{\bar{\phi}_{g,i,j}}\,, \tag{4.11b}$$

$$\bar{D}^{-}_{g,i,j+1/2} = \frac{-\bar{J}^{-}_{x,g,i,j+1/2} - \frac{1}{2\Delta y_{j+1/2}} D_{g,i,j+1/2}(\bar{\phi}_{g,i,j+1} - \bar{\phi}_{g,i,j})}{\bar{\phi}_{g,i,j+1}}\,, \tag{4.11c}$$

$$\bar{D}^{+}_{g,i,j+1/2} = \frac{\bar{J}^{+}_{x,g,i,j+1/2} + \frac{1}{2\Delta y_{j+1/2}} D_{g,i,j+1/2}(\bar{\phi}_{g,i,j+1} - \bar{\phi}_{g,i,j})}{\bar{\phi}_{g,i,j}}\,, \tag{4.11d}$$

where the partial currents $\bar{J}^{\pm}_{\alpha,g}$ are defined by the solution of the high-order transport problem and hence

$$\bar{J}^{\pm}_{x,g,i+1/2,j} = \sum_{j' \in \eta_j} \Delta y_{j'} \tilde{J}^{\pm}_{x,g,n_x(i-1)+1/2,j'}, \tag{4.12a}$$

$$\bar{J}^{\pm}_{y,g,i,j+1/2} = \sum_{i' \in \eta_i} \Delta x_{i'} \tilde{J}^{\pm}_{y,g,i',n_y(j-1)+1/2}, \tag{4.12b}$$

are integrals of the current on the fine mesh

$$\tilde{J}^{+}_{x,g,i+1/2,j} = \sum_{m:\Omega_{x,m} \geq 0} \Omega_{x,m} \psi_{g,m,i+1/2,j} w_m\,, \tag{4.13a}$$

$$\tilde{J}^{-}_{x,g,i+1/2,j} = \sum_{m:\Omega_{x,m} \leq 0} \Omega_{x,m} \psi_{g,m,i+1/2,j} w_m\,, \tag{4.13b}$$

$$\tilde{J}^{+}_{y,g,i+1/2,j} = \sum_{m:\Omega_{y,m} \geq 0} \Omega_{y,m} \psi_{g,m,i+1/2,j} w_m\,, \tag{4.13c}$$

$$\tilde{J}^{-}_{y,g,i+1/2,j} = \sum_{m:\Omega_{y,m} \leq 0} \Omega_{y,m} \psi_{g,m,i+1/2,j} w_m\,, \tag{4.13d}$$

$$\tilde{J}_{x,g,i+1/2,j} = \tilde{J}^{+}_{x,g,i+1/2,j} + \tilde{J}^{-}_{x,g,i+1/2,j}, \quad \tilde{J}_{y,g,i+1/2,j} = \tilde{J}^{+}_{y,g,i+1/2,j} + \tilde{J}^{-}_{y,g,i+1/2,j}. \tag{4.13e}$$

Here $\psi_{g,m}$ is the angular flux for the discrete direction $\mathbf{\Lambda}_m$ and w_m is the quadrature weight.

The first-moment equations can be cast as

$$J_{x,g,i+1/2,j} = -\frac{1}{\Delta x_{i+1/2}} \left(D^{+}_{g,i+1/2,j} \phi_{g,i+1,j} - D^{-}_{g,i+1/2,j} \phi_{g,i,j} \right), \tag{4.14a}$$

$$J_{y,g,i,j+1/2} = -\frac{1}{\Delta y_{j+1/2}} \left(D^{+}_{g,i,j+1/2} \phi_{g,i,j+1} - D^{-}_{g,i,j+1/2} \phi_{g,i,j} \right), \tag{4.14b}$$

where the factors

$$D^{\pm}_{g,i+1/2,j} = D_{g,i+1/2,j} + \tilde{D}^{\mp}_{x,g,i+1/2,j} \Delta x_{i+1/2}\,, \tag{4.15a}$$

$$D^{\pm}_{g,i,j+1/2} = D_{g,i,j+1/2} + \tilde{D}^{\mp}_{y,g,i,j+1/2} \Delta y_{j+1/2} \tag{4.15b}$$

are modified diffusion coefficients of the generalized Fick's law. Substituting equation (4.14)

into the balance equation (4.10a) yields the diffusion-like equation

$$\mathbb{L}_g[D_g^{\pm}]\phi_{g,i,j} + \Sigma_{t,g,i,j}A_{i,j}\phi_{g,i,j} = A_{i,j}\sum_{g'=1}^{G}\Sigma_{s,g'\to g,i,j}\phi_{g',i,j} + \frac{1}{k}A_{i,j}\chi_{g,i,j}\sum_{g'=1}^{G}\nu\Sigma_{f,g',i,j}\phi_{g',i,j}, \quad (4.16a)$$

$$\begin{aligned}\mathbb{L}_g[D_g^{\pm}]\phi_{g,i,j} = &- \left[\frac{(D^+_{g,i+1/2,j}\phi_{g,i+1,j} - D^-_{g,i+1/2,j}\phi_{g,i,j})}{\Delta x_{i+1/2}} - \frac{(D^+_{g,i-1/2,j}\phi_{g,i,j} - D^-_{g,i-1/2,j}\phi_{g,i-1,j})}{\Delta x_{i-1/2}}\right]\Delta y_j \\ &- \left[\frac{(D^+_{g,i,j+1/2}\phi_{g,i,j+1} - D^-_{g,i,j+1/2}\phi_{g,i,j})}{\Delta y_{j+1/2}} - \frac{(D^+_{g,i,j-1/2}\phi_{g,i,j} - D^-_{g,i,j-1/2}\phi_{g,i,j-1})}{\Delta y_{j-1/2}}\right]\Delta x_i\,. \quad (4.16b)\end{aligned}$$

where the leakage operator $\mathbb{L}_g$ is defined by the five point stencil as the NDA equations.

4.4 Hierarchy of Equations and Multigrid Algorithms

A hierarchy of these coarse mesh equation are formulated for the low-order problem as described in Section 3.3. The set of low-order equations is solved using the multigrid cycles similar to those described in Sec. 3.4. The pV-Γ cycle for the multilevel coarse mesh methods is defined in Algorithm 10. Figure 4.1 shows an example of the pV-3 cycle with a coarse mesh and demonstrates that grids $\gamma = 0$ and $\gamma = 1$ have the same energy grid, but different spatial meshes. All of the low-order grids ($\gamma = 1, 2, 3$) have the same spatial mesh. Forming the low-order problem is done using a projection over both angle and space. The low-order problem is then solved as described in Sec. 3.4. Once the low-order flux is updated on grid $\gamma = 1$, an additional prolongation in space step is done between the low-order and high order meshes. The low-order solution is used to update the high-order solution on the fine mesh using shape functions. The shape function $\bar{F}$ is defined as a correction factor, similar to the constant energy correction factors in Sec. 2.3.

$$\bar{f}_{g,i,j} = \frac{\Delta x_i \Delta y_j \hat{\phi}_{g,i,j}}{\sum_{i'\in\eta_i}\sum_{j'\in\eta_j}\Delta x_{i'}\Delta y_{j'}\tilde{\phi}_{g,i',j'}}. \quad (4.17)$$

This spatial correction factor is used to update the transport solution

$$\tilde{\phi}_{g,i',j'} \leftarrow \bar{f}_{g,i,j}\tilde{\phi}_{g,i',j'}, \quad \text{for} \quad i' \in \eta_i \quad \text{and} \quad j' \in \eta_j. \quad (4.18)$$

Similar algorithms are defined for the pW-Γ($\gamma*$,μ) cycles.

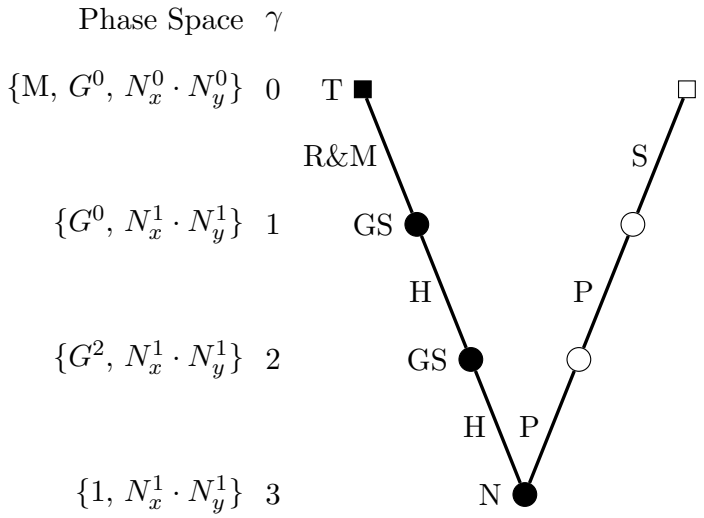

Figure 4.1: Multigrid pV-3 cycle with coarse mesh. GS - Gauss-Seidel iteration over groups on Ω_E^γ, R - projection over angle, M - projection over space, H - homogenization over energy, N - Newton iteration, P - prolongation in energy, S - prolongation in space

Solve $\boldsymbol{\psi} = \mathcal{T}^{-1}\mathcal{S}\boldsymbol{\psi} + \dfrac{1}{k}\mathcal{T}^{-1}\mathcal{P}\boldsymbol{\psi}$
Calculate CMQD/CMFD/pCMFD factors and average the high-order equations over angle and space to form $\mathcal{A}_1$, $\mathcal{B}_1$, $\mathcal{C}_1$
for $\gamma \leftarrow 1$ *to* $\Gamma - 1$ **do**
  Solve $\boldsymbol{\phi}^\gamma = \mathcal{A}_\gamma^{-1}\mathcal{B}_\gamma\hat{\boldsymbol{\phi}}^\gamma + \dfrac{1}{k}\mathcal{A}_\gamma^{-1}\mathcal{C}_\gamma\hat{\boldsymbol{\phi}}^\gamma$
  Perform homogenization in energy to form $\mathcal{A}_{\gamma+1}$, $\mathcal{B}_{\gamma+1}$, $\mathcal{C}_{\gamma+1}$
end
Solve the eigenvalue problem $\mathcal{C}_\Gamma^{-1}\mathcal{A}_\Gamma\boldsymbol{\phi}^\Gamma = k\boldsymbol{\phi}^\Gamma$ to update k and $\boldsymbol{\phi}^\Gamma$
for $\gamma \leftarrow \Gamma - 1$ *to 1* **do**
  Perform prolongation $\hat{\boldsymbol{\phi}}^\gamma = I_\alpha^{\gamma \leftarrow \gamma+1}\boldsymbol{\phi}^{\gamma+1}$
end
Calculate shape function $\bar{F}$ and update the high-order flux $\boldsymbol{\psi} \leftarrow \bar{F}\boldsymbol{\psi}$

Algorithm 10: pV-Γ. The multigrid algorithm with the partial V-cycle.

4.5 Numerical Results

4.5.1 Analysis of Multilevel CMFD

Numerical results are presented for test problems A (2.2) and B (2.3) with 44 groups in energy. These problems both have a square mesh with the high order mesh size of $h = h_x = h_y = 0.09cm$. Tables 4.1 and 4.2 show the results for Test A and B respectively. Coarsening was done equally in each x and y direction for each grid so $n_x = n_y$. The first two columns show the

Table 4.1: Test A with 44 Group Cross Sections using multilevel CMFD.

Algorithm	N_t	N_{lo}	N_t	N_{lo}	N_t	N_{lo}	N_t	N_{lo}
	h		2h		7h		14h	
2 Grid Sequence {44,1}								
pV-2	21	991	22	1036	U/C		U/C	
pW-2(2,1)	12	1171	13	1261	U/C		U/C	
pW-2(3,1)	11	1531	11	1621	U/C		U/C	
3 Grid Sequence {44,2,1}								
pV-3	13	659	13	659	U/C		U/C	
pW-3(2,1)	12	1176	13	1317	U/C		U/C	
pW-3(3,1)	11	1599	11	1693	U/C		U/C	
3 Grid Sequence {44,8,1}								
pV-3	13	743	13	743	U/C		U/C	
pW-3(2,1)	11	1273	11	1273	U/C		U/C	
3 Grid Sequence {44,22,1}								
pV-3	18	1274	18	1274	U/C		U/C	
pW-3(2,2)	12	1171	14	1351	U/C		U/C	
pW-3(2,1)	11	1609	11	1609	U/C		U/C	
4 Grid Sequence {44,22,4,1}								
pV-4	12	924	14	1066	U/C		U/C	
pW-4(2,1)	11	1705	11	1705	U/C		U/C	
5 Grid Sequence {44,22,8,2,1}								
pV-5	12	1002	14	1156	U/C		U/C	
pW-5(2,1)	11	1849	11	1849	U/C		U/C	
6 Grid Sequence {44,22,8,4,2,1}								
pV-6	13	1135	14	1216	U/C		U/C	
pW-6(2,1)	11	1945	11	1945	U/C		U/C	

U/C - Unconverged

number of transport iterations and low-order group-wise solves when the low order mesh is the same as the high order mesh (h). The next set of columns show the results for a coarsening by a factor of two (2h). Coarsening by a factor of seven (7h four spatial cells for each pin cell) resulted in the problem not converging for Test A. This also occurred with the factor of fourteen (14h corresponds to one spatial cell for each pin cell) for both Test A and B. The size of the low-order problem decreases as a square of the coarsening factor. So a coarsening of 7h is a 14 fold reduction in the dimensionality of the low-order problem.

For Test A the 2h mesh reduces the size of the low-order problem by a factor of 4. The most efficient algorithm is pV-3(2,1) on grids {44,8,1}. For Test B the 7h mesh is the smallest and has a factor of 14 reduction in the dimensionality of the low-order problem. The best algorithm on this grid is pW-5(2,4) on grids {44,22,8,2,1}.

Table 4.2: Test B with 44 Group Cross Sections using multilevel CMFD.

Algorithm	N_t	N_{lo}	N_t	N_{lo}	N_t	N_{lo}	N_t	N_{lo}
	h		2h		7h		14h	
2 Grid Sequence {44,1}								
pV-2	27	1261	25	1171	28	1306	U/C	
pW-2(2,1)	15	1396	14	1351	15	1441	U/C	
pW-2(3,1)	10	1441	10	1486	10	1486	U/C	
pW-2(4,1)	8	1531	8	1621	8	1621	U/C	
3 Grid Sequence {44,2,1}								
pV-3	13	659	14	706	15	753	U/C	
pV-3	8	847	8	847	8	847	U/C	
3 Grid Sequence {44,8,1}								
pV-3	18	1008	17	955	14	796	U/C	
pW-3(2,1)	10	1114	10	1167	8	955	U/C	
pW-3(3,1)	9	1485	9	1591	8	1432	U/C	
pW-3(4,1)	8	1803	8	1909	8	1803	U/C	
3 Grid Sequence {44,22,1}								
pV-3	25	1743	23	1609	23	1609	U/C	
pW-3(2,1)	13	1810	12	1743	12	1743	U/C	
pW-3(3,1)	9	1944	9	2011	9	2011	U/C	
pW-3(4,1)	8	2279	8	2413	8	2413	U/C	
4 Grid Sequence {44,8,2,1}								
pV-4	9	551	9	551	9	551	U/C	
pW-4(2,2)	8	595	8	595	8	595	U/C	
5 Grid Sequence {44,22,8,2,1}								
pV-5	8	694	8	694	9	771	U/C	
pW-5(2,4)	8	721	8	721	8	721	U/C	
6 Grid Sequence {44,22,8,4,2,1}								
pV-6	8	730	8	730	9	811	U/C	
pW-6(2,4)	8	793	8	793	8	793	U/C	

U/C - Unconverged

These results demonstrate that coarsening in space can lead to cases where there are instabilities with the CMFD method. For most cases the behavior of various sets of energy grids is not significantly effected by coarsening in space. However, it can be noted for some cases (specifically sets of grids with many groups like {44,22,1}) that coarsening in space can decrease the number of transport iterations for a given multigrid algorithm. In other cases the number of transport iterations can increase with spatial coarsening. For every set of grids tested it was possible to get the same target number of transport iterations with some additional cycles in the low-order problem.

4.5.2 Analysis of Multilevel CMQD

The results of the coarse mesh QD methods for tests A and B are shown in Tables 4.3 and 4.3 for different coarse meshes. These results are with a constant in energy prolongation operator. These results are similar to those with multilevel CMFD. The the multilevel CMQD method

Table 4.3: Test A with 44 Group Cross Sections using multilevel CMQD.

Algorithm	N_t	N_{lo}	N_t	N_{lo}	N_t	N_{lo}	N_t	N_{lo}
	h		2h		7h		14h	
2 Grid Sequence {44,1}								
pV-2	21	991	22	1036	U/C		U/C	
pW-2(2,1)	12	1171	13	1261	U/C		U/C	
pW-2(3,1)	11	1486	12	1756	U/C		U/C	
pW-2(4,1)	11	2161	11	2161	U/C		U/C	
3 Grid Sequence {44,2,1}								
pV-3	13	659	14	706	U/C		U/C	
pW-3(2,1)	12	1176	13	1317	U/C		U/C	
pW-3(3,1)	11	1599	11	1693	U/C		U/C	
3 Grid Sequence {44,8,1}								
pV-3	12	690	14	796	U/C		U/C	
pW-3(2,1)	11	1273	12	1379	U/C		U/C	
pW-3(3,1)	11	1909	11	1909	U/C		U/C	
4 Grid Sequence {44,8,2,1}								
pV-4	12	716	13	771	U/C		U/C	
pW-4(2,1)	11	1321	12	1431	U/C		U/C	
pW-4(3,1)	11	1981	11	1981	U/C		U/C	
5 Grid Sequence {44,22,8,2,1}								
pV-5	12	1002	14	1156	U/C		U/C	
pW-5(2,1)	11	1849	11	1849	U/C		U/C	
6 Grid Sequence {44,22,8,4,2,1}								
pV-6	12	1054	14	1216	U/C		U/C	
pW-6(2,1)	11	1945	11	1945	U/C		U/C	

U/C - Unconverged

does not converge in Test A with a coarse grids 7h and 14h or in Test B with a coarse grid 14h. These are the same cases where the multilevel CMFD method does not converge.

In Test A as the mesh is coarsened the number of transport iterations increases for the pV on each grid set. If pW cycles are used it is possible to converged in 11 iterations for both spatial meshes. For the grids {44,1}, {44,8,1}, and {44,8,2,1} additional pW cycles are needed to get to the target 11 iterations. For the case where the low-order mesh uncoarsened the algorithm

Table 4.4: Test B with 44 Group Cross Sections using multilevel CMQD.

Algorithm	N_t	N_{lo}	N_t	N_{lo}	N_t	N_{lo}	N_t	N_{lo}
	h		2h		7h		14h	
2 Grid Sequence {44,1}								
pV-2	28	1306	26	1216	32	1486	U/C	
pW-2(2,1)	15	1396	15	1441	18	1711	U/C	
pW-2(3,1)	11	1486	11	1621	16	2296	U/C	
pW-2(4,1)	12	1756	9	1801	15	2881	U/C	
pW-2(5,1)	8	1936	9	2251	15	3601	U/C	
3 Grid Sequence {44,2,1}								
pV-3	13	659	14	706	15	753	U/C	
pW-3(2,1)	8	847	9	941	14	1411	U/C	
3 Grid Sequence {44,8,1}								
pV-3	19	1061	18	1008	19	1061	U/C	
pW-3(2,1)	10	1114	10	1167	16	1803	U/C	
pW-3(3,1)	9	1485	9	1591	15	2545	U/C	
pW-3(4,1)	8	1803	9	2121	15	3393	U/C	
4 Grid Sequence {44,8,2,1}								
pV-4	9	551	10	606	14	826	U/C	
pW-4(2,2)	8	595	9	661	14	991	U/C	
5 Grid Sequence {44,22,8,2,1}								
pV-5	9	771	10	848	14	1156	U/C	
pW-5(2,3)	8	793	9	881	14	1321	U/C	
6 Grid Sequence {44,22,8,4,2,1}								
pV-6	8	730	10	892	15	1297	U/C	
pW-6(2,4)	8	793	10	969	14	1321	U/C	
pW-6(2,3)	8	865	9	961	14	1441	U/C	

U/C - Unconverged

with the fewest transport iterations and low-order solves is pW-3(2,1) on grids {44,8,1}. For the grid coarsened by 2h the algorithm pW-3(3,1) on grids {44,2,1} has the fewest low-order solves for the target number of iterations.

For Test B the target number of transport iterations increases as the spatial mesh is coarsened. The fewest transport iterations is 8, 9, and 14 for the low-order meshes of h, 2h, and 7h respectively. The pV cycle on grids {44,1} and {44,2,1} the 2h mesh takes fewer transport iterations than the h mesh. For all other combination of grids and cycles, coarser grids have equal or greater number of transport iteration. For each spatial mesh the grid sequence {44,8,2,1} gives the fewest transport iterations with the least low-order solves. On this grid the pW-4(2,2) cycle for meshes h and 2h the pW-4(2,2) cycle and for mesh 7h give the target transport iterations.

4.5.3 Analysis of Multilevel pCMFD

Numerical results for the multilevel pCMFD methods are presented for Tests A and B with 44 groups. The same mesh coarsening of h, 2h, 7h, and 14h are used. Tables 4.5 and 4.6 summarize the results.

Table 4.5: Test A with 44 Group Cross Sections using multilevel pCMFD.

Algorithm	N_t	N_{lo}	N_t	N_{lo}	N_t	N_{lo}	N_t	N_{lo}
	h		2h		7h		14h	
2 Grid Sequence {44,1}								
pV-2	21	991	22	1036	31	1441	30	1396
pW-2(2,1)	12	1171	13	1261	17	1621	21	1981
pW-2(3,1)	12	1666	11	1621	14	2026	19	2701
pW-2(4,1)	11	2071	11	2071	14	2701	19	3601
3 Grid Sequence {44,2,1}								
pV-3	13	659	13	659	17	847	23	1129
pW-3(2,1)	11	1129	12	1223	15	1505	19	1881
pW-3(3,1)	11	1693	12	1834	13	1975	19	2821
3 Grid Sequence {44,8,1}								
pV-3	12	690	13	743	21	1167	32	1750
pW-3(2,1)	11	1273	12	1379	21	2333	32	3499
4 Grid Sequence {44,22,4,1}								
pV-4	12	924	13	995	15	1137	25	1847
pW-4(2,1)	11	1705	12	1847	21	3125	19	2841
5 Grid Sequence {44,22,8,2,1}								
pV-5	12	1002	12	1002	15	1233	25	2003
pW-5(2,1)	11	1849	12	2003	20	3234	19	3081
6 Grid Sequence {44,22,8,4,2,1}								
pV-6	12	1054	12	1054	15	1297	23	1945
pW-6(2,1)	11	1945	12	2107	13	2269	19	3241

For the case where the low-order mesh is the same as the high-order mesh the multilevel pCMFD method behaves similarly to the NDA method. The target number or iterations for Test A is 11 and for Test B is 9. Whereas the multilevel CMFD methods stopped converging for mesh 7h and 14h for Test A and for mesh 14h for Test B, the multilevel pCMFD converges for all of the coarse meshes. However, for some of the coarser meshes the target number of transport iterations increases. In Test A on mesh 7h and 14h the target number of iterations is 13 and 19 respectively. In Test B the target number of transport iterations on mesh 14h is 10. These meshes are also the meshes where the multilevel CMFD does not converge. For Test

Table 4.6: Test B with 44 Group Cross Sections using multilevel pCMFD.

Algorithm	N_t	N_{lo}	N_t	N_{lo}	N_t	N_{lo}	N_t	N_{lo}
	h		2h		7h		14h	
2 Grid Sequence {44,1}								
pV-2	28	1306	26	1216	29	1351	27	1261
pW-2(2,1)	15	1396	15	1441	16	1531	16	1531
pW-2(3,1)	11	1486	11	1621	12	1756	13	1891
pW-2(4,1)	9	1666	9	1801	10	1981	11	2161
pW-2(5,1)	9	2251	9	2251	10	2476	10	2476
pW-2(6,1)	9	2701	9	2701	9	2701	10	2971
3 Grid Sequence {44,2,1}								
pV-3	14	706	14	706	16	800	16	800
pW-3(2,1)	10	988	9	941	10	1035	11	1129
pW-3(3,1)	9	1317	9	1317	9	1411	10	1552
3 Grid Sequence {44,8,1}								
pV-3	18	1008	18	1008	17	955	15	849
pW-3(2,1)	10	1114	11	1273	11	1273	11	1273
pW-3(3,1)	10	1591	10	1750	10	1750	12	2068
pW-3(4,1)	9	1909	9	2121	9	2121	11	2545
pW-3(7,1)	9	3711	9	3711	9	3711	10	4082
3 Grid Sequence {44,22,1}								
pV-3	25	1743	24	1676	24	1676	24	1676
pW-3(2,1)	14	1944	13	1877	14	2011	14	2011
pW-3(3,1)	11	2212	10	2212	10	2212	11	2413
pW-3(4,1)	9	2480	9	2681	10	2949	11	3217
pW-3(5,1)	9	3351	9	3351	9	3351	11	4021
4 Grid Sequence {44,8,2,1}								
pV-4	9	551	9	551	10	606	11	661
pW-4(2,2)	9	661	9	661	9	661	10	727
5 Grid Sequence {44,22,8,2,1}								
pV-5	9	771	9	771	10	848	11	925
pW-5(2,3)	9	881	9	881	9	881	10	969
6 Grid Sequence {44,22,8,4,2,1}								
pV-6	9	811	9	811	10	892	10	892
pW-6(2,5)	9	841	9	841	9	841	10	925

A the 14h mesh is the smallest low-order problem, but the increase in the number of transport iterations is likely too significant for this mesh to be the most efficient.

4.6 Summary

This chapter presented the multilevel method with multigrid in both energy and space. This is done by formulating the low-order equations on a coarser mesh in space. For the NDA simply becomes the CMFD method when formulated on a coarser spatial mesh. Numerical results showed that coarsening in space can significantly reduce the work in the low-order problem. However this coarsening can also lead to problems that make the CMFD method unstable. A consistent discretization of the QD equations was also formulated on a coarse spatial mesh. The multilevel method was also formulated using the pCMFD equations which address the instability issues with the CMFD method. The numerical results showed that the multilevel method works well on coarser energy grids. Various energy grid sequences behave differently on different spatial meshes. Multiple energy grids can be particularly helpful on coarse spatial meshes.

Chapter 5

Conclusions

This dissertation presents new methods for solving eigenvalue neutron transport problems using multilevel in energy methodology. New iteration methods for solving eigenvalue problems for multigroup diffusion equations have been developed. They are based on multigrid-in-energy approach. The nonlinear projection operator is formulated by means of averaging the group diffusion equations over energy on the hierarchy of energy grids. We defined several variants of prolongation operators based on multiplication correction of the grid solutions. The new prolongation operators use linear interpolation in energy between neighboring grids. We apply the partial V- and W-cycles to move through the hierarchy of energy grids. The estimation of the eigenvalue is performed on the coarsest grid with just one energy group. Thus, the eigenvalue problem is solved in the space with the smallest dimensionality. The proposed methods with multigrid in energy were derived for the second-order finite volume spatial approximation of the diffusion equation. They can be applied to other spatial discretizations as well, for example, finite element methods. The obtained numerical results on realistic model reactor-physics problems with 44 groups demonstrated efficiency of the developed algorithms with multigrid in energy. They enable to reduce significantly total number of diffusion solves. Involving additional coarse energy grids can accelerate iterations and decrease computational costs. The proposed multilevel methods can be applied to solve multigroup transport problems with very large number of groups.

In the transport problem the multilevel methodology was applied by formulating the low-order equations of the NDA and QD methods on multiple grids in energy. The results presented here showed that different sets of grids behaved differently depending on numbers of groups on each grid. Even the same set of grids behaved differently for different problems. The optimal set of grids is problem dependent, however some insight was gained on how to select grids. The use of a two group grid was beneficial for almost sets of grids. For more complex problems, with more coupling between space and energy, an advantage was seen in using sets with many grids.

For these problems using a finer grid along with coarser grids, like two-groups, was seen to work well. For coarser energy grids it was seen that the behavior of the convergence depended primarily on the group structure of the thermal groups. This means that fewer groups could be used in the fast groups without effecting the convergence. Hybrid cycles effectively accelerate the transport iterations with reduced work in the low-order problem compared to the standard cycles.

The multilevel method with coarsening in energy and space was also presented. This method used the multigrid in energy methodology on a low-order problem on a coarser spatial mesh, namely, CMFD and coarse mesh QD. The multilevel in energy and space method was also presented using the pCMFD equations which have some advantaged over standard CMFD. Coarsening in space for the low-order problem can significantly reduce the work in that problem, but it can also reduce the rate of convergence. Multiple grids in energy was found to be useful in solving the low-order problem on coarse meshes.

5.1 Continuing Lines of Investigation

This methodology was found to be effective and has some promising results. Further research is can be done to improve its efficiency and apply it to other types of problems. Future work will include a more detailed analysis of this family of algorithms, and the development of advanced prolongation operators and coarsening strategies based on formal algorithms for analysis of group cross sections. Fourier analysis would give a better understanding of the behavior of the method and identify the slowest converging error modes. This could also help define a better way of choosing each coarse energy grid. To develop fast solvers for the algebraic system of low-order equations, it is necessary to improve the efficiency of preconditioners for Krylov iterative methods. A multilevel method with simultaneous coarsening in space and energy can be developed.

The methodology could be used with the method of long characteristics and other transport schemes. Although this method is formulated for equations discretized on a rectangular spatial mesh, it can be extended to unstructured meshes and curved surfaces. Finite elements have been used to discretize both the NDA and QD equations. This multilevel hierarchy can also be applied to those equations with finite elements. Problems with anisotropic scattering can also be treated using this methodology. The low-order equations also solve for the current which can be used to accelerate the first moment term of the scattering source. We note that the proposed method can be used to solve other kinds of eigenvalue problems, such as α-eigenvalue or critical parameter problems. It can also be applied to solve fixed source problems for shielding applications and adjoint multigroup transport problems.

REFERENCES

[1] A. V. Averin and A. M. Voloschenko. Consistent P_1 synthetic acceleration method for outer iterations. *Transport Theory and Statistical Physics*, 23:701 – 730, 1994.

[2] B. C. Yee, B Kochunas, and E. W. Larsen. A Multilevel in Space and Energy Solver for Multigroup Diffusion Eigenvalue Problems. *Nuclear Engineering and Technology*, 49(6):1125 – 1134, 2017.

[3] B. C. Yee, B. Kochunas, and E. W. Larsen. Space-dependent Wielandt shifts for multigroup diffusion eigenvalue problems. *Nuclear Science and Energy*, 188:140–169, 2017.

[4] B. Chang, T. Manteuffel, S. McCormick, J. Ruge, and B. Sheehan. Spatial multigrid for isotropic neutron transport. *SIAM Journal on Scientific Computing*, 29(5):1900–1917, 2007.

[5] B. Cho and N. Z. Cho. Nonoverlapping local/global iteration with 2-D/1-D fusion transport kernel and p-CMFD wrapper for transient reactor analysis-II: Parallelization and Predictor-Corrector Quasi-Static method application. *Annals of Nuclear Energy*, 90:284–302, 2016.

[6] B. Collins and S. Stimpson. Acceleration Method for Whole Core Reactor Simulations Using VERA. *Transaction of the American Nuclear Society*, 118:929–932, 2018.

[7] B. T. Adams and J. E. Morel. A two-grid acceleration scheme for the multigroup S_n equations with neutron upscattering. *Nuclear Science and Engineering*, 115:253 – 264, 1993.

[8] D. A. Knoll, H. Park, and C. Newman. Acceleration of k-Eigenvalue/Criticality Calculations Using the Jacobian-Free Newton-Krylov Method. *Nuclear Science and Engineering*, 167:133–140, 2011.

[9] D. Gill, Y. Azmy, J. Warsa, and J. Densmore. Newton's method for the computation of k-eigenvalues in S_N transport applications. *Nuclear Science and Engineering*, 167:141–153, 2011.

[10] D. J. Miller, K. A. Matthews, and C. R. Brennan. Split-cell discrete ordinates transport on an unstructured grid of triangular cells. *Transport Theory and Statistical Physics*, 25:833 – 867, 1996.

[11] D. Mihalas and B. Weibel-Mihalas. *Foundation of radiation hydrodynamics*. Oxford University Press, 1984.

[12] D. Y. Anistratov. Nonlinear quasidiffusion acceleration methods with independent discretization. *Transactions of the American Nuclear Society*, 95:553–555, 2006.

[13] D. Y. Anistratov, E. N. Aristova, and V. Ya. Gol'din. A Nonlinear Method for Solving the Problems of Radiation Transfer in a Physical System. *Mathematical Modeling*, 8(12):3–28, 1996. In Russian.

[14] D. Y. Anistratov, L. R. Cornejo, and J. P. Jones. Stability analysis of nonlinear two-grid method for multigroup neutron diffusion problems. *Journal of Computational Physics*, 346:278–294, 2017.

[15] D. Y. Anistratov and V. Ya. Gol'din. Nonlinear methods for solving particle transport problems. *Transport Theory and Statistical Physics*, 22:42–77, 1993.

[16] J. J. Duderstadt and W. R. Martin. *Transport Theory*. John Wiley & Sons, New York, 1979.

[17] D.Y. Anistratov. Multilevel NDA Methods for Solving Multigroup Eigenvalue Neutron Transport Problems. *Nuclear Science and Engineering*, 174:150 – 162, 2013.

[18] D.Y. Anistratov and V. Ya. Gol'din. Solution of the multigroup transport equation by the quasi-diffusion method. *Preprint of the Keldysh Institute for Applied Mathematics*, 128:19 pp, 1986. (in Russian).

[19] D.Y. Anistratov and V. Ya. Gol'din. Multilevel quasidiffusion methods for solving multigroup transport k-eigenvalue problems in one-dimensional slab geometry. *Nuclear Science and Engineering*, 169:111 – 132, 2011.

[20] D.Y. Anistratov and V.Ya. Gol'din. Numerical Solution of the Time-Dependent Transport Equation Coupled with the Burnup and Reactor Kinetics Equations. In *International Symposium on Numerical Transport Theory*, pages 33–36, May 26-28, 1992, Moscow, Russia, Nuclear Society,, 1992.

[21] E. W. Larsen. A Grey Transport Acceleration Method for Time-Dependent Radiative Transfer Problems. *Journal of Computational Physics*, 78:459–480, 1988.

[22] E. W. Larsen. The asymptotic diffusion limit of discretized transport problems. *Nuclear Science and Engineering*, 112:336 – 346, 1992.

[23] E. W. Larsen and G. C. Pomraning. The P_N theory as an asymptotic limit of transport theory in planar geometry-I: analysis. *Nuclear Science and Engineering*, 109:49 – 75, 1991.

[24] E.N. Aristova, V.Ya. Gol'din, and A.V. Kolpakov. Multidimensional Calculations of Radiation Transport by Nonlinear Quasi-Diffusion Method. In *Proceeding of International Conference on Mathematics and Computation, Reactor Physics and Environmental Analysis in Nuclear Applications (M&C 99)*, pages 667–676, Sept. 27-30, 1999, Madrid, Spain, 1999.

[25] H. G. Cho and C. J. Park. A Comparision of Coarse Mesh Rebalance and Coarse Mesh Finite Difference Accelerations for the Neutron Transport Calculations. In *Int. Conf. Nuclear Mathematical and Computational Sciences (M&C 2003)*, 2003.

[26] H. Park, D. A. Knoll, and C. Newman. Nonlinear Acceleration of Transport Criticality Problems. *Nuclear Science and Engineering*, 172:52–65, 2012.

[27] I. K. Abu-Shumays. Angular quadratures for improved transport computations. *Transport Theory and Statistical Physics*, 30(2&3):169 – 204, 2001.

[28] J. Dorning. Homogenized multigroup and energy-dependent diffusion equations as asymptotic approximations to the boltzmann equation. *Transaction of the American Nuclear Society*, 89:313–316, 2003.

[29] J. E. Morel, E. W. Larsen, and M. K. Matzen. A synthetic acceleration scheme for radiative diffusion calculations. *J. Quant. Spectrosc. Radiat. Transfer*, 34:243–261, 1985.

[30] J. E. Morel, T.-Y. B. Yang, and J. S. Warsa. Linear multifrequency-grey acceleration recast for preconditioned krylov iterations. *Journal of Computational Physics*, 227:244–263, 2007.

[31] J. Willert, H. Park, and D. A. Knoll. A comparison of acceleration methods for solving the neutron transport k-eigenvalue problem. *Journal of Computational Physics*, 274:681–694, 2014.

[32] J. Xu and L. Zikatanov. *Algebraic Multigrid Methods*. Cambridge University Press, 2017.

[33] J. Y. Cho, H. G. Joo, K. S. Kim, and S. Q. Zee. Cell Based CMFD Formulation for Acceleration of Whole-core Method of Characteristics Calculations. *Journal of the Korean Nuclear Society*, 34(3):250–258, 2002.

[34] K. P. Keady and E. W. Larsen. Stability of S_n k-Eigenvalue Iterations Using CMFD Acceleration. In *Joint Int. Conf. on Math. and Comp. (M&C), Supercomp. in Nucl. Appl. (SNA) and the Monte Carlo (MC) Method*, 2015. Nashville, TN, United States, April 19-23, on CD-ROM.

[35] K. S. Kim and M. D. DeHart. Unstructured partial- and net-current based coarse mesh finite difference acceleration applied to the estended step charateristics method in NEWT. *Annals of Nuclear Energy*, 38:527 – 534, 2011.

[36] K. S. Smith. Nodal Method Storage Reduction by Nonlinear Iteration. *Trans. Am. Nucl. Soc.*, 44:265, 1984.

[37] K. S. Smith. Assembly homogenization techniques for light water reactor analysis. *Progress in Nuclear Energy*, 17:303–335, 1986.

[38] K. Smith and J. Rhodes III. Full-core, 2-D, LWR core calculations with CASMO-4E. In *Proceedings of PHYSOR 2002*, 2002. Seoul, Korea, October 7-10.

[39] K. Stuben. A review of algebraic multigrid. *Journal of Computational and Applied Mathematics*, 128(1&2):281 – 309, 2001.

[40] L. Cornejo, D. Anistratov, and K. Smith. Iteration Methods with Multigrid in Energy for Eigenvalue Neutron Diffusion Problems. *Nuclear Science and Engineering (submitted for publication in July, 2018).*

[41] L. J. Rhodes and K. Smith. CASMO-5/CASMO-5M a fuel assembly burnup program methodology manual, SSP-08/405 Rev. 0. Technical report, 2008. Studsvik Scandpower, Inc.

[42] L. R. Cornejo and D. Y. Anistratov. Nonlinear diffusion acceleration method with multigrid multiplicative corrections for multigroup eigenvalue transport problems. In *Joint Int. Conf. on Math. and Comp. (M&C), Supercomp. in Nucl. Appl. (SNA) and the Monte Carlo (MC) Method*, 2015. Nashville, TN, United States, April 19-23, on CD-ROM.

[43] L. R. Cornejo and D. Y. Anistratov. Multilevel Quasidiffusion Method with Multiplicative Corrections For Eigenvalue Neutron Transport Problems. In *PHYSOR 2016*, 2016. Sun Valley, ID, United States, May 1-5, on CD-ROM.

[44] L. R. Cornejo and D. Y. Anistratov. Nonlinear Diffusion Acceleration Method with Multigrid in Energy for k-Eigenvalue Neutron Transport Problems. *Nuclear Science and Engineering*, 184:514–526, 2016.

[45] L. R. Cornejo and D. Y. Anistratov. The multilevel quasidiffusion method with multigrid in energy for eigenvalue transport problems. *Progress in Nuclear Energy*, 101:401–408, 2017.

[46] E. W. Larsen. Diffusion theory as an asymptotic limit of transport theory for nearly critical systems with small mean free paths. *Annals of Nuclear Energy*, 7:249–255, 1980.

[47] E. W. Larsen and R.P. Hughes. Homogenized diffusion approximations to the neutron transport equation. *Nulcear Science and Engineering*, 73:274–285, 1980.

[48] E. W. Larsen, J. E. Morel, and J. M. McGhee. Asymptotic derivation of the multigroup p_1 and simplified p_n equations with anisotropic scattering. *Nulcear Science and Engineering*, 123:328–???, 1996.

[49] E. E. Lewis, M. A. Smith, N. Tsoulfanidis, G. Palmiotti, T. A. Taiwo, and R. N. Blomquist. Benchmark specification for deterministic 2-D/3-D MOX fuel assembly transport calculations without spatial homogenization (C5G7). Expert Group on 3-D Radiation Transport Benchmarks NEA/NSC/DOC(2001)4, 2001.

[50] M. Ainsworth, J. Levesley, M. Marletta, and W. A. Light. *Wavelets, Multilevel Methods and Eleptic PDEs*. Oxford University Press, 1997.

[51] M. I. Bakirova, V. Ya. Karpov, and M. I. Mukhina. A characteristic-interpolation method for solving a transfer equations. *Differential Equations*, 22:788–794, 1987.

[52] M. L. Adams and E. W. Larsen. Fast iterative methods for discrete-ordinates particle transport calculations. *Progress in Nuclear Energy*, 40:3–159, 2002.

[53] M. T. Calef, E. D. Fichtl, J. S. Warsa, M. Berndt and N. N. Carlson. Nonlinear Krylov acceleration applied to a discrete ordinates formulation of the k-eigenvalue problem. *Journal of Computational Physics*, 238:188–209, 2013.

[54] N. Z. Cho. The Partial Current-Based CMFD (p-CMFD) Method Revisited. In *Transactions Korean Nuclear Society*, 2012. Gyeongju, Korea. October 25-26.

[55] N. Z. Cho, G. S. Lee, and C. J. Park. Partial Current-Based CMFD Acceleration of the 2D/1D Fusion Method for 3D Whole-Core Transport Calculations. *Transaction of the American Nuclear Society*, 88:594–596, 2003.

[56] R. E. Grove. The slice balance approach (SBA): a characteristic-based, multiple balance S_N approach on unstructured polyhedral meshes. In *Proceedings of International Confrence on*

Mathematics and Computations, Supercomputing, Reactor Physics and Nuclear Biological Applications (M&C 2005), page 12, 2003. ANS, Avignon, France, September.

[57] R. Ferrer, J. Rhodes, and L. Li. Implementation of Coarse-mesh Nolinear Diffusion Acceleration for Hexagonal Geometry in CASMO5. In *PHYSOR 2016*, 2016. Sun Valley, ID, United States, May 1-5, on CD-ROM.

[58] R. N. Slaybaugh, T. M. Evans, G. G. Davidson and P. P. H. Wilson. Multigrid in energy preconditioner for Krylov solvers. *Journal of Computational Physics*, 242:405–419, 2013.

[59] R. P. Fedorenko. A relaxation methods for solving elliptic difference equations. *USSR Comput. Math. Phys.*, 1:1092–1096, 1961.

[60] R. P. Fedorenko. The speed of comvergence of one iterative process. *USSR Comput. Math. Phys.*, 4:227–235, 1964.

[61] S. G. Hong, K. Kim, and J. S. Song. Fourier Convergence Ananlysis of the Rebalance Methods for Discrete Ordinates Transport Equations in Eigenvalue Problems. *Nuclear Science and Engineering*, 164:33 – 52, 2010.

[62] S. Schunert, Y. Wang, F. Gleicher, J. Ortensi, B. Baker, V. Laboure, C. Wang, M. DeHart, and R. Martineau. A Flexible Nonlinear Diffusion Acceleration Method for the S_N Transport Equations Discretized with Discontinuous Finite Elements. *Journal of Computational Physics*, In Press:Accepted Manuscript, 2017.

[63] S. Schunert, Y. Wang, J. Ortensi, F. Gleicher, B. Baker, M. DeHart, and R. Martineau. A Flexable Nonlinear Diffusion Acceleration Method for the First Order Eigenvalue S_n Equations Discretized with Discontinuous FEM. In *PHYSOR 2016*, 2016. Sun Valley, ID, United States, May 1-5, on CD-ROM.

[64] S. Yuk and N. S. Cho. Whole-Core Transport Solutions with 2-D/1-D Fusion Kernel via p-CMFD Acceleration and p-CMFD Embedding of Nonoverlapping Local/Global Iterations. *Nuclear Science and Engineering*, 181:1–16, 2015.

[65] R. Sanchez. Assembly homogenization techniques for core calculations. *Progress in Nuclear Energy*, 51:14–31, 2009.

[66] SCALE. A comprehensive modeling and simulation suite for nuclear safety analysis and design, ornl/tm-2005/39, Version 6.1. Technical report, 2011. Oak Ridge National Laboratory, Oak Ridge, TN.

[67] K. Stüben. An introduction to algebraic multigrid, 2001. in book: U. Trottenberg, C. Oosterlee, A. Schuller, Multigrid, Academic Press, pp. 413-532.

[68] T. M. Evans and K. T. Clarno. A Transport Acceleration Scheme for Multigroup Discrete Ordinates with Upscattering. *Nuclear Science and Engineering*, 165:292–304, 2010.

[69] V. Ya. Gol'din. A quasi-diffusion method of solving the kinetic equation. *USSR Comp. Math. and Math. Phys.*, 4:136, 1964.

[70] V. Ya. Gol'din. On mathematical modeling of problems of non-equilibrium transfer in physical systems. In *Modern Problems of Mathematical Physics and Computational Mathematics*, pages 113–127. Nauka, Moscow, 1982. in Russian.

[71] V. Ya. Gol'din, D. A. Gol'dina, A. V. Kolpakov, and A. V. Shilkov. Mathematical modeling of hydrodynamics processes with high energy density radiation. *Problems of Atomic Science and Engineering: Methods and Codes for Numerical Solution of Mathematical Physics Problems*, 2:59–88, 1986. (in Russian).

[72] V.Ya. Gol'din and D.Y. Anistratov. Fast Neutron Reactor in a Self-Adjusting Neutron-Nuclide Regime. *Mathematical Modeling*, 7(10):12–32, 1995. In Russian.

[73] W. Boyd, S. Shaner, L. Li, B. Forget, and K. Smith. The OpenMOC method of characteristics neutron particle transport code. *Annals or Nuclear Energy*, 68:43–52, 2014.

[74] W. L. Briggs, V. E. Henson, and S. F. McCormick. *A Multigrid Tutorial*. Society for Industrial and Applied Mathematics, 2000.

[75] W. L. Briggs, V. E. Henson, and S. F. McCormick. A multigrid tutorial. *SIAM*, 2000.

[76] M. M. R. Williams. *Mathematical methods in particle transport theory.* Butterworh & Co, 1971.

[77] Z. Zhong, T. Downar, Y. Xu, M. DeHart, and K. Clarno. Implementation of Two-Level Coarse-Mesh Finite Difference Acceleration in an Arbitrary Geometry, Two-Dimensional Discrete Ordinates Transport Method. *Nuclear Science and Engineering*, 158:289 – 298, 2008.